

Universiteit
Leiden
The Netherlands

Advances in quantitative coronary and vascular angiography

Janssen, J.P.

Citation
Janssen, J. P. (2012, October 11). *Advances in quantitative coronary and vascular angiography*. Retrieved from https://hdl.handle.net/1887/19946

Version:	Corrected Publisher's Version
License:	Licence agreement concerning inclusion of doctoral thesis in the Institutional Repository of the University of Leiden
Downloaded from:	https://hdl.handle.net/1887/19946

Note: To cite this publication please use the final published version (if applicable).

Cover Page



Universiteit Leiden



The handle http://hdl.handle.net/1887/19946 holds various files of this Leiden University dissertation.

Author: Janssen, Jasper
Title: Advances in quantitative coronary and vascular angiography
Date: 2012-10-11

Advances in Quantitative Coronary and Vascular Angiography

Jasper Janssen

2012

Printed by: Gildeprint Drukkerijen

ISBN: 978-94-6108-341-8

©2012, J.P.Janssen, Leiden, the Netherlands. All rights reserved. No part of this publication may be reproduced or transmitted in any form or by any means, electronic or mechanical, including photocopying, recording, or any information storage and retrieval system, without prior permission in writing from the copyright owner.

Advances in Quantitative Coronary and Vascular Angiography

Proefschrift

ter verkrijging van

de graad van Doctor aan de Universiteit Leiden,

op gezag van de Rector Magnificus prof.mr. P.F. van der Heijden,

volgens besluit van het College voor Promoties

te verdedigen op donderdag 11 oktober 2012

klokke 15.00 uur

door

Johannes Petrus Janssen

geboren te Heteren

in 1976

Promotiecommissie

Promotor:	Prof. dr. ir. J.H.C. Reiber	
Co-promotor:	Ir. G. Koning	
Overige leden:	Prof. dr. A. de Roos	(LUMC)
	Prof. dr. W.J. Niessen	(Erasmus MC)
	Prof. dr. ir. M.J.T. Reinders	(TU Delft)

Financial support by the Dutch Heart Foundation for the publication of this thesis is gratefully acknowledged.

Financial support for the publication of this thesis was kindly provided by:

- Bontius Stichting inz. Doelfonds Beeldverwerking, LUMC
- Medis medical imaging systems bv, Leiden

Contents

1 General Introduction **1**
- 1.1 Coronary heart disease . . . 2
- 1.2 Imaging techniques: X-ray . . . 2
- 1.3 Other imaging techniques . . . 4
- 1.4 QCA . . . 7
- 1.5 Outline of the thesis . . . 9

2 Inventory Contour Detection Algorithms **13**
- 2.1 Introduction . . . 14
- 2.2 Methods . . . 14
- 2.3 Discussion . . . 20

3 A novel approach for the detection of pathlines in X-Ray angiograms: the wavefront propagation algorithm **23**
- 3.1 Introduction . . . 25
- 3.2 Methods . . . 25
- 3.3 Results . . . 30
- 3.4 Discussion . . . 31
- 3.5 Conclusion . . . 34

4 Validation of a New Method for the Detection of Pathlines in Vascular X-ray Images **37**
- 4.1 Introduction . . . 39
- 4.2 Materials and Methods . . . 40
- 4.3 Results . . . 45
- 4.4 Discussion . . . 48
- 4.5 Conclusion . . . 49

5 A new approach to contour detection in X-ray arteriograms: The Wavecontour 51
5.1 Introduction . . . 53
5.2 Materials and methods . . . 55
5.3 Results . . . 60
5.4 Discussion and conclusion . . . 64

6 New approaches for the assessment of vessel sizes in quantitative (cardio-) vascular X-ray analysis 65
6.1 Introduction . . . 67
6.2 Methods and materials . . . 67
6.3 Results . . . 76
6.4 Discussion . . . 79
6.5 Conclusions . . . 81

7 Dedicated bifurcation analysis: basic principles 83
7.1 Introduction . . . 85
7.2 Bifurcation analysis . . . 85
7.3 Validation . . . 91
7.4 Conclusion . . . 92

8 Clinical validation of the new T- and Y-shaped models for the quantitative analysis of coronary bifurcations: An inter-observer variability study 93
8.1 Introduction . . . 95
8.2 Material and Methods . . . 96
8.3 Material . . . 103
8.4 Results . . . 104
8.5 Discussion . . . 106
8.6 Conclusion . . . 109

9 Discussion 111
9.1 Objective . . . 111
9.2 Wavepath . . . 111
9.3 Wavecontour . . . 111
9.4 Diameter Function . . . 112
9.5 Overall QCA . . . 113
9.6 External developments . . . 114
9.7 Future of QCA . . . 115
9.8 In Conclusion . . . 116

Summary and Conclusion 117

Samenvatting en Conclusie 121

References 123

Acknowledgements **135**

Publications **137**

Curriculum Vitæ **139**

CHAPTER 1

General Introduction

1.1 Coronary heart disease

Cardiovascular disease (CVD) is the leading cause of death and disability among adults in the developed countries today. As the burden of heart disease and stroke continues to grow, it is expecting to be the leading cause of death worldwide within 10 years. It causes half of the total number of deaths in the western world and the overall worldwide death rate for cardiovascular disease is 355 per 100,000 people.

The American Heart Association estimated that in 2006 about 1.2 million Americans would have a first or recurrent coronary attack and about 479,000 of these people would die. Coronary heart disease is American's single leading cause of death [1], with 831000 deaths in 2006 followed by cancer with 560000 deaths in the same year. According to the European Heart Network, CVD causes over 4.35 million deaths in Europe, nearly half of the total number of deaths (49%). CVD is the main cause of years of life lost from early death in Europe - around a third of years of life lost from early death are due to CVD. Overall CVD is estimated to cost the EU economy 169 billion a year [2]. From data of the World Health Organization, it is estimated that worldwide 17 million people die of CVDs, particularly heart attacks and strokes, every year [3].

The major cause of cardiovascular disease is atherosclerosis, the forming of plaque in the coronary arteries. These coronary arteries are the arteries that supply blood to the muscle of the heart itself (Fig. 1.1). This plaque mostly consists of fatty substances, cholesterol, cellular waste products and calcium, and can lead to a severe narrowing of the vessel lumen, called stenosis, which can disturb the blood flow dramatically and even totally occlude the vessel (Fig. 1.2). In case of an occlusion a part of the heart muscle is exempt from oxygen carried by the blood flow, which usually leads to a myocardial infarction. Furthermore, when a plaque ruptures, embolies (blood clots) can travel through the vascular system and get stuck elsewhere, causing a blockage of an artery and/or vein (embolism), which can lead to a myocardial infarction if one of the coronaries is blocked, stroke when one of the cranial arteries is occluded, or pulmonary embolism when one of the lung vessels is blocked.

1.2 Imaging techniques: X-ray

Over the years, cardiologists have been looking for ways to detect these atherosclerotic lesions at an early stage and assess the progression of the disease over time [4]. This monitoring of the progression of coronary atherosclerosis was made possible by making use of the much earlier discovery of X-rays by Röntgen [5, 6] and their ability to penetrate the human body. The first introduction of "selective" coronary X-ray arteriograms was done by Sones in 1958 [7]. X-ray angiography is a technique that uses an X-ray system (X-ray source at one side of the patient and a detector at the other side, Fig. 1.3) and a contrast agent that is administered into the artery, which absorbs a substantial amount of the X-ray beam that is passing through. This results in an image that shows the projection of the lumen of the arteries under study as can be seen in Figure 1.4.

Much earlier, already in the 30's, the concept of coronary X-ray arteriograms was introduced by Castellanos [8]. However, the quality of the images was very poor, due to weak radiographic generators that required long exposure times and therefore resulted in motion artifacts. Further-

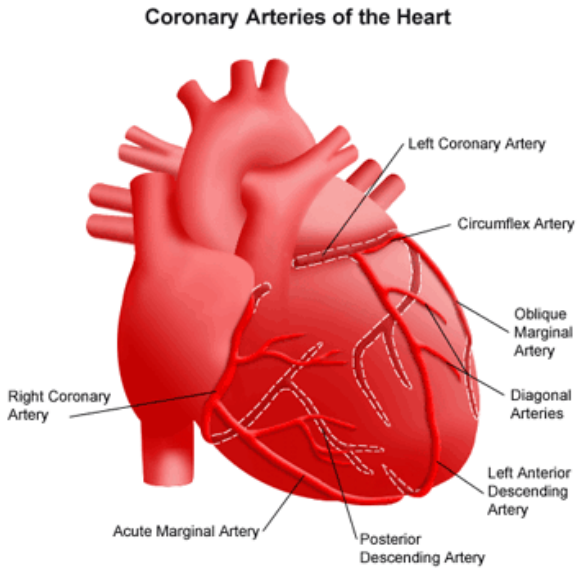


Figure 1.1: Schematic representation of the heart and its coronary arteries. (image from www.yalemedicalgroup.org)

more, the injection of the contrast medium was too slow causing a poor filling of the coronary arteries. In 1945, it was Radner who published the first attempt to visualize coronary arteriograms in living humans. In 1956, Arnulf developed a method to visualize the coronary arteries much better by inducing a cardiac arrest and to administer the contrast by direct needle punc-

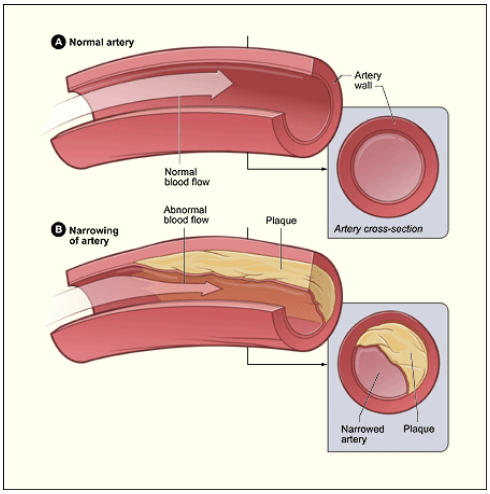


Figure 1.2: Atherosclerosis: the forming of plaque inside an artery. (image from wikimediafoundation.org)

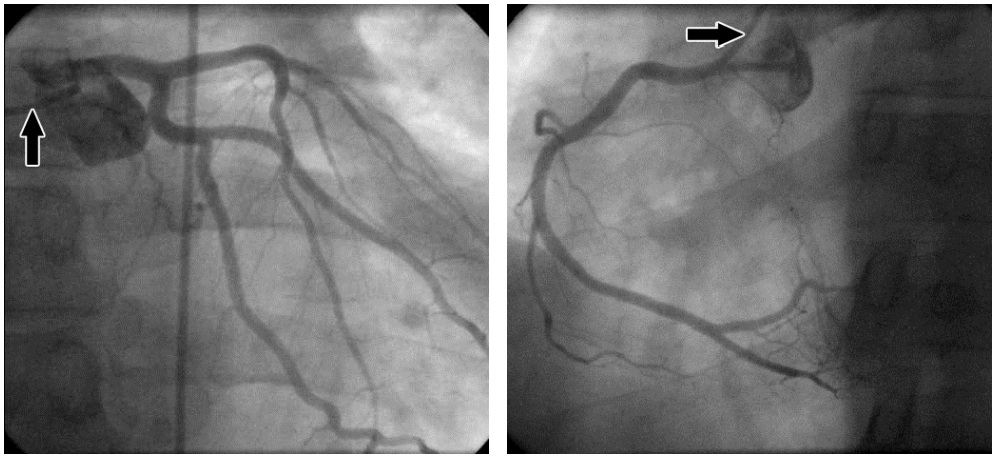


Figure 1.3: Modern X-ray system with a source on one side and a detector on the other side of the patient, both mounted on a so-called c-arm.

ture in the aortic arch [9]. Then, in 1958, Sones managed to achieve the first selective angiogram, that was really usable in clinical practice; the technique was not published until 1962 [7]. He developed a method that uses only small amounts of the contrast agent and delivers it directly into the coronary arteries. In the 60's, the procedure was further improved by Judkins [10] and Amplatz [11], resulting in transfemoral catheter techniques (injection of contrast agent via the femoral artery) using pre-bent catheters, quite similar to the techniques used today. Later on, the imaging equipment was developed further and further for example by the introduction of rotating gantries and linking the image intensifiers to TV screens. Systems that allow caudo-cranial recordings were developed, as described by Ludwig and Bruschke [12]. A problem with this technique in relation to the atherosclerosis, is that the vessel wall cannot be seen in an X-ray image, and therefore the earliest stage of the coronary artery disease cannot be detected. In this stage, the forming of plaque doesn't cause a narrowing of the lumen yet, but results in a thickening of the vessel wall. This is called arterial remodeling as described by Glagov et al [13]. Only when the disease continues and the outer vessel wall cannot be stretched further, the lumen becomes affected and this can be detected by means of the X-ray angiograms as can be seen in Fig. 1.5.

1.3 Other imaging techniques

In order to image the coronary vessel wall itself, another technique has been developed, namely Intravascular Ultrasound (IVUS). This technique provides real-time cross-sectional images using ultrasound that is transmitted and received by the tip of the catheter which is inserted in the artery under study. An advantage of this technique is that the early stage of atherosclerosis can be detected. However, there are also significant disadvantages associated with the technique, such as: the catheter cannot be inserted in the smallest coronary vessels, only one vessel can be imaged at a time, but most seriously, the catheter manipulation can damage the arterial wall, resulting in a puncture of the wall, or even worse small pieces of plaque could become



(a) (b)

Figure 1.4: Example of a typical coronary angiogram. At the left hand side, the left coronary system is depicted, on the right hand side the right coronary system. The arrow depicts the catheter that is positioned in the ostium of the artery and through which the contrast medium is administered. This is an example of a normal angiogram without any narrowings in the vessels.

loose, resulting in embolization of the distal vessels. Although such serious events do not happen very often, the interventional cardiologists in general do not wish to manipulate the catheter in the coronary artery more than is absolutely necessary. Another technique that images the vessel wall from the inside has been developed in the last decade: Optical Coherence Tomography (OCT). This technique uses interferometric imaging typically with near-infrared light to produce cross-sectional images of micrometer resolution. The relatively long wavelength allows the light to penetrate into the surrounding tissue. Similar to IVUS, OCT is an invasive, catheter-based technique that can image only one vessel at a time, making it perfect for studying complex lesions and the malapposition of stent struts, but less suitable for diagnostic purposes. The advantage of OCT with respect to IVUS is its much higher axial resolution, whereas its disadvantage is the limited penetration in the vessel wall. OCT is perfectly suitable to study the thin fibrous cap and the positions of the stent struts, but does not allow the assessment of the plaque composition. In that sense, OCT and IVUS are complementary imaging techniques; intravascular imaging companies are therefore also developing new catheters with both IVUS and OCT elements on the same tip.

In the last decades, a new noninvasive technique for imaging vessels has been developed, namely CTA (Computer Tomographic Angiography). This technique provides a three-dimensional image of the vessels under study, allowing the analyst to select the view in which the lesion is best visible. The problem of overlapping vessels doesn't occur when using this new modality. Over the years, this technique has been improved and the resolution has been increased making it now possible to image the coronary arteries.

As described by Achenbach [14] and Schuijf [15], the quality of coronary CT angiography is increasing rapidly nowadays. The spatial and temporal resolution of the modern multi-slice-CT

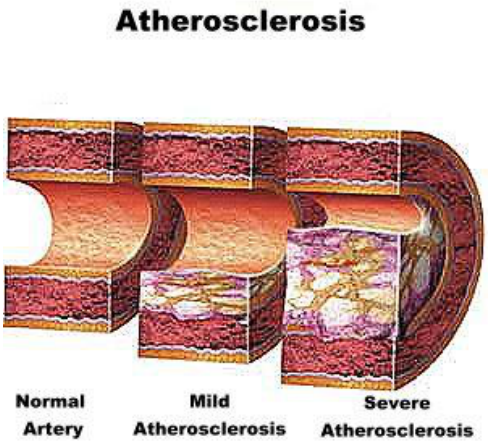


Figure 1.5: Progression of atherosclerosis: left a healthy vessel, in the middle the early stage of atherosclerosis: arterial remodeling and at the right a severely diseased vessel. (image from www.fitnessavenue.net)

scanners (MSCT) however, is still limited compared to the X-ray angiography, which makes accurate stenosis quantification more difficult [16, 17]. Furthermore, the reproducibility of the measurements is not optimal [18]. However, the development of more automatic methods reduced the variability in the outcomes and therefore improved the precision of the methods, as shown by [19, 20]. Moreover, the dose of radiation remains a big concern in CT-imaging.

On the other hand, a big advantage of MSCT is that the same images that were used for stenosis quantification can hopefully also be used for plaque characterization [21, 22, 23]. When a multi-frame CT is recorded (a 3-dimensional image for a number of phases in the heart beat), also the left ventricular function [24, 25, 26] and even mitral and aortic valve anatomy [27, 28, 29] can be assessed, making it a very efficient and versatile imaging technique.

Another new noninvasive vessel imaging technique that has been developed in the last decades is MRA (Magnetic Resonance Angiography), which is also a three-dimensional technique. Similarly to CTA, there are lots of developments currently going on in MRA and its quality has increased substantively. Quantitative methods have been developed to assess the degree of stenosis in diseased vessel segments [30, 31]. Furthermore, MRA can be extended with Vessel Wall Imaging (VWI), allowing visualization of the arterial wall, and even of the composition of the plaque components [32, 33]. Most of this research is performed on the carotid arteries and only very little is done on the coronary arteries [34] since the limited spatial resolution makes it very hard to image the vessel wall in the (smaller) and rapidly moving coronary arteries. Fusion of the MRA and VWI data will provide a better accuracy of the luminal dimensions and the wall visualization and quantization as was demonstrated by Adame et al [35]. This will work even better with the new 3T MRI systems.

CTA is used more and more for diagnostic purposes since it is still being improved and image quality is getting better and better due to newer scanners and better reconstruction algorithms. However, it is not to be expected to replace traditional invasive coronary angiography on a wide

scale yet. Not only because the spatial resolution is still not as high as in the X-ray angiographic images, but mainly because this technique (and the same holds for MRA) cannot be used during an intervention. X-ray, on the other hand, is the only available technique that is applicable during an intervention. Physicians use the X-ray projection images during a catheterization to steer the catheter towards the vessel of interest, while injecting contrast agent from time to time to see the artery tree in which the guide wire and imaging catheter is positioned. Since X-ray is the only technique that makes this possible, it is still the most commonly used technique in the catheterization laboratories for the visualization of the coronary arteries.

1.4 QCA

Currently, three different methods are used to assess the presence and extent of possible narrowings from X-ray arteriograms. The first method is the purely visual interpretation of the images to estimate the percentage diameter stenosis, which is generally seen as the most important parameter when assessing the severity of the lesion and the need for an intervention. Despite the relatively low accuracy and reproducibility and the strong observer dependence, this is still the most widely used method in routine clinical practice. The second method of assessing parameters from X-ray arteriograms is measuring the obstruction diameter using a caliper, a single line piece drawn by the observer, but this is of course very inaccurate and poorly reproducible. The last method, the one we have focused our research on, is the Quantitative Coronary and Vascular Angiography (QCA/QVA) [36, 37, 38, 39, 40].

Apart from the methods that rely on X-ray arteriograms, there are other ways of assessing the severity of a stenosis, for example by determining the functional significance in terms of blood flow, using pressure catheters. Several different methods have been developed to measure flow and flow reserve [41]. Nevertheless, they all suffer from the same problem: there is too much variation in normal values to distinguish between normal and pathological cases [42]. As a solution for this problem, the Fractional Flow Reserve (FFR) can be determined, as introduced by Pijls et al [43, 44, 45, 46]. This FFR is defined as the maximum achievable blood flow in the presence of a stenosis divided by the maximum blood flow in case the vessel had not been diseased. These values are derived from the mean arterial pressure, the central venous pressure and the pressure measurement distal to the stenosis in the diseased vessel. As a result, FFR appears to be a good indicator for the severity of the lesion; it has been demonstrated that an FFR <0.75 means that the obstruction is functionally significant and therefore should be treated by the interventional cardiologist. The advantage of this method is that not the geometric dimensions of the stenosis are measured, but its functional severity in terms of reduction in blood flow. The disadvantage is that a pressure catheter is needed for the measurement and there are problems assessing very severe stenoses and total occlusions.

QCA is a quantitative tool that provides objective and reproducible data about the narrowings in the vessels. Over the past 30 years, many developments have taken place, from using manual calipers, drawing the vessel contours on projected cinefilm images, to automated edge detection techniques. QCA requires user-interaction by selecting the segment that is under study and performing a calibration, usually on the catheter that is inserted into the ostium of the vessel to administer the contrast agent. The QCA-tool detects the segment and the lumen contours of

this segment and calculates the diameters of the lumen over the entire length of the segment. From these diameter measurements and an estimation of the lumen in a healthy situation, the stenosis parameters are calculated.

Over the last several decades, QCA has been generally accepted as the proper method for accurate and reproducible assessment of coronary artery disease from X-ray angiograms and the quantification of the severity of coronary artery lesions. Its precision and accuracy have been widely proven in several studies, using phantom data as well as clinical patient data [39]. QCA facilitates the choice of the proper recanalization devices during interventional cardiology as well as the evaluation of the development of a disease over time, by extracting clinically relevant parameters such as diameter stenosis, minimal lesion diameter and estimated reference diameter, as well as lesion length. Furthermore, QCA is used by core laboratories for the evaluation of the outcomes of clinical and pharmaceutical research trials, for example to determine the effects of statins, and stent trials, to assess the effect of new types of (drug-eluting) stents.

Since the early times of QCA, technical developments have proven their importance in the catheterization laboratories, facilitating the use of QCA and improving the analysis results. The 35mm cinefilm has been replaced by digital images in DICOM-format, stored on CD or in a PACS-system. This not only facilitates copying the original images and transferring these copied images to other physicians or core labs for further analysis, but also preserves the quality of the images. Furthermore, the introduction of the flat-panel systems as a replacement for the conventional image intensifier and CCD camera has removed a large amount of the spatial distortions from the X-ray system and preserved more of the X-ray signals, making the angiograms better and therefore the QCA analysis more accurate and more suitable for measurements or other post processing applications. The automated software packages that were developed in our group over the last decades provide reliable results and are generally seen as one of the leading applications in QCA [39, 40]. This application that was originally called QCA-CMS and later changed into QAngio XA, achieves a precise and accurate measurement of a stenosis in the coronary arteries. The system is applicable in online situations, during an intervention, as well as in offline situations, in both hospital and core laboratory environments. Its accuracy and precision were demonstrated by several extensive validation studies using both phantom and clinical data [39]. Furthermore, the system was validated by measuring the inter- and intra-observer variabilities and even inter- and intra-core lab variabilities [39, 47, 48].

Although the measurements are very fast and accurate, it is still not a fully automatic method, which means that there is still some user interaction required to perform the analysis. Therefore, there is still some variation in the results of a lesion quantification when a single segment is measured repeatedly by different analysts (inter-observer) or even by the same analyst (intra-observer). Besides this variation, there are still some difficulties when analyzing complex lesion morphologies and strongly curved vessels, which can lead to less accurate measurements. Furthermore, the interventional approaches that were originally designed for cardiac applications, are no longer restricted to the coronary arteries nowadays, but extended to the peripheral vessels as well, for example the aorta, the renal, iliac, femoral and carotid arteries. This extension of the intervention methods implies the inclusion of a whole new range of vessel sizes, much larger than the size of the coronary arteries. In addition to that, the analysis method had to be extended to be able to cope with new vessel morphologies, namely ostial segments and bifurcation segments, which cannot be measured properly with the conventional "straight"

segment analysis method.

The developments of these new intervention techniques have led to additional requirements for the automatic analysis software, such as measuring the exact location and quantifying the severity of vascular lesions at the position of the ostium of a sidebranch and at the position of an arterial bifurcation. These new requirements combined with the variation in the existing analysis results are the basis of our research towards new algorithms for the improvement of quantitative coronary and vascular analyses.

From our point of view, a quantitative coronary or vascular analysis consists of four steps that are performed subsequently: First, the rough position of the vessel is detected and usually this is done by finding a pathline or centerline through the vessel from a user-defined startpoint to endpoint, see Figure 1.6(a). The second step is finding the exact outlines of the vessel, using the already detected pathline as a definition of the segment under study, see Figure 1.6(b). This contour detection is a very important part of the analysis since the accuracy of the contours determines to a large extend the accuracy of the measurements. The third step is measuring the luminal diameters and estimating the diameters as they would have been in a healthy case, which we call the reference diameters, see Figure 1.6(c). The fourth and last step consists of measuring the stenosis parameters such as minimal lumen diameter (MLD), percentage diameter stenosis and obstruction length. In order to achieve a correct, reliable and reproducible lesion measurement, it is essential that all steps in this analysis perform equally well: the system is as precise and as robust as its weakest link in the chain of the analysis. Therefore, the overall goal of this research is to find new algorithms and improve all steps of the quantitative analysis to achieve a better overall result. Furthermore, the new algorithms should make it possible to extend the current analysis in order to cope with peripheral vessels and different vessel morphologies, such as sidebranches and bifurcations.

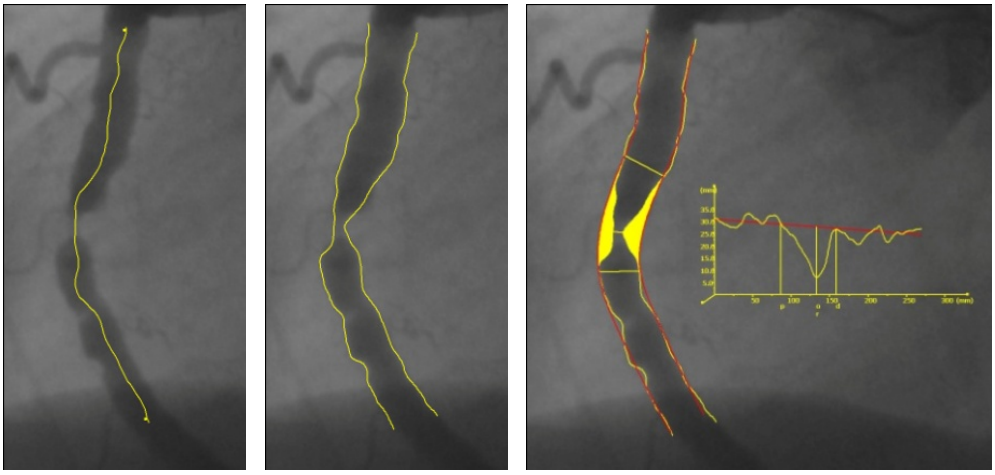
1.5 Outline of the thesis

The structure of the remaining part of this thesis is as follows:

In chapter 2, a general overview is presented of the main contour detection techniques that exist within the medical applications. Many methods are listed here and the most important advantages and disadvantages are discussed. This overview was the starting point of our contour detection research and led to the overall choice of the most promising technique for our application.

In chapter 3, our novel method for detecting pathlines in digital coronary angiograms is introduced. This new method that we denote Wavepath is based on the wavefront propagation method (fastmarching levelset-method). Wavepath was developed to reduce the influence of the user-defined start- and endpoint and results in a more stable, reproducible pathline, as demonstrated in the validation study that was performed on coronary angiograms. Furthermore, this method expands the possibilities of the pathline, making it suitable for different morphologies required for the new ostial segment and bifurcation segment analyses.

Chapter 4 describes the application of the Wavepath in peripheral applications, analyzing vessels with various sizes and morphologies. The extended validation was performed on a large variety of images, showing various vessels and morphologies. This validation proves the robust-



(a) (b) (c)

Figure 1.6: Example of a typical coronary angiogram. At the left hand side, the left coronary system is depicted, on the right hand side the right coronary system. The arrow depicts the catheter that is positioned in the ostium of the artery and through which the contrast medium is administered. This is an example of a normal angiogram without any narrowings in the vessels.

ness of the Wavepath, since the resulting pathline has proven to be virtually independent of the user-variation in placing the start- and endpoints.

Chapter 5 discusses our novel approach for the contour detection in X-ray angiograms, that we denote the Wavecontour. As the name already suggests, this method is also based on the wavefront propagation principle and performs the detection in a two-stage approach. The method was developed with the major goal to improve the robustness and reproducibility of the contour detection and to be a solution for the problems the other contour detection techniques suffer from, such as the detection of the contour in sharp corners (for example the contour between the two distal branches in a bifurcation segment) and at the position of complex lesions and side-branches. In addition to the description of the methods that we use in this approach, we also discuss the validation study that was performed to demonstrate the precision and accuracy of this new method. In this validation study, both in-vivo patient data and phantom data were used to show the improvement in accuracy and reproducibility that was achieved with the Wavecontour.

Chapter 6 describes the new approach for the measurement of the diameters and the estimation of the reference diameters of the blood vessels. This new approach was developed to overcome the problems that were encountered with the direction of the measurements in strongly curved vessels or strange vessel morphologies. Furthermore, this new approach optimizes the diameter measurement of the proximal part of an ostial lesion, as well as the estimation of the vessel as it would have been without disease. This diameter calculation method improves the accuracy of the lesion measurement substantially. Besides that, we also discuss the new analysis methods that were designed to analyze a bifurcation segment and measure all its diameters and stenosis parameters at the same time. We introduce two different models, the Y-shape and T-

shape model, which together cover the whole range of different bifurcation morphologies. These analyses provide data for the proximal segment and the two distal segments as well as data for the central part of the bifurcation, which was previously not possible to measure. In a phantom validation study, the accuracy and the precision of this new analysis method is calculated and discussed.

In chapter 7, the total bifurcation analysis is discussed, including our two new bifurcation models and the newly introduced edge segment analysis that provides data for stent segments and the corresponding stent- and ostial edge segments. This can be done for both the Y-shape and the T-shape model, representing the different intervention techniques. Furthermore, the results of the first validation study on clinical material are presented, which shows the intra-observer variability, proving the good reproducibility of our new bifurcation analysis.

Chapter 8 describes an extended validation study that was performed on clinical data using both the Y-shape and the T-shape model. This validation study assesses the inter- and intra-observer variability on pre- and post-intervention data showing the robustness of our newly developed bifurcation analysis methods.

Chapter 9 provides discussions for each of the previous chapters and an overall conclusion. For each of the newly developed methods, it is discussed to what extend our research goals have been met and which issues are still left for further research and improvement. Finally, the goals of the whole research are considered and overall conclusions are drawn.

CHAPTER 2

Inventory Contour Detection Algorithms

2.1 Introduction

Quantitative coronary arteriography (QCA) has been widely used for the detection and accurate assessment of the morphology of coronary vessels and the localization and measurement of obstructions from X-ray arteriograms. The accurate derivation of clinical parameters such as obstruction diameter and percentage diameter stenosis has proven to be very useful in clinical trials as well as in online applications in interventional cardiology.

In spite of the high accuracy and precision that has been shown by several packages [49, 36, 50, 51, 52] and the increasing complexity in cardiovascular interventions, the use of QCA and QVA (Quantitative Vascular Analysis) tools is still limited because of the manual interactions and corrections that are needed in routine clinical practice, and therefore the majority of the angiograms is still visually interpreted. This is obviously not the case in clinical trials, which are almost exclusively analyzed by the QCA approach, and which allow more time for the analysis. Currently there is still insufficient motivation by the interventional cardiologists to use QCA during the procedure, despite the fact that it may result in cost savings, better prognosis for the patient, etc; this will change if the insurance companies and the hospitals themselves are going to demand a quantitative proof of the need for the intervention and for the number and types of stents to be used, that is evidence based medicine. It may also change if the procedures become so complicated that absolute vessel sizes are needed to obtain acceptable results, such as in the case of complex bifurcation stenting.

A substantial part of the research that has been done for the current QCA packages focused on the automated detection of the borders of the vessel in order to achieve a robust and reproducible measurement. Nevertheless there are some difficulties that still have to be overcome in order to achieve a robust tool that works with all kind of images in a reproducible way. For example there is always a trade-off that has to be made between the smoothness of the contour and the ability to detect complex lesions. A smooth contour is more robust with respect to noise but cannot follow complex stenoses, whereas a contour with more freedom can detect the irregular lesions but also tends to be influenced by the noise in the image.

In this chapter, an overview will be given of the work that has been done in the field of contour detection approaches for QCA applications, which will point out the advantages and disadvantages of these approaches.

2.2 Methods

In general, several mathematical algorithms have been commonly used for contour detection purposes, and a number of them have already been tried for QCA applications. The algorithms are grouped by category and discussed below.

2.2.1 Thresholding

One of the most straight-forward approaches is a simple thresholding or region growing. These approaches have proven to be not very suitable for contour detection in vascular X-ray angiograms since they are quite coarse, (no sub-pixel accuracy) and require a fixed threshold as input, which is very difficult or even impossible to choose in X-ray images.

2.2.2 Edge detection and grouping

A large category of contour detection algorithms is based on the principle of edge detection and grouping of the candidate edge points. A number of these approaches are used widely in the QCA field and are discussed below.

Minimal Cost Algorithm (MCA)

This contour detection method consists of a derivative approach in combination with dynamic programming. This approach is present in the existing version of the QAngioXA package. The basic derivative approaches are based mainly on a combination of the first and the second derivative of the image intensity function [53, 54, 55, 56]. Edge-points can be localized by finding the extrema of the first order derivative or by finding the maxima of the second order derivative. Due to uncertainty in the images, for example due to the noise of the imaging system or the unknown shape and orientation of the vessel, the first order derivative tends to find edges inside the vessel, whereas the second order derivative is more likely to find edges outside the vessel area. In order to correct for these systematic errors, a weighted average of the localization using the first and second order derivatives is calculated to give the best estimation of the edge localization. Nevertheless, tuning the algorithm by finding the optimal weights is certainly not trivial and the approach is still quite sensitive to the noise in the image [57].

In the MCA method, this problem of uncertainty in edge location and direction is solved by the dynamic programming technique [54, 55, 56]. This approach mainly consists of using an estimate of the vessel's centerline to construct scanlines perpendicular to it. Along the scanlines the image is resampled into a matrix in which the weighted sum of the first and second order derivatives determines the local cost. The dynamic programming technique minimizes the costs of a path through the matrix. This minimum cost path is warped back onto the image as the resulting contour. This approach that will result in a continuous path, will work well under the condition that it is a normal vessel whose contours are relatively smooth, see Fig. 2.1. The overall accuracy that can be achieved is 0.001 mm and the overall precision in this case is 0.096 mm, measured with plexiglass phantoms of varying diameter. On the other hand, applying this technique to a complex lesion leads to incorrect contours because of the continuity of the algorithm and the fact that intercepting scanlines in sharp corners can cause incorrect contours, because the undersampling on the outside can miss edges and the oversampling on the inside can produce misleading edges.

Furthermore the results of the algorithm depend strongly on the positions of the start- and endpoints that are defined by the user, since not only the position of the pathline, but also its length determines the positioning of the scanlines and therefore the resampling of the image. Therefore, the contours cannot be found in a totally reproducible way.

Another problem that occurs using this approach is the overestimation of the diameter of small vessels. A postprocessing method is needed to correct for this imperfection, but this does not take into account the different edge profiles that are present at small vessel boundaries compared to the ones at large vessel boundaries [58, 59, 60]. When the correct edge profile had been taken into account, the boundary of these small vessels would be found with higher accuracy.

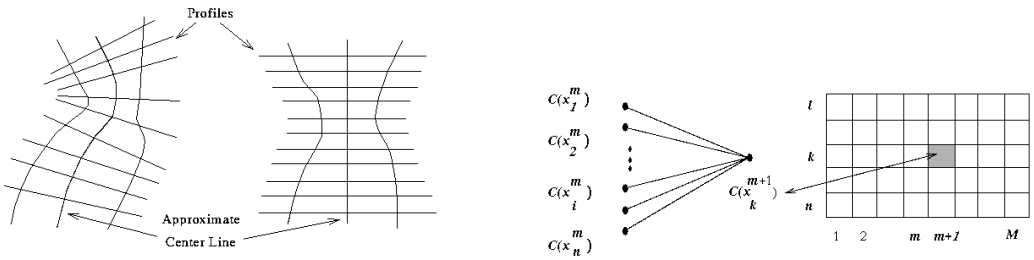


Figure 2.1: MinCost Algorithm: a) Resampling and b) Dynamic Programming

Finally, the approach is solely based on edge information and does not take the grey value itself into account. This means that the algorithm does not have knowledge about the intensity in the background, which can cause the algorithm to lock onto the wrong contour, for example the catheter inside the vessel.

Gradient Field Transform

As improvement of the mincost approach, the Gradient Field Transform (GFT) was developed [54, 50] as well as the Sequential Edge Detection (SED) algorithm [56]. These algorithms are based on the same approach, i.e. a detected centerline is used to determine scanlines along which the image is resampled. In this matrix the possible derivative based edge points are given cost values associated with the edge strength as well as the edge direction, see Fig. 2.2. Minimum cost approaches are subsequently used to find a path through the possible edge points which results in the initial edges. Next, these edges are used to achieve a better approximation of the vessel centerline which is very important in order to achieve a finer edge determination.

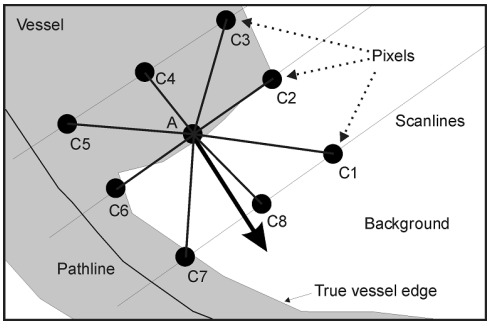


Figure 2.2: The principles of the GFT (figure from Zwet et al. [54])

Using the same plexiglass phantoms of varying diameter, the overall accuracy was found to be 0.004 mm and the overall precision 0.114 mm. The advantage of this algorithm over the previously discussed mincost approach, is that the directional information of the edges is taken into account in the cost function which leads to a more accurate determination of the edge

location. Furthermore, the algorithms are not restricted to only one single edge point on each scanline, which results in an ability to follow more complex lesion morphology.

However, the model that is used for the detection of the initial edges has a big influence on the detected contours. In case of irregular lesions, the model has to be smoothed heavily and resampled uniformly in order for the scanlines not to intersect. This causes the approach to perform worse in case of sharp edges and the calculation of the vessel diameter will be less accurate.

Just as the mincost algorithm, this approach also depends strongly on the position of the start- and endpoint. Therefore, the contours cannot be found in a very reproducible way, when analyzing an image repetitively. The problem of overestimation of the diameter of small vessels that is present using the mincost approach is also a part of this approach, since the edge profile is not adjusted for the diameter of the vessel. To improve the performance of these above mentioned edge detection based methods, the matched filters estimations have been developed. Van der Zwet and Nettesheim described a method to derive an optimal filter to detect the edges of coronary arteries [60]. This method takes into account the point-spread function of the cardiovascular X-ray system and derives an optimal filter to detect the edge profile, associated with the given diameter. It shows that the systematic errors are close to zero and the standard deviation is in the order of 0.02 mm. Similar research has been carried out by Jalali et al. [61] where they try to find an approximation of the edge profile (in this case without additional knowledge about the transfer function of the imaging system) and derive an optimal filter to detect the estimated edge-profile. Miles et al. [59] derive a matched filter assuming that the vessel has a blurred half elliptical profile.

One problem with this approach is that the edge profile is not antisymmetric (as assumed by Petrou [62], an extended version of Canny's edge detector [63]) and thus the profile of the optimal detector is not symmetric. This implies that it is not simple to extend the 1-dimensional profile to a 2-dimensional one. This is a problem that has to be solved in order to get rid of the scanlines and use edge detectors that can detect edges in any orientation.

Morphological Filtering

Another approach, that still uses the principle of edge detection and grouping, is the morphological filtering [64]. This approach is quite similar to the mincost approach in the sense that it uses image resampling and dynamic programming techniques to obtain the vessel contours. The difference is that the cost function is now determined by morphological instead of derivative based edge detection operators, for example grey value erosions and dilations.

A number of limitations characterize this approach. The analyzed segment should not contain bifurcations, no other vessels should be in the neighborhood and since the scanlines should be perpendicular to the vessel, it has to be more or less straight. The algorithm does not take into account the width and the orientation of the vessel, which generally leads to inferior results.

2.2.3 Model-based

Another category of algorithms are the model-based approaches. These methods try to make a model of the total imaging system, background, arteries, noise [57]. This is matched to the

image intensities and the parameters of the model are estimated using a mean square error method. This method needs a joint optimization process for the combination of parameters, which are subsequently used for the estimation of the vessel statistics. This method has a few disadvantages, such as the simplicity of the model that is used, the processing time of the algorithm and the dependency on the detected vessel centerline. Moreover, in case of a stenosis in the vessel that may perpendicularly align with the centerline, more than one edgepoint may exist, which cannot be detected by this approach.

2.2.4 Active contours

Active contours (snakes) [65, 66, 67, 68, 69] form another group of contour detection algorithms that have been used for the detection of vessel borders. Snakes are parametric curves that deform under the influence of internal and external forces to find the object contour. The internal forces are a measure for the degree of deformation of the spline, whereas the external forces are determined usually by some kind of edge detection method. Klein et al. used a deformable spline model to detect the coronary artery borders [70, 71]. In small diameter measurements, an accuracy of -0.19 pixels and a precision of 0.53 pixels were obtained.

A big advantage of this method is its ability to create a smooth, continuous contour, even through areas where there is very little edge information, for example at the position of a side-branch. However, this ability also results is difficulties when trying to follow complex lesions. The smoothness of the model will cause the algorithm to underestimate the severity of very short stenoses simply because it cannot make a sharp turn. The initialization of the model can have a big influence on the final result of the segmentation. The minimum that is found by the algorithm is not necessarily the global minimum.

As an improvement to the regular snake algorithm, a new approach was developed, the gradient vector flow snake, that uses a gradient vector field (GVF) as external force for the active contour model [72, 73]. This approach is less sensitive to the initialization. It is designed to find the global maximum in all situations and not to stop in a local maximum. Furthermore, this type of snake is able to follow strange morphological structures such as convex curves which is virtually impossible with a regular snake. A disadvantage of using this method is that a closed contour must be produced and that the algorithm cannot adjust the edge profile according to the diameter of the vessel since the vector field is already made before the model is matched onto the image. This algorithm has been tested, but never validated for vascular images.

Another extension to the normal active contour models is the Topology adaptive snake, T-snake [74]. The advantage of this approach over the regular snake models is its ability to change topology. The snake can split into two parts, join another snake, create a hole and so on. It may be used for an initialization with multiple pieces (one piece around the startpoint and one around the endpoint, for example). However, this freedom can also cause the algorithm to find non-continuous contours.

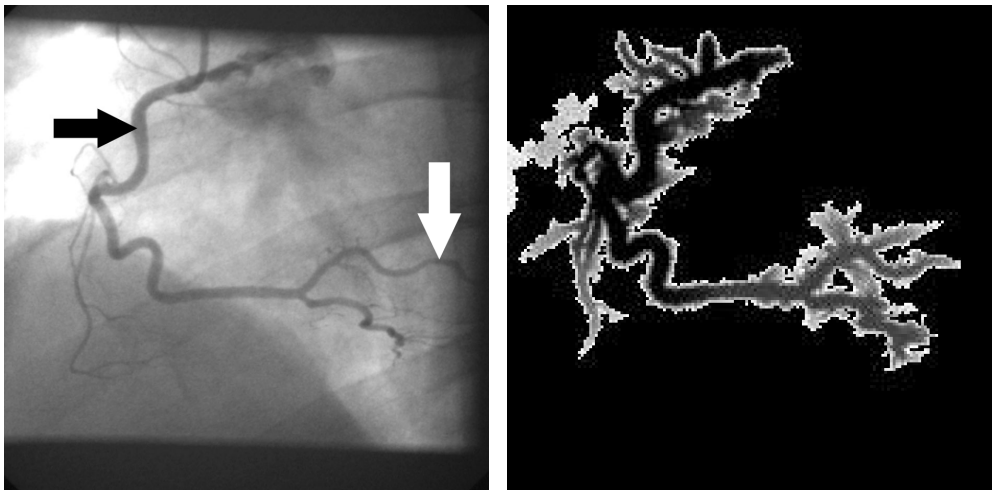
Another approach, an attractable snake that is based on the greedy algorithm for contour extraction [75] has been designed to make the active contour model more robust. An overall optimal edge detector is used to avoid local minima and to make the approach less dependent on the initialization. An adaptive interpolation scheme is used to sense the details of object shapes, also convex shapes. This approach also requires the definition of an edge profile before

the algorithm starts, which makes it impossible to adjust this profile according to the estimated diameter of a vessel.

2.2.5 Level set

Another type of algorithms is the level set based approaches. Level sets are geometric models that can segment an image into regions with smooth interiors [76, 77, 78, 79]. The computation of level sets however is generally a costly operation and it remains difficult to achieve consistent boundaries in noisy images because it is not bound to a certain topology. The fastmarching level set segmentation, also called wavefront propagation [80, 81], is a very fast method to calculate the position of monotonically advancing fronts. This method initiates a wavefront in the image and progresses with a speed dependent on the grey-value of the pixels. When it is stopped at the correct moment, a segmentation of the vessel segment [82, 83] can be obtained by taking the envelope of the area that the wave has reached as the resulted contours.

Since the algorithm is very robust and does not depend on scanlines and image resampling, the detected contours are stable and robust. The problem of under- and oversampling in sharp corners is eliminated since no scanlines are used. The algorithm is able to follow structures with a complex morphology and also global structures with the use of the different parameters. However, the issue of when to stop the algorithm, which is the most important part of the segmentation, is not trivial (see Fig. 2.3). This may cause an inaccuracy in the detected contours. Furthermore, there is the problem of leaking, when another vessel or background structure is projected on top of the vessel of interest.



(a) (b)

Figure 2.3: Wavefront Propagation: a) Initial image with startpoint (black) and endpoint (white) and b) Resulting image after propagation (figure from Janssen et al. [84])

2.2.6 Watersheds

Very common in image processing is the method that consists of using watersheds [85] to divide the image in separate regions, which coincide with the different objects in the image. Although the watershed transformation is a powerful method, the main problem using this algorithm for edge detection is that it depends strongly on the gradient operator that has been used before applying the watershed transform. The scale of the gradient operator determines the amount of edges that are found and also the size of these edges. Although more research has been performed to solve this problem [86], noise still remains a major problem.

2.2.7 Markov Random Fields

The next method, Markov Random Fields (MRF) [87], is a region-based approach that tries to group pixels whose intensities are statistically similar, making it more robust with respect to localized image noise compared to using the edge-information. However, when there's a strong inhomogeneity present in the contrast filling of the arteries, the MRF has great difficulties separating the foreground from the background and it often results in small holes/islands inside the segmented object.

2.2.8 Graph Cuts

Another technique that is used for segmentation problems nowadays is Graph Cuts [88, 89, 90]. This approach uses graph theory to segment an image into different regions by maximizing the flow through a graph that is representing the image. This is done by defining a source and a sink in the image (foreground and background) and removing the minimal edges, the edges that connect pixels with large differences in intensity. In this way the optimal cut to separate the foreground from the background is found. The results however are strongly dependent on the initialization and the algorithm has difficulties detecting the edges when there is only little contrast in the image.

2.2.9 Statistical models

Other sophisticated algorithms have been developed like Active Shape Models (ASM) and Active Appearance Models (AAM) [91], both statistical models trained from examples and describing the object boundaries in terms of variations to the mean. These algorithms use high-level knowledge about the object to constrain the deformations of the model, which makes them robust for image interpretation. These methods have proven their value in other fields of medical image processing, such as magnetic resonance imaging [92, 93, 94, 95] but are not useful in X-ray applications because of the large variation in images, in vessels shape and in background structures that are present in this field.

2.3 Discussion

In order to become widely applicable in practical use, a QCA contour detection approach must satisfy a number of criteria. The method must be robust towards the selection of start- and

endpoints and it must be able to achieve reproducible measurements in the sense that the same contours must be found, when analyzing the same segment repetitively. Also, it must be minimally dependent on the size of the image intensifier that is used. Furthermore it must not suffer from a systematic over- or underestimation, neither for small, nor for large vessels. The approach should have enough freedom to follow complex lesions, but at the same time be smooth enough to be relatively insensitive to the noise in the image and be able to cross side-branches. Finally it must be fast enough for online applications.

Since there can be a large variety in the morphology of the target vessels, as well as in the background, especially in images of peripheral arteries, the model based contour detection techniques are less suitable for the QCA/QVA applications. Most of the commonly used contour detection methods are in the category of "edge detection and grouping", which is understandable since the edge information is the only reliable contour information in the images.

However, the introduction of scanlines for resampling causes variation in the detected contours when the start- and endpoints are shifted only slightly. Furthermore, scanline-based methods suffer from oversampling and undersampling in sharp corners, which can lead to failures in those areas. To avoid these problems, a global filtering method is needed that can detect edges in any direction to identify candidate edge-points and an algorithm that can connect the most probable candidate edge-points forming the resulting contour. For the grouping of these edge-points, the wavefront propagation is a good method to be used, since it has proven its reproducibility and speed in the pathline tracing algorithm 'Wavepath'. When the wavefront propagation is given the edge information as input instead of the grey-value, it is able to follow edges in any direction. However, the requirement for smoothness, for example in order to be able to cross side-branches, requires an additional solution. The accuracy of the detected contours relies mostly on the accuracy of the edge-detection filter that is used. To ensure maximum accuracy, the optimal edge-profile can be used as described by the matched filter from Van der Zwet. This approach computes the optimal filter as a function of the vessel diameter, which causes the need for a two-stage approach, with the first stage a detection of preliminary contours and an initial estimate of the diameter of the vessel, and a second stage to apply the optimal filter and fine-tune the contours.

CHAPTER 3

A novel approach for the detection of pathlines in X-Ray angiograms: the wavefront propagation algorithm

This chapter was published as:

Janssen JP, Koning G, de Koning PJH, Tuinenburg JC, Reiber JHC.
A novel approach for the detection of pathlines in X-ray angiograms:
the wavefront propagation algorithm.
Int J Cardiovasc Imaging. 2002;18(5):317-324

Abstract

This article presents a new pathline approach, based on the wavefront propagation principle, and developed in order to reduce the variability in the outcomes of the quantitative coronary artery analysis. This novel approach, called wavepath, reduces the influence of the user-defined start-and endpoints of the vessel segment and is therefore more robust and improves the reproducibility of the lesion quantification substantially. The validation study shows that the wavepath method is totally constant in the middle part of the pathline, even when using the method for constructing a bifurcation or sidebranch pathline. Furthermore, the number of corrections needed to guide the wavepath through the correct vessel is decreased from an average of 0.44 corrections per pathline to an average of 0.12 per pathline. Therefore, it can be concluded that the wavepath algorithm improves the overall analysis substantially.

3.1 Introduction

Quantitative coronary arteriography (QCA) has been widely accepted as the method for the accurate assessment of the morphology of coronary vessels and the location and severity of coronary obstructions from X-Ray arteriograms [36]. The accurate derivation of clinically relevant variables, such as the obstruction diameter, interpolated reference diameter, percent diameter stenosis and plaque area, not only facilitates the objective evaluation of clinical research trials, but has also proved to be useful for the selection of the appropriate recanalization devices in interventional cardiology [37, 96]. Over the years, we have developed analytical software packages for both cinefilm [38] and on-line digital applications [39]. The high accuracy and precision of these packages have been established and described elsewhere [36, 37, 96, 38, 39].

In spite of the demonstrated accuracy and precision of the packages, there is still some variability demonstrated in the outcomes of the coronary lesion quantification parameters, when analyzing the same segment repeatedly. This variability is caused by different start-and endpoint positioning and different corrections of the detected contours. The analysis results are computed on the basis of the arterial contours of the segment under study, which have been detected automatically using a method based on the minimal cost algorithm [40] and/or the gradient field transform [50]. These methods require a pathline as input [97], which is a rough approximation of the centerline of the vessel segment to be analyzed. The image is resampled along scanlines that are perpendicular to and evenly distributed along the pathline. The resulting contours depend therefore on the resampling of the image data along the scanlines and thus on the pathline that is found.

The pathline itself depends on the start-and endpoints that are defined by the user. Therefore, a small variation in the start-and endpoints may result in a significant variation in the coronary lesion parameters due to the pathline algorithm. In an attempt to minimize the influence of the user-defined start-and endpoints of the vessel segment, we have developed a new pathline algorithm, based on a wavefront propagation. This method, that is called the wavepath, is (within a certain range) independent of the start-and endpoint positions and consequently improves the reproducibility of the lesion quantification sub-stantially.

More research has been performed by other people that also aimed at reducing the variability in QCA measurements, introduced by the analyst. One approach aimed at detecting the entire coronary tree using a skeletonization process [98] and another approach used the wavefront propagation in order to perform a coronary segmentation (contour detection) without the use of a pathline [82]. We chose to use the wavefront propagation for the detection of the pathline of the vessels. In our opinion the wavefront is not precise enough to perform a contour detection.

In this paper, we will first describe the new pathline method and its validation and subsequently compare the results with the ones obtained with the existing pathline method.

3.2 Methods

To be applicable in the environment of the QCA system, the algorithm must satisfy the following criteria: (1) the resulting pathline must remain within the vessel boundaries over its entire length; (2) its course must be insensitive to small variations in the user-defined start-and endpoints,

which have to be located inside the artery under study; (3) it should be fast enough for on-line applications; and, (4) it should also be suitable for functioning as a model for the contour detection of more complex morphology, such as a bifurcation or sidebranch. The new algorithm that we have developed is based on the wavefront propagation principle [80].

A wavefront is initiated in the image and expands using a local speed that depends on the local in-tensity-value of the image. A parallel can be drawn between the algorithm and an actual surface wave, that is induced by a stone that is thrown into water. If the substance in which the wave propagates (in this case water) is homogeneous, the wave will expand uniformly in all directions (the expanding circles in the water). On the other hand, if the substance is inhomogeneous, the resistance is not constant and therefore the speed of the wave will differ with the location. It is analogous to the stone that is thrown into a fluid in which the viscosity would vary significantly with the position. In such a case, the velocity of a traveling wave in the material varies locally and the wave expands nonuniformly in the material.

3.2.1 Preprocessing

Our approach of pathline detection consists of the following steps: (1) an appropriate preprocessing that consists of a smart subsampling [97] and a filtering to reduce the influence of background shading; and (2) the wavefront algorithm. The nonlinear subsampling is applied mainly to decrease the processing time of the algorithm and results in an image that is three times smaller in its dimensions. A grey level morphology filter is applied in this low-resolution image. The filter enhances the interesting structures (the coronary arteries) that are present in the image and reduces the shading in the background caused by overlaying structures. Therefore, it provides an appropriate input for the wavefront algorithm.

3.2.2 Wavefront propagation

The purpose of the wavefront algorithm is to find the fastest path from the user-defined startpoint to the endpoint. In the filtered low-resolution image an eight-connected wave is initialized from the startpoint, after defining a speedfunction for the wave, which connects to every possible grey level in the image a value that represents the velocity of the wavefront (e.g. a step function, a ramp function or a sigmoid). Starting from the single start-point, the algorithm calculates the arrival times of the wave for all neighbors according to the associated speed. The neighbors are added to a collection of points that is called the wavefront. The point with the lowest arrival time in the wavefront is set 'accepted' since there is no faster way to reach that point. This point is removed from the wavefront and its neighbors are added to the wavefront after their arrival times have been calculated. For a point that already has been assigned a certain arrival time, this time is updated when the new arrival time is earlier than the previous one. This procedure is repeated recursively until the endpoint has been reached, resulting in an image that represents the local arrival times of the wave, as can be seen in Figure 3.1, showing the initial image and the result of the propagation.

After the wave has been propagated, the backtrack algorithm finds the fastest way back through the wave using the arrival time image, resulting in a low-resolution pathline that is subsequently transformed back into high-resolution and smoothed to obtain the final resulting

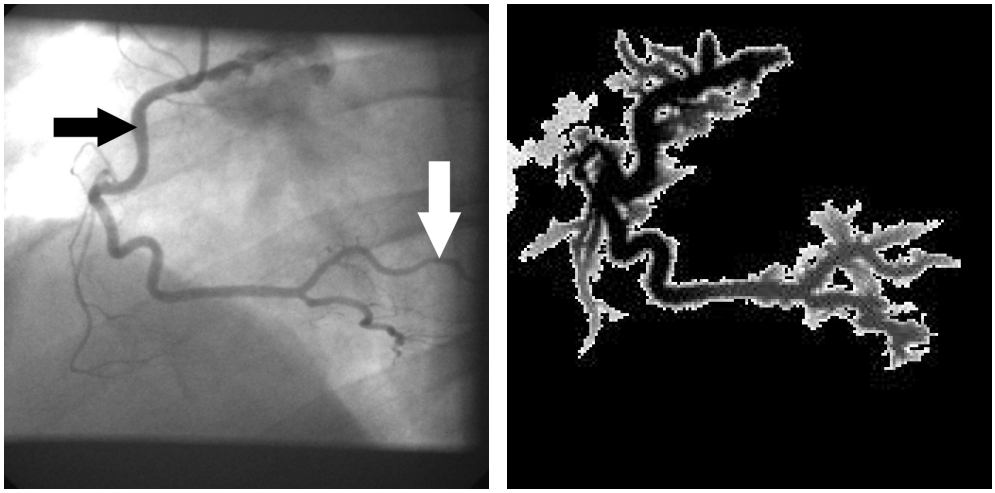
pathline. In some cases the pathline follows an erroneous path and must therefore be rejected, for example when two arteries overlap. The user has the option to add an additional point to force the path through a certain part of the image. In this case, two waves are initiated subsequently. The first one travels from the startpoint to the additional point and the second wave is sent from the endpoint back to the additional point. These partial path-lines are then combined into one final pathline.

Another option has been developed, denoted the 'live-wire'. This principle has been used earlier to detect object boundaries [99]. In this case the wavefront propagation algorithm proceeds until it has processed the entire image. In that case one is able to move the endpoint over the entire image and immediately find the pathline between the fixed startpoint and the variable endpoint using the (very fast) backtrack algorithm.

3.2.3 Bifurcation and sidebranch

In the analysis of an artery, either being a coronary or a peripheral artery, three different situations can be distinguished that require different protocols. The first case is the analysis of a single segment that is supported by the known quantitative coronary artery packages. The second case is the analysis and quantification of a vessel bifurcation, such as occurs in a carotid artery or major vessels in the coronary tree, and the third case is the sidebranch analysis, which applies to e.g. renal artery analysis, but also to a diagonal branch of an LAD artery. The first case requires just a single pathline from start-to endpoint. The protocol for constructing this pathline was discussed above. The other two situations require a more sophisticated pathline in order to appropriately detect all arterial boundaries. In the case of a bifurcation, we need the pathline algorithm to provide an initial model for the detection of three contours. To achieve this, one proximal point and two distal points are needed, one in each branch of the bifurcation (see Figure 3.2). Basically, we are constructing two different pathlines to connect those three points, starting in the proximal point and ending in each distal point. Since the startpoint for both waves is identical, we can use solely one single wave and let it propagate until it has reached both endpoints. Subsequently the backtracking from both endpoints back to the startpoint is carried out.

The procedure for constructing a pathline in the situation of a sidebranch is slightly different from the case of the bifurcation. In this case the pathline algorithm has to provide a model for two contours. The three points that are needed in this case consist of two different proximal points and one distal point (see Figure 3.3). This would mean that two different waves are needed to detect the two pathlines. Since there is no difference in the resulting path between sending a wave from A to B and sending a wave from B to A, we can transform this protocol into the protocol of the bifurcation. This means that one single wave is sent out from the distal point to the two proximal points. Again these two pathlines are combined into one final pathline. This approach of transforming the side-branch pathline into a bifurcation pathline decreases the processing time of the algorithm by almost 50%.



(a) (b)

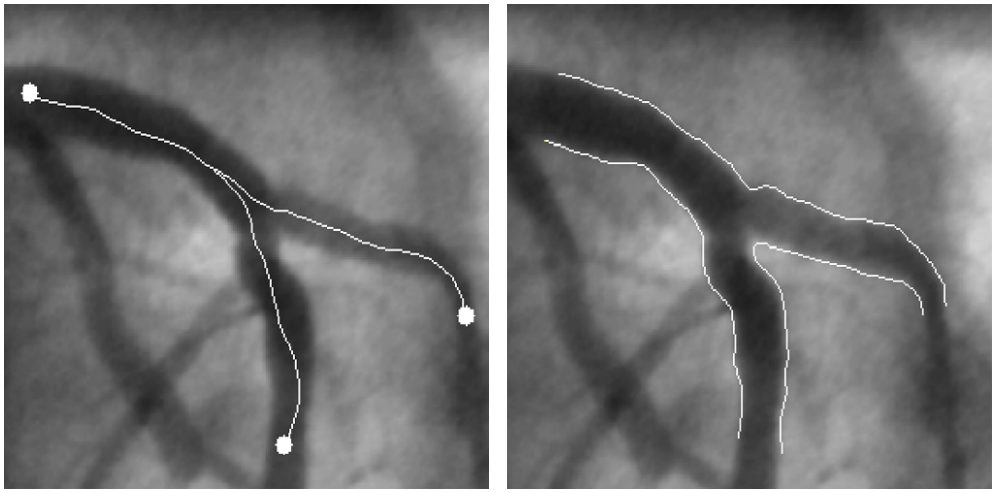
Figure 3.1: Wavefront Propagation: a) Initial image with startpoint (black) and endpoint (white) and b) Resulting image after propagation.

3.2.4 Validation

Since the goal of this research is to achieve a reliable and reproducible method for pathline detection, the performance of our wavepath algorithm can be determined relative to the existing pathline, by moving the start-and endpoints in certain areas and calculating the variabilities in the pathline positions. Obviously the number of corrections needed for the pathline to be acceptable (i.e. it must lie within the assumed arterial bounds over its entire length) is also an important criterion for the validation procedure. In order to measure the local variability of the pathline we varied the start-and endpoints in a certain window around the originally manually defined points and calculated a pathline for every different combination of points. To this end, a 5 x 5 matrix of points with a subsequent distance of three pixels between the points, was used, resulting in 625 pathlines between the 25 start-and 25 endpoints.

In order to compute the variations between the pathlines, the straight line between the middle of the start-matrix and end-matrix was taken and 50equidistant scanlines perpendicular to this line were constructed (Figure 3.4). For all pathlines the intersection points with each of the scanlines are determined and the distances of the intersection points to the straight line are calculated. This allows the calculation of an average distance (which is not relevant for the comparison) and the standard deviation of these distances for each individual scanline. This standard deviation is a measure for the local variability of the pathline. The same method was used to calculate the standard deviation for the existing pathline algorithm.

For the validation experiment a set of 49 coronary segments was used, selected from 33 digital coronary arteriograms (512^2 x 8 bits) from the Philips Digital Cardiac Imaging system. The selection was performed such that the resulting set of segments was as diverse as possible, containing long and short, obstructed and nonobstructed, right and left coronary arterial



(a) (b)

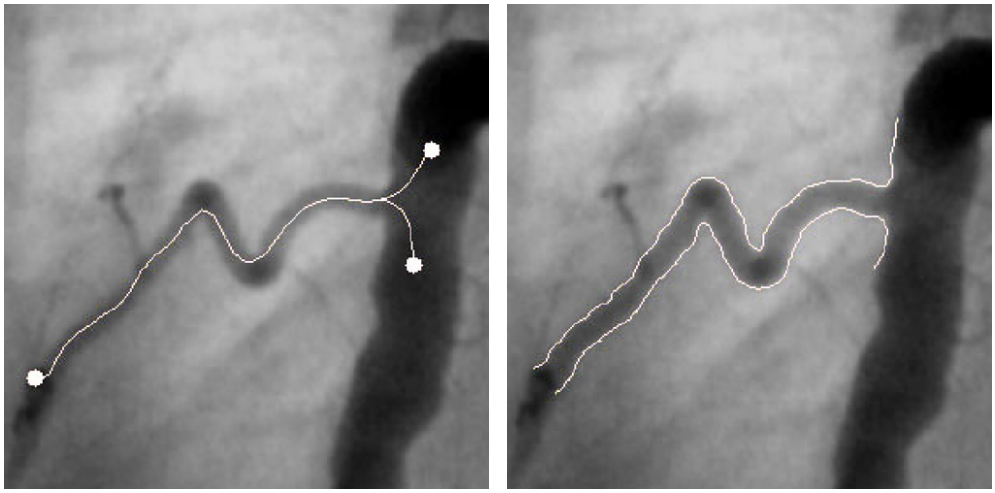
Figure 3.2: Bifurcation analysis: a) Pathlines for bifurcation and b) Contours for bifurcation.

segments, with and also without overlap of other arteries or anatomic structures. As a result, for each segment the 625 pathlines using both our new and the existing pathline method were computed and analyzed. In case a number of pathlines did not satisfy the criterion of lying within the artery over its entire length, the incorrect (unaccepted) pathlines were selected and all selected pathlines were provided with one single additional point simultaneously. All the selected pathlines were then computed again with the use of the additional point.

This procedure of correcting the incorrect pathlines was repeated until all pathlines remained entirely within the artery. The standard deviation per scanline and the number of corrections for the accepted pathlines were calculated, for the new wavefront algorithm as well as the existing path-line method.

3.2.5 Bifurcation and sidebranch validation

The second validation experiment concerned the bifurcation and sidebranch pathline. Since the existing pathline method can only calculate one single pathline, it is not possible to make a comparison between the old and the new method. Obviously, the criteria for the bifurcation and sidebranch versions of our new algorithm are identical to those for the 'normal' case we discussed above: the variations in the pathline as a result of a variation in the proximal or distal points as well as the number of corrections to make the pathline acceptable (entirely within the vessel) have to be minimized. In case of the bifurcation pathline, one is dealing with one start-and two endpoints, which were varied in a 3 x 3 matrix with a mutual distance of 5 pixels, resulting in 729 pathlines. Each pathline can be divided into three different parts: a common (proximal) part and two separate distal parts. In order to calculate the variation of the pathlines, the location of the separation point of the first pathline is detected and from this point three lines to the proximal and distal points with 25 perpendicular scanlines are drawn (Figure 3.5). The calculation of the



(a) (b)

Figure 3.3: Sidebranch analysis: a) Pathlines for sidebranch and b) Contours for sidebranch.

variations per scanline is similar to the procedure described in the previous section.

Note that since the separation point of the first pathline that is computed, is used to calculate the variations, a possible dislocation of the separation point between different pathlines would result in a local variation at that point that is not equal to zero. The validation study was carried out on 43 coronary segments which were derived from 38 different digital arteriograms.

The sidebranch pathline is very similar to the bifurcation pathline, with the exception that there are two startpoints and one single endpoint. Therefore, the bifurcation validation method was used for the validation of this pathline. Since the two proximal parts of the pathline are usually relatively short, only 10scanlines for these parts were used to assess the variation, in stead of 25, used in the bifurcation analysis. The results of the validation procedure were based on 43 segments derived from 37 digital arterial images.

3.3 Results

As indicated before, there are situations where correction points had to be defined, before the pathline could be accepted (i.e. remains entirely within the artery). The average number of corrections needed in each situation is shown in Table 3.1. As can be seen, our wavepath approach requires much less corrections than the existing pathline method. Looking at the distribution of these corrections as shown in Table 3.2, it is clear that in contrast to the existing method, our new method requires at the most one single correction to guide it through the correct artery.

The results of the single pathline detection with both methods, averaged over all 49 segments are presented in Figure 3.6. It is clear, that the existing pathline method shows variations over its entire length, due to the fact that small changes in start-and endpoints lead to different pathlines. The new method, however, shows variability only at the start and end of the pathline, whereas the essential middle part of each pathline (approximately 72% of its length) is exactly

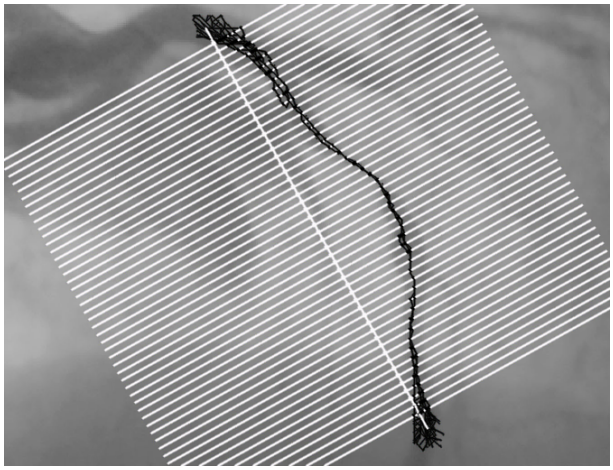


Figure 3.4: Scanlines for calculation of the local variation in pathlines

the same for all 625 path-lines. Figure 3.7 shows the results of the local variation calculation for the wavepath algorithm in case of a bifurcation. Over all 43 segment analyzed, the values were averaged. Again, it can be seen that the pathlines show some variability at the start and end, whereas the central parts of all 729 pathlines are exactly identical. Note that the separation point is at the exact same location for all pathlines in each segment!

The sidebranch results are presented in Figure 3.8. Again, in the middle part of the pathlines the variation is zero and only at the beginning and end, a certain amount of variation can be seen. Note that again the separation point is at the exact same location for all pathlines in each segment!

Table 3.1: Average number of corrections per pathline for all pathline methods.

	number of corrections per pathline
Existing pathline	0.4426
Wavepath (straight segments)	0.1224
Wavepath (Bifurcation)	0.1783
Wavepath (Sidebranch)	0.1163

3.4 Discussion

In this paper we have presented a novel approach for the (semi-)automatic detection of arterial pathlines in digital arteriograms, that is also suitable for constructing a bifurcation or side-branch pathline. The main goal of this new development was to gain a better reproducibility, as that also affects the reproducibility of the entire lesion quantification process. In addition, the robustness of the algorithm is also important, which implies the reduction of the number of user corrections needed for the pathline to satisfy all criterions. The validation study shows that the

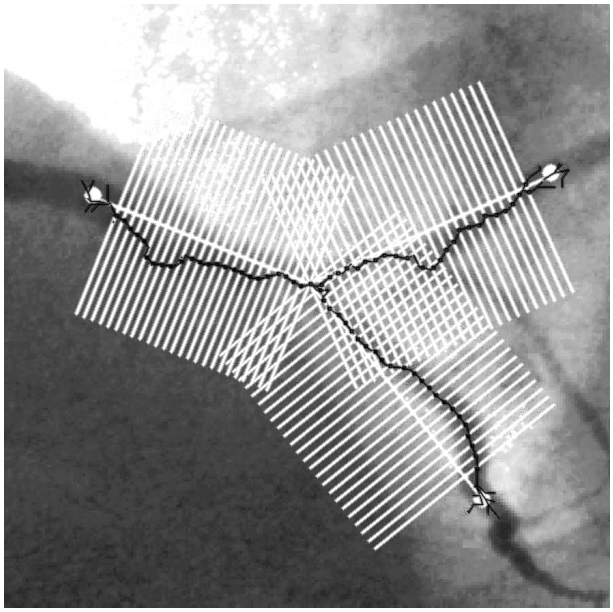


Figure 3.5: Scanlines for calculation of the local variation in bifurcation pathlines

Table 3.2: Distribution of corrections for each of the pathline methods for the total number of 30625 (31347 for the bifurcation and side-branch) analyses carried out.

	number of corrections per segment								
	0	1	2	3	4	5	6	7	8
Existing pathline	22721	4096	1258	754	333	131	5	1	1
Wavepath (straight segments)	26875	3750	0	0	0	0	0	0	0
Wavepath (Bifurcation)	25758	5589	0	0	0	0	0	0	0
Wavepath (Sidebranch)	27702	3645	0	0	0	0	0	0	0

new algorithm meets these two criteria. The traced pathline is for the larger part independent of changes in start-and endpoint, except for the parts that are very near to the start-and endpoint, obviously. This means that we can achieve a constant pathline over a certain distance by setting the start-and endpoints a certain distance outside that range. It was also demonstrated that our new method is appropriate for detecting a bifurcation or sidebranch pathline. This opens the way for the quantification of lesions located within a bifurcation or sidebranch. Concerning the robustness, it is evident that the number of corrections needed to guide the pathline through the correct vessel is much lower than it was using the old algorithm. This means that the amount of user interaction is further minimized which benefits the reproducibility of the whole system further.

The measured values for variation of the path-lines may be not precisely correct, since the variation was assessed along a scanline perpendicular to the straight line from start-to endpoint. When the detected path is approximately parallel to the straight line, the measured variations

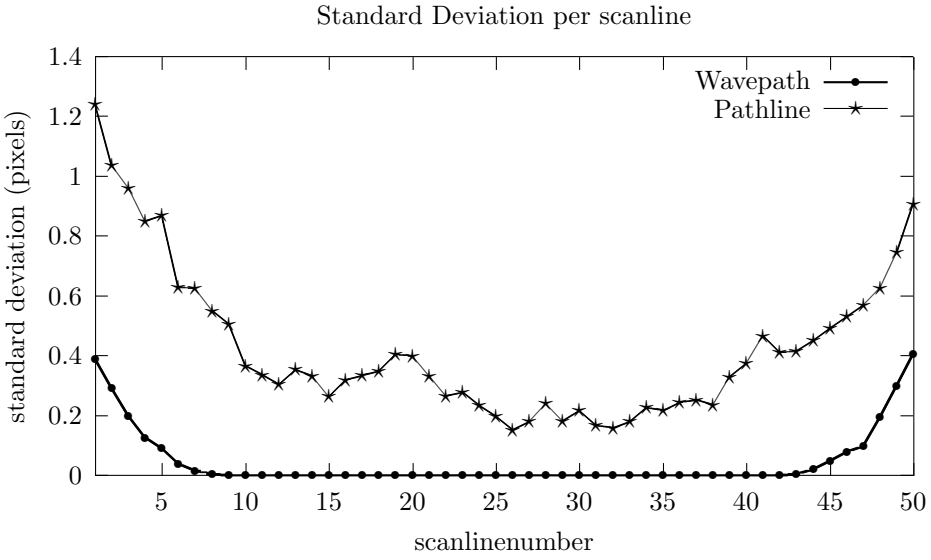


Figure 3.6: Mean local variations of the wavepath approach and the existing pathline method in single vessel segments.

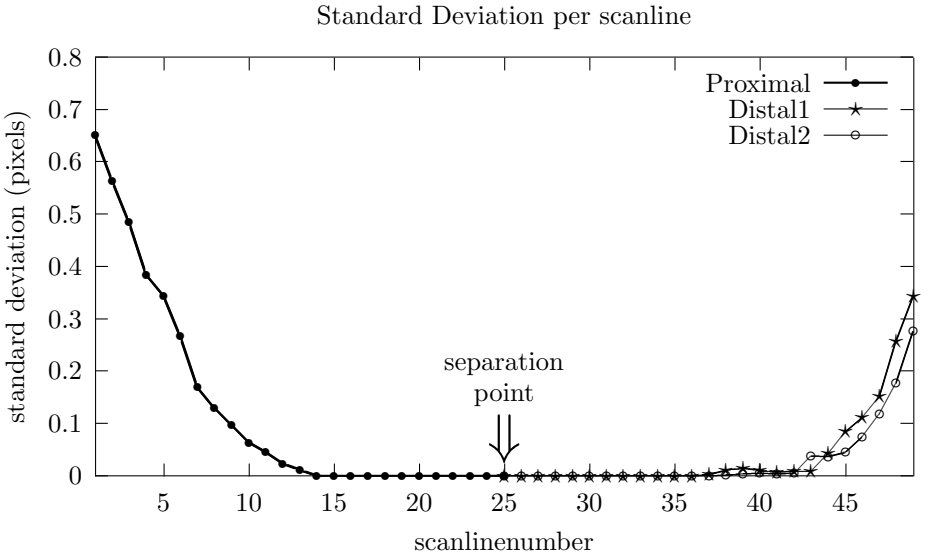


Figure 3.7: Mean local variations of the wavepath approach in the bifurcation version.

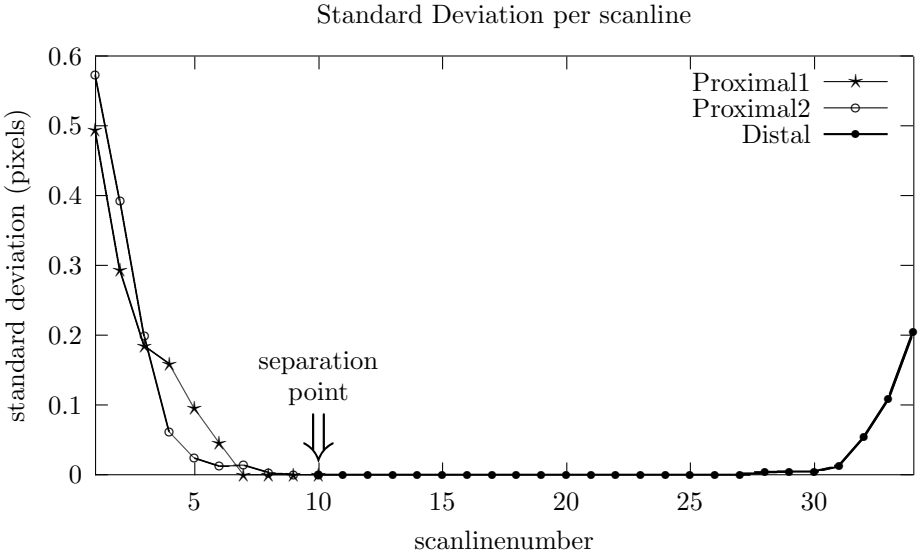


Figure 3.8: Mean local variations of the wavepath approach in the sidebranch version.

are correct. However when the found pathline is not parallel to the straight line, the variations are overestimated. Since the latter holds for mainly the end and beginning of the pathline and not for the most important intermediate part, this incorrectness is not essential for the final conclusions.

Although in the validation study, the wavepath was only tested on digital images (512^2 x 8 bits) from the Philips Digital Cardiac Imaging system in one single resolution, pilot experiments show that the principles can be generalized towards other types of images and even to other vascular applications. Minor changes in the filtering and tuning of the wavepath, make the algorithm suitable for these other applications, which will be tested in the future.

The overall goal of our research is to make the entire QCA analysis more reproducible, and the new pathline method is one part of it. That doesn't mean that a robust pathline algorithm in itself makes the total analysis more reproducible. As indicated, the image is resampled along scanlines, perpendicular to and evenly distributed along the pathline. Obviously, the total length of the path-line will change when the start-and endpoint change, in spite of the robustness of the pathline in the important area. Therefore, since the resampling of the pathline for the contour detection is dependent upon the position of the start-and endpoint as well as the length of the pathline, this last mentioned dependency must be solved as well, in order to make the entire QCA analysis more re-producible.

3.5 Conclusion

The new approach for the automated detection of pathlines (wavepath) in digital coronary arteriograms, has proven to outperform the existing pathline algorithm. Validation results of

the wavepath algorithm have demonstrated that it is very reproducible and the need for user interaction has been minimized. The algorithm is also suitable for application in bifurcation or sidebranch analysis in coronary vessels.

CHAPTER 4

Validation of a New Method for the Detection of Pathlines in Vascular X-ray Images

This chapter was published as:

Janssen JP, Koning G, de Koning PJH, Tuinenburg JC, Reiber JHC.
Validation of a new method for the detection of pathlines in vascular x-ray images.
Invest Radiol. 2004;39(9):524-530

Abstract

This article presents the validation of a new pathline approach, based on the wavefront propagation principle, on a large variety of vascular images. The purpose of the novel approach, called wavepath, was to minimize the variability of the measurements in the quantitative vascular analysis by reducing the variability that is introduced by manually placing the start and end points of the vessel segment. This results in a robust and reproducible pathline detection that is subsequently used in the analysis and lesion quantification. The validation study that was performed concerned a large variety of vessel segments and showed that the approach results in a pathline that is totally constant in its middle part. This holds not only for the straight segment version but also for the bifurcation version and ostial version of the algorithm. Moreover, the average number of additional points per pathline needed to guide the wave-path through the correct vessel is minimized to 0 for the straight segments, 0.06 for aortic bifurcations, 0.25 for carotid bifurcations, and 0.08 for the ostial segments. In conclusion, our new approach performs very well in all types of vascular x-ray images, resulting in a stable and robust pathline detection.

4.1 Introduction

Since more and more techniques have become available over the last years to treat obstructions in peripheral vessels, the need has risen to characterize and quantify these lesions from vascular x-ray arteriograms. The accurate measurement of clinically relevant parameters (obstruction diameter, obstruction length, estimated reference diameter, percentage diameter stenosis) is useful for the selection of recanalization devices that are needed in vascular interventions and for the exact evaluation of clinical research studies.

At this moment, 3 methods are available to obtain the clinical parameters from the x-ray arteriograms: The most widely used method is the visual interpretation of the images to estimate a percentage diameter stenosis. Obviously, this method is not quite accurate and highly dependent on an observer. The second method uses the peak systolic blood flow velocity, which is measured with an endovascular Doppler technique to discriminate between obstructed and nonobstructed arteries [100]. The last method uses a pressure catheter or wire to measure the pressure drop over an obstructed vessel segment. Because these last 2 methods are highly invasive, quantitative vascular analysis (QVA) of the x-ray arteriograms should be a widely applicable technique to obtain the accurate measurements that are needed for a proper planning and follow-up of an interventional procedure. In coronary angiography, such quantification tools have been used for many years. The quantitative coronary arteriography package QCA-CMS® has proven its value in the quantification of coronary artery stenoses and is widely accepted as the golden standard [37, 96, 38, 36]. In contrast to coronary arteriography, a much larger variety of images is present in general vascular applications. First of all, the vessels under study can be totally different. For example, the renal arteries, the aorta bifurcation, the iliac arteries, the femoral arteries, and the carotid arteries differ significantly in morphology and size. Second, we need different types of analyses to characterize stenoses in the different morphologies. In addition to the straight segment analysis, bifurcation and sidebranch analysis approaches are needed to measure the lesion at the exact location of a bifurcation or sidebranch, respectively. Third, there is the possibility of a subtraction. Because overlying structures in the vascular images are very common, background subtraction often is needed to perform an accurate measurement of the stenosis. This is done frequently on the x-ray acquisition console, but can also be performed afterward.

The last variety in the images concerns the method of calibration. In addition to the catheter calibration that is most common in QCA analyses, other methods are needed to calibrate objects like marker wires, coins, and centimeterrulers that are present in these images. Note that there also is a large variety in the results of the calibration (ie, the pixel size) because the field of view in vascular images depends strongly on the type of segment that is under study.

To obtain an accurate tool for quantitative vascular angiography, a first version of a QVA package was developed [101] that is able to quantify the severity of renal artery stenoses. Despite the good results that have been achieved using this newly developed tool, there are still some difficulties to overcome. One of the problems is the variability that occurs in the outcomes of the lesion quantification parameters, when analyzing the same segment repeatedly. This variability is caused by different start and end point locations of the vessel segment of interest and different user interactions to correct the detected contours. The analysis results are computed on the basis of the arterial contours of the segment, which have been detected automatically using a method based on the minimal cost algorithm [40]. This method requires a pathline as input [97], which

is a rough approximation of the centerline of the vessel segment under study. Subsequently, a resampling of the image is performed along scanlines that are perpendicular to and evenly distributed along the pathline. In this resampled image, the vessel contours are detected and therefore the contours depend strongly on the resampling process and thus on the pathline that was found. The pathline itself depends on the start and end points that are defined by the user and therefore, a small variation in these points may result in a significant variation in the stenosis quantification parameters. Another problem is the definition of a pathline in case of a sidebranch or bifurcation. Such a pathline consists actually of 2 pathlines that have one part in common.

In an attempt to overcome these problems, we have developed a new pathline algorithm based on a wavefront propagation algorithm [80]. This method, that is called the Wavepath [84], has proven to be (within a certain range) independent of the start and end point positions in QCA applications. Consequently, the reproducibility of the coronary lesion quantification was improved substantially. Also, the definition of bifurcation and sidebranch pathlines in coronary arteries has been demonstrated to be highly successful using this algorithm. In this article, the new pathline method will be described first, followed by a description of the validation procedure on the different types of vascular images, and finally the results of the validation are presented and discussed.

4.2 Materials and Methods

4.2.1 Methods

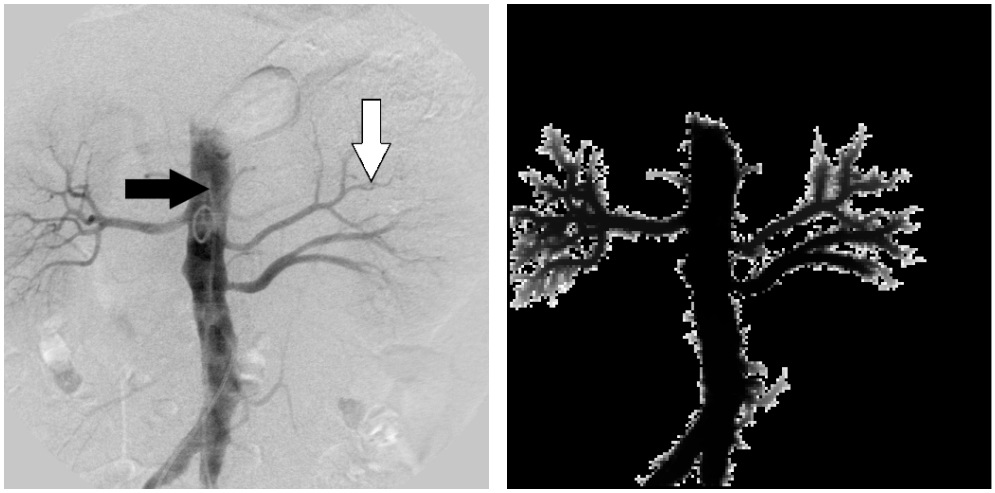
To be practically useful in vascular applications, the algorithm must satisfy the following criteria: (1) the resulting pathline must lie within the assumed vessel boundaries over the entire length of the vessel segment; (2) its trajectory must be insensitive to small variations in the user-defined start and end points, which have to be located inside the artery under study; (3) it must be fast enough for online applications; (4) the method must require no or at least very little user interaction; (5) it must be suitable as a model for the contour detection of more complex morphology, such as a bifurcation or sidebranch, which occur frequently in vascular applications.

The new algorithm we have developed is based on the wavefront propagation principle introduced by Adalsteinsson and Sethian [80]. A wavefront that uses a local speed, depending on the local intensity value of the image, is initiated in the image and propagates according to the local speed until it has reached an end criterion. The wavefront propagation algorithm can be compared with an actual surface wave. If the image is homogeneous, the wave will expand uniformly in every direction. This can be compared with a stone that is thrown into the water, which will generate expanding circles on the surface of the water. If the image is inhomogeneous, the wave will have a different speed locally, which will cause the wave to expand faster in some directions than in others. This can be compared with a stone that is thrown into a fluid, whose viscosity varies significantly from one location to another. In that case, the resistance of the fluid will vary locally and therefore the surface wave will not expand in circles, but go faster in one direction than in another.

The first step of our approach is a preprocessing of the image to achieve a better performance of the propagation. It consists of a smart subsampling [97] (with a factor of 3 for 512^2 images and

5 for 1024^2 images) and a gray-level morphology filter that is designed to enhance the interesting structures and reduce the artifacts of background shading.

The next step of the algorithm is the wavefront propagation, which finds the optimal path from the user-defined start point to the end point, using a speed function, which assigns a speed value to every possible gray level in the image. From the start point the wavefront expands eightconnected, calculating the optimal arrival times, until it has reached the user-indicated end point. The image that will remain after this propagation represents the local arrival time of the wave, as can be seen in Figure 4.1, showing the initial image as well as the resulting image after the propagation.



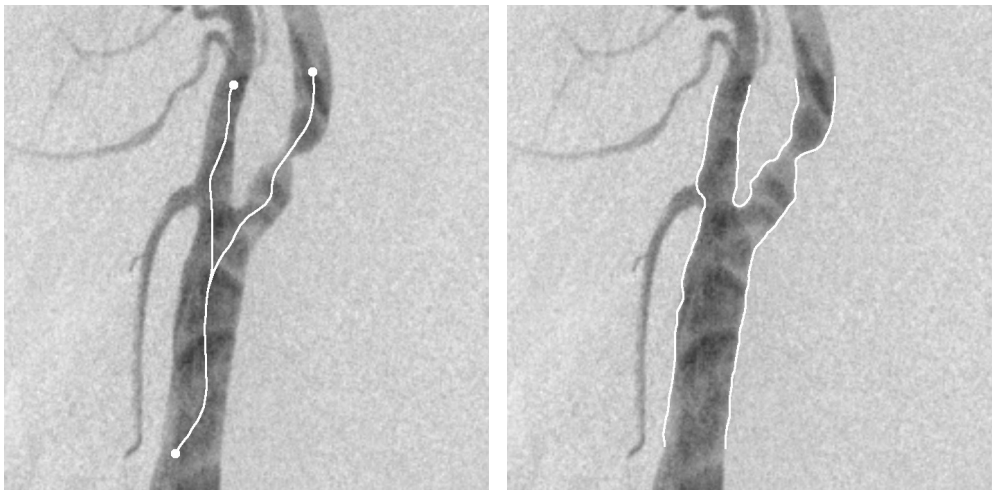
(a) (b)

Figure 4.1: Wavefront Propagation: a) Initial image with startpoint (black arrow) and endpoint (white arrow) and b) Resulting image after propagation.

The final step of the algorithm is the backtracking that finds the way back from the end point to the start point through the arrival time image. This line is subsequently transformed back into the high-resolution image and slightly smoothed to obtain the final resulting pathline. When the pathline does not follow the correct path, for example, when 2 vessels overlap and the overlapping vessel has more contrast than the one under study, the user has the possibility to add an additional point to the pathline to force the algorithm through a certain region of the image. Two waves are then initiated subsequently, the first one travels from the start point to the additional point and the next one from the additional point to the end point. Subsequently, these partial pathlines are combined into one final pathline. In an exceptional situation where more than one additional point is needed, there is also a wave initiated from one additional point to the other, eventually combining 3 partial pathlines into the final solution.

4.2.2 Bifurcation and Sidebranch

As indicated earlier, one of the major variances in peripheral vessel analysis is the type of vessel segment, the morphology of the artery under study. A simple vessel segment without any branches requires only a straight analysis, whereas other morphologies (in this case we discuss the bifurcation and the sidebranch analysis) need a different, more complex analysis. As an illustration of the bifurcation case, one can think of the major aorta bifurcation or the bifurcation in the carotid arteries. Because obstructions often occur at these junctions, a straight segment is not the proper model to assess the stenosis quantification parameters. In these cases one needs to analyze the entire bifurcation structure, which means that 3 contours of the vessel segment need to be detected (Fig. 4.2). To be able to detect these 3 contours, the pathline algorithm must provide a model for all 3 contours. To achieve this, one start point and 2 end points are needed, one in each branch of the bifurcation (Fig. 4.2). To this end, 2 pathlines are constructed to connect these 3 points: one starting from the start point and stopping at the first end point, the other starting in the start point and stopping in the other end point. Because the start point is functioning as a start point for both pathlines, the use of one single wavefront propagation from this start point is sufficient to find both pathlines.

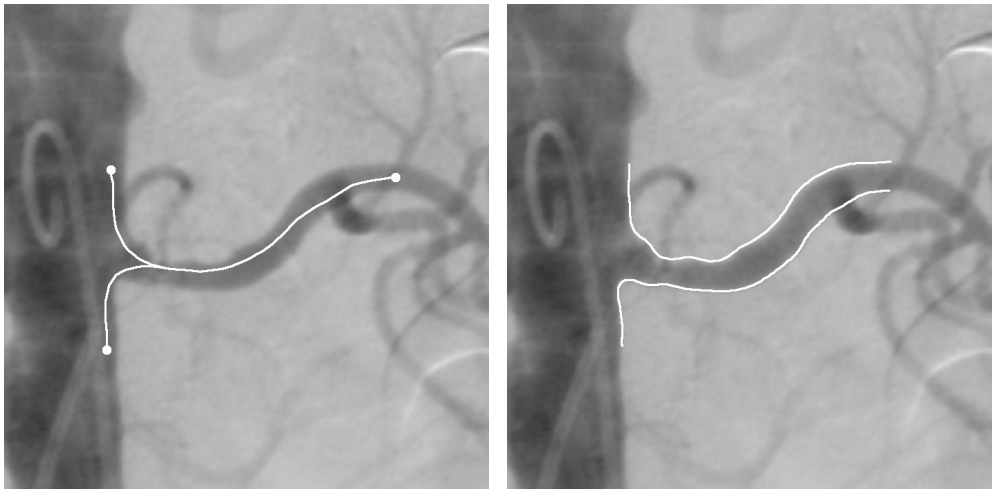


(a) (b)

Figure 4.2: Bifurcation analysis: a) Pathlines for bifurcation and b) Contours for bifurcation.

This time, we only have to continue the propagation until it has reached both end points. Performing the backtracking twice, once for each end point, provides the 2 pathlines needed. Also the analysis in case of a sidebranch requires a different approach. For example, to analyze a lesion in a renal artery, which often occurs at the ostium of the artery, a straight segment analysis would not be able to find a proper segmentation of the proximal part of the vessel.

To solve this problem, an ostial segment measurement method was developed [101], which also uses 3 points, in this case 2 start points and 1 end point. These 3 points are subsequently used to generate 2 pathlines, 1 from the first start point and 1 from the second start point,



(a) (b)

Figure 4.3: Sidebranch analysis: a) Pathlines for sidebranch and b) Contours for sidebranch.

both to the end point (Fig. 4.3). Because both pathlines have a different start point, this would normally mean that we have to perform the wavefront propagation twice. Nevertheless, because the resulting pathline does not depend on the direction of search, we can perform the search from the end to the start point and in this way, a single wavefront propagation suffices. The wave is sent out from the end point and the backtracking is performed from both start points. Again, these 2 pathlines are combined into 1 final sidebranch pathline.

4.2.3 Validation

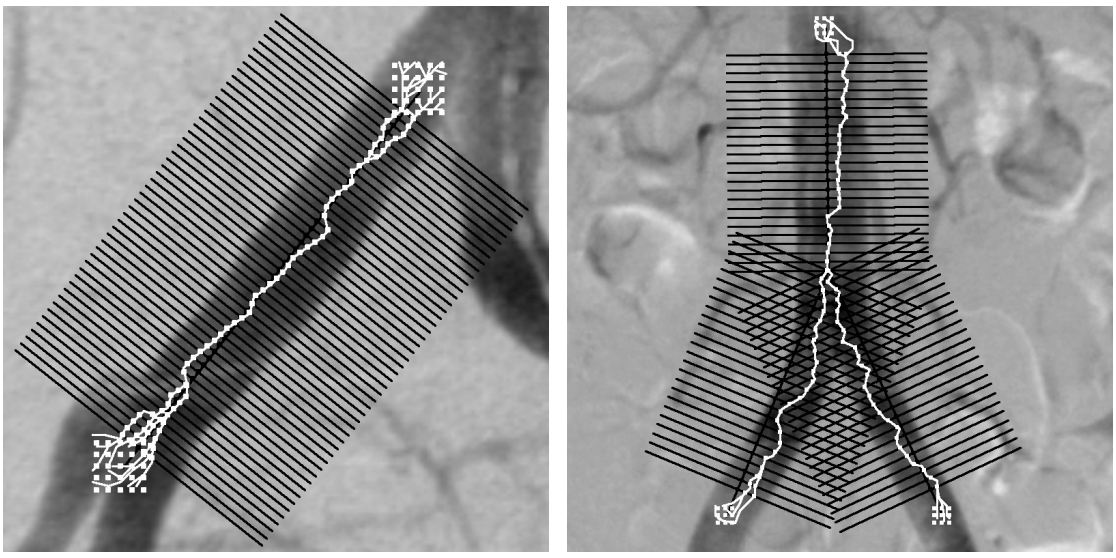
To assess the performance of the new pathline approach, the criteria mentioned earlier were used: First of all, the pathline must be robust for small changes in the location of the start and end points. To assess this sensitivity, these points were relocated in certain regions around the manually defined points and the variations in the resulting pathlines were calculated. Second, the number of additional points that the user must provide to achieve a correct pathline was evaluated. A correct pathline in this case means a line that remains within the assumed arterial boundaries over its entire length. Because there is a large variety in possible vessel segments, the experiments for the validation procedure were divided into groups that represent one type of vessel each. In this way we were able to assess the performance of the pathline approach in each of the different types of arteries. To assess the dependency of our pathline approach on the exact location of the start and end points, an area around the point, indicated by an expert, was defined, and the point was varied within this area. For each combination of start and end points, the pathline was calculated, all the different pathlines were compared, and their local variability was measured.

4.2.4 Materials

Straight Segment

For the straight segment validation, a 5 x 5 matrix of points with a distance of 3 pixels between the neighboring points was used for the variation of the start and end points. This resulted in a total number of 625 pathlines. From the manually defined start point, a straight line was drawn to the manually defined end point. Perpendicular to this line 50 scanlines were defined, equally distributed along the line (Fig. 4.4(a)). For all pathlines the intersection points with each of the scanlines were determined, and the distances of the intersection points to the straight line were calculated. From all the distances per scanline, the mean and the standard deviation were calculated. This standard deviation is a measure for the local variability of the pathline along the scanline.

For the validation experiment 3 different sets of vascular segments were selected, each representing a different type of vessel. The first set consisted of 26 aortic segments selected from 26 angiographic images, the second set consisted of 36 femoral segments selected from 29 images, and the third set of 31 iliac segments selected from 17 images. The selection was performed such that the resulting set of images represented a large variety in sizes, ranges and types, containing digital and digitized cinefilm, subtracted and nonsubtracted, 512^2 and 1024^2 matrices, 8-bit and 16-bit angiographic images, from different imaging systems. The resulting set of segments also was selected to be as diverse as possible, containing long and short, obstructed and nonobstructed, arterial segments.



(a) (b)

Figure 4.4: Scanlines for calculation of the local variation in pathlines: a) Straight segment and b) Bifurcation.

Bifurcation and Sidebranch

The bifurcation pathline validation is slightly different from the straight segment validation. Because 3 points of importance are now present, 1 start and 2 end points, the number of variations is reduced for all the points. A 3 x 3 matrix is used, with a mutual distance of 5 pixels, resulting in 729 pathlines. Each pathline can be divided into 3 different parts: The proximal part, where the 2 calculated pathlines are identical, and the 2 distal parts, each representing the pathline of one branch of the bifurcation. To calculate the variation of the pathlines, the location of the separation point of the first pathline is detected, and from this point 3 lines are drawn to the start and end points, each containing 25 perpendicular scanlines that are evenly distributed along this line segment (Fig. 4.4(b)). For each segment, the calculation of the local variation is performed similarly to the procedure described in the straight segment case. Note that a possible dislocation in the separation point between different pathlines would result in a local variation at that point that is not equal to zero. This should be clearly visible for all 3 line segments.

The validation of the sidebranch pathline is similar to the bifurcation pathline discussed above, only now there are 2 start points and 1 end point. The difference is that for the 2 proximal parts of the pathline only 10 scanlines were used to assess the variation, instead of 25 used in the bifurcation analysis, because these 2 parts of the pathline are usually relatively short.

The validation study of the bifurcation pathline was conducted on 2 sets of vascular images, one containing 32 aortic bifurcations and the other containing 39 carotid bifurcation segments, again selected in such a way that the sets were as diverse as possible. The sidebranch pathline validation was performed on one set of 75 renal artery segments selected from 51 angiographic images.

4.3 Results

4.3.1 Straight Segment

As indicated before, there are situations where correction points had to be defined, before the pathline could be accepted (ie, remained entirely within the vessel). The average number of corrections needed was 0 in each type of segment, ie, the aorta, the femorals and the iliaca as can be seen in Table 4.1. This number of support points can be seen as a measure for the correctness of the algorithm. Note that the new method required no corrections to guide it through the correct vessel.

Table 4.1: Average number of corrections needed per pathline.

	Straight segment			Bifurcation		Sidebranch
	Aorta	Femorals	Iliaca	Aortic	Carotid	Renal
# corrections	0	0	0	0.062	0.249	0.079

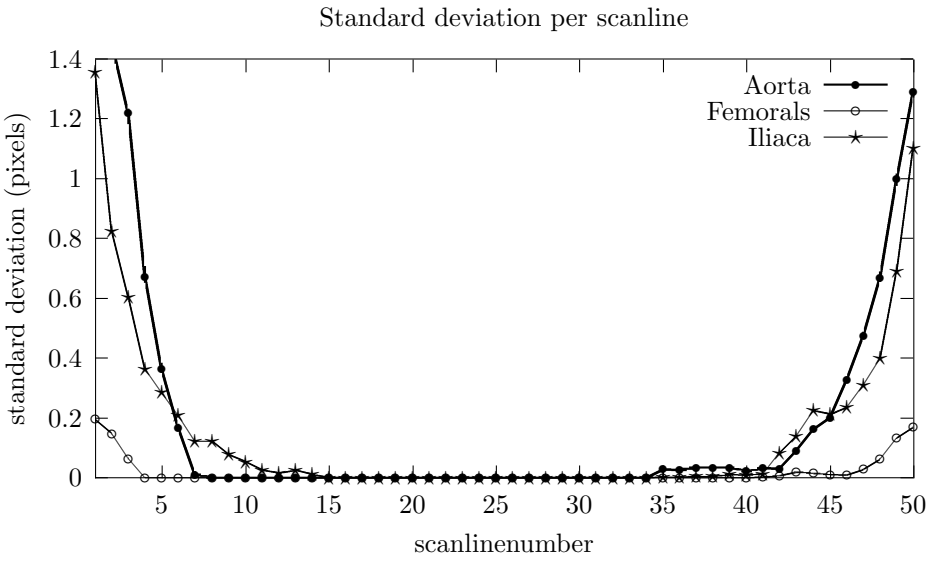


Figure 4.5: Mean local variations of the wavepath approach in the straight segment version.

The results of the variation measurement for the straight segment pathline detection, averaged over all segments per set, are presented in Figure 4.5. This can be seen as a measure for the reproducibility of the algorithm. It is clear that the new method shows variability only at the start and end of the pathline, whereas the essential middle part of each pathline (approximately 60% of its length) is exactly the same for all 625 pathlines per segment.

4.3.2 Bifurcation and Sidebranch

Figure 4.6 shows the results of the local variation calculation for the wavepath algorithm in bifurcation segments. Over all segments per set, the values were averaged. Analog to the straight segment pathline, these bifurcation pathlines show some variability at the start and end, whereas the central parts of all 729 pathlines per segment are exactly identical. From the fact that the variation is zero in the central point, where the proximal part meets the 2 distal parts, follows that the separation point is at the exact same location for all pathlines in each segment! The sidebranch results are presented in Figure 4.7. Again, the variation is zero in the middle part of the pathlines and only close to the start and end point, a certain amount of variation can be seen.

Note that the separation point is at the exact same location for all pathlines in each segment, as follows from the fact that the variation is zero at the point where the proximal parts meet the distal part.

The average number of correction points needed to guide the algorithm through the correct vessel was calculated for each set of bifurcation segments and the sidebranch segment set. This resulted in an average of 0.062 support points for the aortic bifurcation segments, 0.249 for the carotid bifurcation segments and 0.079 for the renal ostial segments. Because each of the

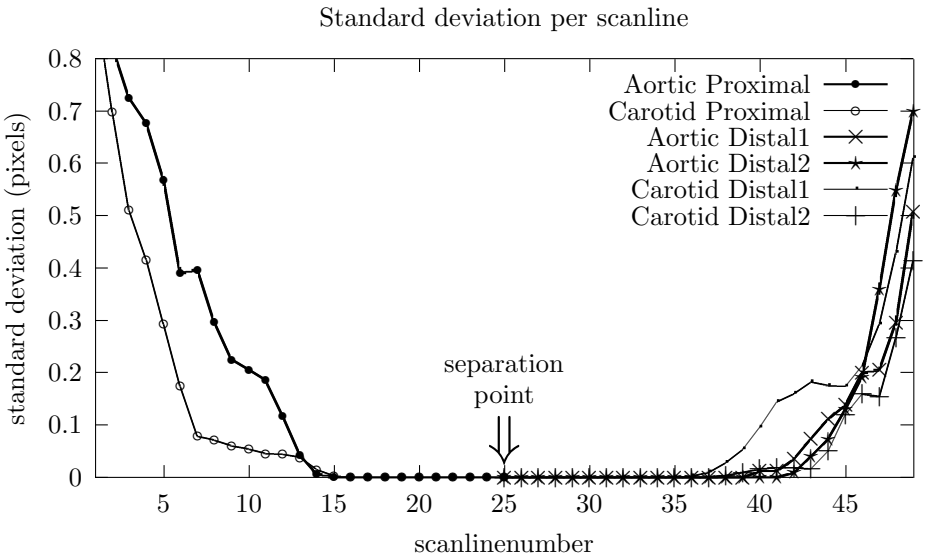


Figure 4.6: Mean local variations of the wavepath approach in the bifurcation version.

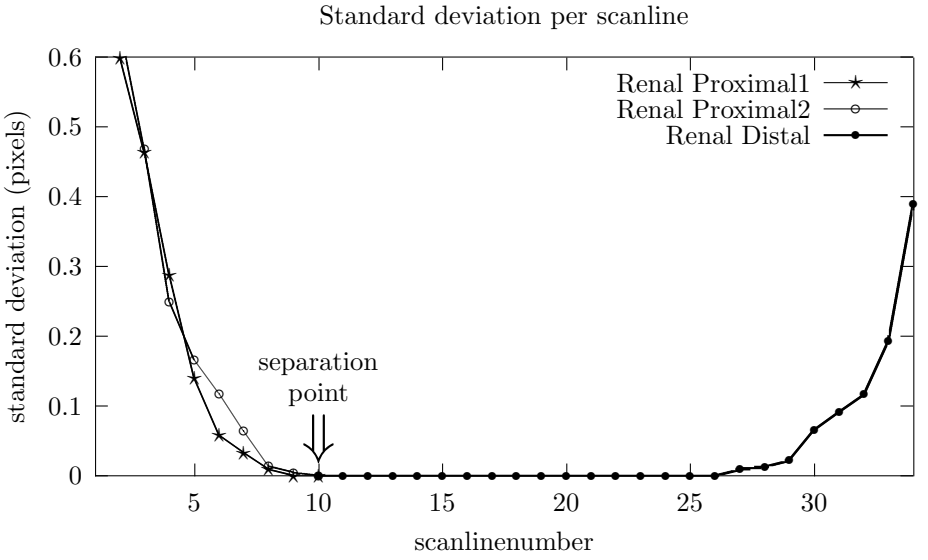


Figure 4.7: Mean local variations of the wavepath approach in the sidebranch version.

bifurcation and sidebranch pathlines consist more or less of 2 "straight" pathlines, a correction point can be set not only in one of the "straight" pathlines but also in the common part, which means that it holds for both "straight" pathlines. Only in one case of the ostial pathline, 2 correction points were needed. Except for that case, the maximal number of user interactions per segment, needed to correct the pathline, was one.

4.4 Discussion

In this article, a novel approach for the detection of pathlines in vascular x-ray images was presented that is able to cope with a large variety of image types and segment types. The aim of the current research was to achieve an excellent reproducibility of the pathline detection in vascular images, which represent other morphologies, such as the bifurcation and sidebranch cases, than the coronary arteries.

The other goal for the development of our new algorithm was the robustness of the new approach, which comes down to minimization of the amount of user interaction that is needed to gain a pathline that satisfies all criteria. As can be seen from the validation study, the new approach satisfied our aims for a wide range of image types and vessel types. The straight segment pathline showed variation only in the neighborhood of the start point and end point, whereas the large and important middle part of the pathline is found at exactly the same location, independent, within a certain range, from the location of the user-indicated start and end point. In other words, we can achieve a unique pathline in a certain section by placing the start and end point outside this region. This holds for all 3 sets of segments that were tested in this morphology: the aortic segments, the iliaca, and the femorals.

Considering the robustness of the algorithm, it can be seen that the average number of correction points that is needed is zero. This means that no corrections have to be made, which obviously benefits the user friendliness and reproducibility of the resulting pathline.

Similar to the straight segment pathline, the validation of the bifurcation pathline and the sidebranch pathline demonstrates the excellent reproducibility of the pathline in the central part of the line. Again, the only variation occurs close to the user-indicated start and end points, which also implies that the separation point is at a fixed location for each segment. This holds for all the different segment sets: aortic and carotid bifurcations and renal ostial segments. The average number of correction points that is needed is still relatively low, considering the fact that the end parts of the vessels can be very close together, which could be a source of failure for a pathline algorithm. This means that also the bifurcation and sidebranch pathlines minimize user interaction, and therefore achieve a good reproducibility.

In the validation study, the wavepath was tested on various types of images and segments. We put effort into making the validation sets as diverse as possible. We used digital arteriograms and digitized films, 512^2 and 1024^2 images, 8 bits and 16 bits, different x-ray equipment, subtracted and nonsubtracted images. Concerning the large variety of the segment sets, it is likely that the approach will perform well on almost every vascular x-ray image. The research described in this article is a part of a much broader research effort that aims at the accurate and reproducible measurement of all vascular lesions. A robust pathline algorithm by itself is not enough for making the total analysis reproducible. More research is needed for a robust and reproducible

contour detection and diameter function calculation. Also, the exact analysis of a bifurcation lesion is still a subject under study, but this pathline approach surely opens the way for the quantification of stenoses located within a bifurcation.

4.5 Conclusion

Our new approach for the detection of pathlines in various segments in vascular x-ray images has proven to be a robust and reproducible method. The required user-interaction is minimal and the pathline is more or less independent from the user-defined start and end points, as is shown in the validation study. This holds for the straight segment as well as the bifurcation and sidebranch versions in a large variety of vessel segment types.

CHAPTER 5

A new approach to contour detection in X-ray arteriograms: The Wavecontour

This chapter was published as:

Janssen JP, Koning G, de Koning PJH, Bosch JG, Tuinenburg JC, Reiber JHC.
A new approach to contour detection in X-ray arteriograms - The Wavecontour.
Invest Radiol. 2005;40(8):514-520

Abstract

Objectives: To develop a novel approach (the Wavecontour) for the detection of contours in vascular X-ray images, designed to eliminate any systematic under-or overestimation for vessel sizes in the range of 0.5 to 15 mm, and further minimize the influence of the user-defined start- and endpoint.

Materials and Methods: The method is based on the Wavefront Propagation principle in a two-stage approach. Two validation experiments were performed: a plexiglass phantom study (tube sizes ranging from 0.51 to 9.9 mm) and an in vivo patient study (114 patients with various degrees of stenosis).

Results: The phantom study demonstrated an accuracy of 0.007 mm and a precision of 0.072 mm. The patient study showed a high similarity between the detected and the expert-drawn contours: 93% for a threshold of 1.0 pixel and 81% for a threshold of 0.5 pixel. Furthermore, the contours are robust in complex lesions and are almost independent in the middle part of the segment from the user-defined start- and endpoint. A variation of only 0.6 pixel exists in the middle 60% of the contours.

Conclusions: Our new Wavecontour approach performs very well on phantom images as well as on clinical data over the whole range of 0.5 to 15 mm and results in more robust QCA/QVA analyses.

5.1 Introduction

Over the last decades, several approaches have been developed for the assessment of coronary artery morphology and the accurate and automatic quantification of coronary arterial lesions. The goal in this field of research of Quantitative Coronary Arteriography (QCA) has been the development of a robust method that can be used in clinical trials as well as during cardiac catheterization interventions, by providing clinically relevant parameters such as percent diameter stenosis, obstruction diameter, estimated reference diameter, obstruction length and others [37, 96]. These parameters can be used to select the proper devices during interventions and to assess accurately the development of the disease process over time.

In order for a method to be acceptable in these applications, it has to be fast, accurate, reproducible, automatic (or at least semi-automatic) and reliable, be able to handle different types of images and different types of vessel morphologies. In our lab, we have developed and validated various generations of such QCA software packages for online and offline usage over the past 25 years [37, 96, 38, 36]. The accuracy and precision data of these different generations of software packages have served as standards in Quantitative Coronary Arteriography.

Despite the proven high accuracy and precision of our software packages [40, 101], it would be highly desirable to even further automate the procedure with associated likely smaller observer variabilities, to apply this contour detection scheme to all possible morphologies including complex lesions, bifurcations and ostial lesions, and to a wider range of vessel sizes, including all peripheral vessels, such as the carotid arteries, aorta, renal arteries, femoral arteries, etc. in order to achieve a broader acceptance in on-line applications. As a first step to minimize the user influence as much as possible, we recently developed the Wavepath [84, 102], a highly reproducible and accurate pathline detection method that is virtually independent of the exact position of the user-defined start- and endpoints of the vessel segment of interest.

However, a stable and reproducible pathline alone is not enough to make the overall measurement more reliable and reproducible. The contour detection methods that were used so far in the QCA-CMS systems, i.e. the Minimal Cost Algorithm (MCA) [40] and the Gradient Field Transform (GFT) [50], also introduce a certain amount of variation, even when the pathline is absolutely stable in the middle part of the segment.

This and other limitations that were encountered with the detection of the arterial contours using the MCA approach, are related to the scanlines, on which the MCA is based. These scanlines are constructed perpendicular to the initial model (i.e. the centerline of the vessel) and are used to calculate the possible edge-points that are subsequently used by the dynamic programming algorithm to calculate the best contours. The fact that only two points can be detected per scanline (one for each side of the vessel), makes this algorithm less suitable for following complex lesion morphologies and also causes an undersampling of the contours at the outside of corners and an oversampling at the inside. The latter can lead to crossing scanlines and therefore loops in sharp corners. This issue is explained in Figure 5.1.

As mentioned above, scanline-based methods suffer from a relatively large variability since the definition of the scanlines is usually dependent on the pathline, which is divided into a fixed number of segments of equal length, making the resampling dependent on the length of the pathline. The use of the Wavepath [84, 102] does not solve this problem since the lengths of the pathlines vary with the manual definition of the start- and endpoints.

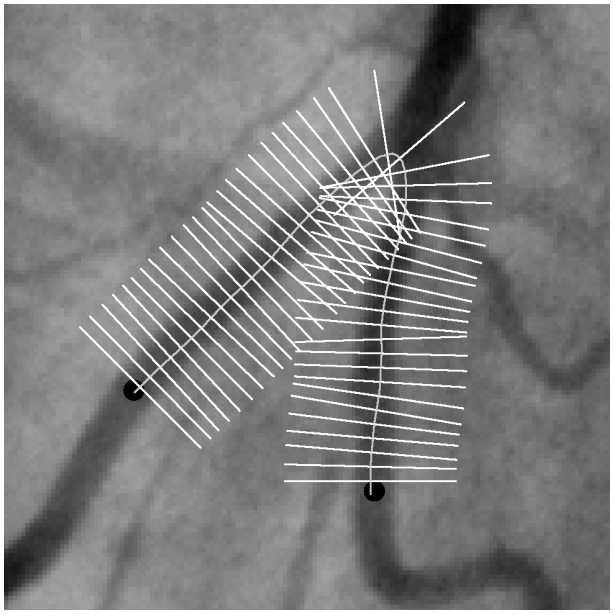


Figure 5.1: Under- and oversampling and crossing scanlines due to a sharp corner in a bifurcation.

To avoid these problems, we decided to design and implement an entirely new contour detection method that does not require scanlines to detect the contours and would indeed benefit clearly from a stable pathline and solve the problems the other algorithms suffer from, such as the difficult trade-off between smooth contours that are not affected by the noise in the image, and more irregular contours that are able to follow complex lesion morphologies.

In addition, the algorithm should also satisfy the requirements for vascular applications, i.e. it should provide accurate measurement data for a much larger range of vessel sizes, up to about 12-15 mm in diameter. Over the last several years we have seen that the coronary interventional techniques are transferred successfully to peripheral applications, in particular in the carotid arteries. This has created great possibilities and challenges for Quantitative Vascular Arteriographic (QVA) applications [103]. As a consequence, the algorithm must also be able to handle other vessel morphologies than the straight vessels in QCA, being ostial segments and bifurcations. At the same time, bifurcation stenting in coronary arteries has attracted more and more attention lately, requiring solutions from the QCA point-of-view [104, 105].

In general, four different types of contour detection approaches can be distinguished: the derivative-based techniques [40, 50, 106, 107], the densitometry based techniques [108, 109], the threshold-based techniques [110, 111] and the model-based techniques [112, 57]. As was shown by Hoffmann et al [113], all techniques can yield highly accurate contour detection results, but no single technique provides accurate sizes for the whole range of vessel sizes that is used in QCA and QVA. In our application, the densitometric methods are not favored since the coronary angiograms show substantial motion, which makes a background subtraction virtually impossible. This difficulty to separate the artery from the background as well as the non-linear transfer-function of the X-ray system, make the densitometric approaches unsuitable. The model-based

techniques require detailed information about the exact characteristics of the imaging system to achieve its theoretical accuracy, which is in many cases not available. Since the threshold-based approaches show the largest error in size measurements and the derivative-based techniques have proven their accuracy in this field of application [40], the new approach is also based on a derivative technique.

This paper describes the new contour detection approach that we have developed to perform successfully in the full range of new applications mentioned above. Next, the results of a validation study are presented, followed by a discussion about the advantages and limitations of this approach.

5.2 Materials and methods

The new approach for contour detection has to meet several criteria in order to be applicable in the practical environment of a QCA and QVA system: 1) The definition of the contours must be very accurate, such that no systematic over- or underestimation of the size of the vessel occurs; 2) the resulting contours must be reproducible; 3) the algorithm must be able to detect the vessel contours of different vessel morphologies, such as straight vessel segments, ostial segments and bifurcations; 4) the approach must be able to cope with complex lesion morphologies, such as an overhang or asymmetric and steep stenosis; 5) the algorithm must be applicable over a wide range of vessel sizes from 0.5 up to about 12 - 15 mm in diameter; and 6) the algorithm must be fast enough for online applications.

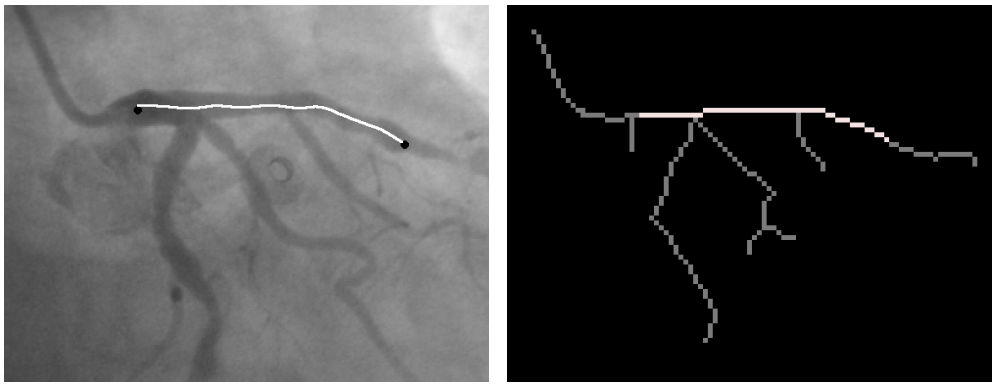
In our approach, the measurement of an arterial stenosis is divided into the following steps: First a pathline through the vessel is detected between the user-defined start- and endpoint. Then, the contour detection is applied, to locate the contours of the arterial segment using the pathline as an initial model. Next, a first estimation of the location of the stenosis is made based on the detected contours. Subsequently, an estimation is made of the vessel segment without the obstruction (i.e. the reference contours), on the basis of the detected contours in the non-stenotic parts of the analyzed vessel. Finally, from these reference contours and the detected contours, the stenosis parameters are calculated. As mentioned earlier, we already developed a new approach for the detection of pathlines through the arteries, the Wavepath, that was designed to minimize any user influence. However, since we want the entire measurement to be robust and user-independent, the contour detection itself must be improved further to achieve a reproducible measurement approach.

5.2.1 Algorithm

To meet the criterion of eliminating all systematic errors, we choose for a two-stage approach. The first stage is meant to roughly find the correct contours and the second stage will adjust the contours to achieve the high accuracy and precision. In this first stage, all edges are detected using the edge filters that were already used in the MCA algorithm. To solve the problem of different vessel morphologies, more information is needed than only the edge strength. Therefore we add high-level information concerning the morphology of the vessel under study.

To extract this information, a Wavefront propagation [80] is used to detect the entire vessel. When analyzing the region that the Wavefront has reached, a binary image is computed that

represents the morphology of the structure of interest. Subsequently, a skeletonization operation is performed that provides us with the information about the location and direction of side-branches and bifurcations, as can be seen in Figure 5.2. This information is taken into account in the different directional edge-images, which were generated in an earlier phase. In this way, the algorithm can be forced to step over an undesired sidebranch, or artifact in the image. This is achieved by locally modifying the detected edge images with a weighted combination of the direction of the edge and the direction of the pathline segment that is closest.



(a) (b)

Figure 5.2: Skeleton extraction: a) Input image and b) the detected skeleton. In white the pathline is shown, in gray the detected sidebranches

The removal of the scanlines allows the algorithm to follow complex lesions, for example with overhangs, and sharp corners, but requires a different approach to the edge detection since the global direction of the contours is unknown. Therefore, all possible edges in all directions must be detected. We use different directional filters to achieve a directional edge-image in each of the possible directions. These directional edge-images are used later on for finding the optimal contour.

In our approach, we use the Wavefront propagation [80] and modified it to use not only one global edge-image as speed-image for the propagation, but also the directional edge images, all at the same time, in one single propagation. In this case, each position is not only assigned one speed value as is the case in the Wavefront algorithm, but also eight different direction dependent speed values. So dependent on the local direction the wavefront is propagating in, one of the extra speed-values is added. This allows the algorithm to find only the contours that lie on the edges in the correct direction.

The resulting contours are subsequently found by performing a traceback from the endpoints to the startpoints. These start- and endpoints of the contours are found by a simple 1-dimensional weighted edgefilter perpendicular to the pathline, at the position of the proximal point and the distal point.

The second stage of the algorithm uses the initial contours as input and refines the contours to achieve the final results, by using the optimal filter approach for the detection of coronary arteries that was defined by Van der Zwet et al [60]. Taking into account the average transfer

function of an X-ray system and assuming that the arteries under study have a circular cross-section shape, a vessel profile is calculated, as can be seen in Eq. 5.1 and Figure 5.3.

$$G(x) = R * \left\{ \begin{array}{l} \left(1 + e^{-2bR}\right) * \left[erf\left(\frac{fx}{2}\right) + erf\left(fR - \frac{fx}{2}\right)\right] - \\ e^{\left(\frac{b^2}{f^2} - bx\right)} * \left[erf\left(\frac{fx}{2} - \frac{b}{f}\right) + erf\left(\frac{b}{f} - \frac{fx}{2} + Rf\right)\right] + \\ e^{\left(\frac{b^2}{f^2} - 2bR + bx\right)} * \left[erf\left(-\frac{b}{f} - \frac{fx}{2} + Rf\right) + erf\left(\frac{b}{f} - \frac{fx}{2}\right)\right] \end{array} \right\} \tag{5.1}$$

with $b = \frac{4.53}{R}$, $\quad f = 0.9 \quad$ and $R =$ the radius of the vessel

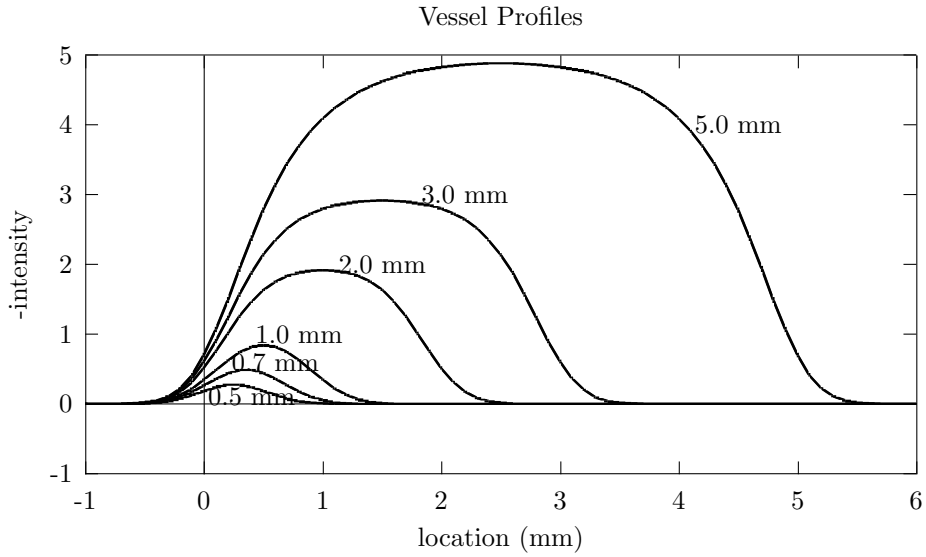


Figure 5.3: The profiles of the projections of circular vessel with different diameters in an X-ray system

For these vessel profiles, the optimal filters for detecting the True Edge Point (TEP) as well as the Most Characteristic Point (MCP) are defined. The TEP-filters are optimized for finding the true edgepoint, whereas the MCP-filters are optimized to find the point on the edge that best matches an anti-symmetrical profile.

These filters are different for different vessel sizes, so an estimation of the width of the vessel is needed to select the proper filter. Since we use this filter in the final step of our two-stage algorithm, we already have initial contours and therefore an initial estimation of the vessel width.

As was shown by van der Zwet et al. the TEP-filters are very different for different vessel sizes, whereas the MCP-filters are quite similar for the different vessel sizes. The MCP-filters need to have a fixed offset to position the edge at the correct edge point. We chose the MCP-filters to

detect the contours in the second stage of our algorithm, which results in the filter-profile that can be seen in Eq. 5.2 and Figure 5.4.

$$
\begin{aligned}
f(x) = & \\
& c_1 e^{sx} cos(sx) + c_2 e^{sx} sin(sx) + \\
& c_3 e^{-sx} cos(sx) + c_4 e^{-sx} sin(sx) + \\
& c_5 * \int_0^{+\infty} \left(\begin{array}{l} e^{(x-t)s} \{sin\,[(x-t)\,s]\} - cos\,[(x-t)\,s] + \\ e^{-(x-t)s} \{cos\,[(x-t)\,s]\} + sin\,[(x-t)\,s] \end{array} \right) \frac{G(t)}{8s^3} dt + \\
& c_6 * \int_0^{+\infty} \left(\begin{array}{l} e^{(x-t)s} \{sin\,[(x-t)\,s]\} - cos\,[(x-t)\,s] + \\ e^{-(x-t)s} \{cos\,[(x-t)\,s]\} + sin\,[(x-t)\,s] \end{array} \right) \frac{G''(t)}{8s^3} dt + c_7
\end{aligned}
\tag{5.2}
$$

with $c_1 - c_7$ and s as parameters to optimize.

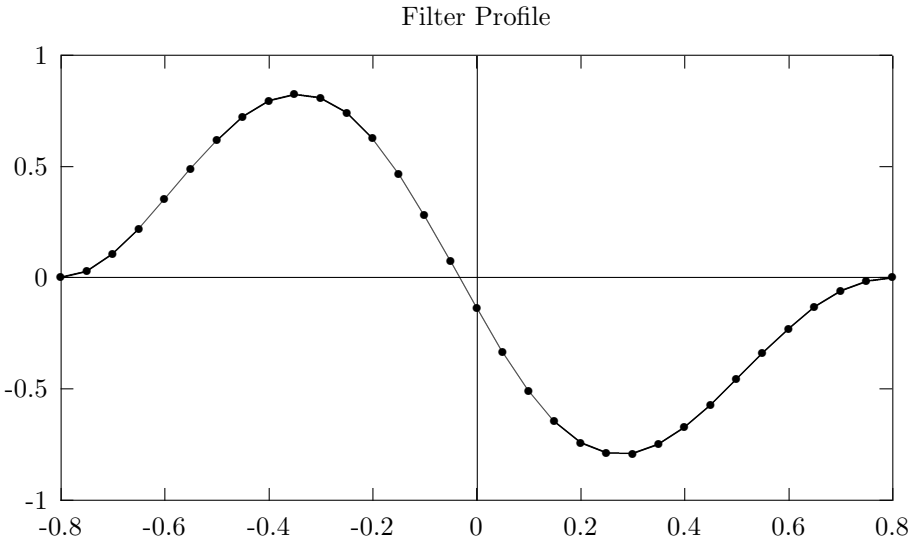


Figure 5.4: The profile of the filter used in the second stage of the algorithm

Finally, in the last phase of our contour detection approach, a contour smoothing is performed to decrease the sensitivity of the contours to noise. To avoid the global edges of the contours to be cut off, an edge-preserved smoothing is used, based on the "Fuzzy Vector Median-based Surface Smoothing", proposed by Shen et al [114]. This filter, which was originally designed for surface smoothing, removes high frequent noise, while preserving the global morphology of the contours.

5.2.2 Validation

In order to assess the performance of our new contour detection approach, we performed two validation studies: one study on phantom images and the other study on clinical patient data.

Plexiglass phantom study

The first part of the validation concerned measuring the accuracy and precision of the Wavecontour approach. This is achieved by analyzing phantom images that were acquired on different imaging systems. Two plexiglass phantoms containing straight tubes with diameters ranging in size from 0.51 mm to 9.9 mm, were filled with 100% contrast agent, placed in the the X-ray system and acquired with different kV-levels (75-90 kV) and different image intensifiers (5 to 9 inch). Also different X-ray machines were used (a Philips cardio-system, a Philips vascular system and a GE cardio-system) in order to make the validation as general as possible.

All these images were analyzed and for each vessel segment, the diameters were measured for all points on the contours and the mean diameter of the segment, calculated from 100 diameter measurements, was compared to the true value. From these results the precision and accuracy of our contour detection approach was assessed.

In Vivo study

The second validation experiment was performed under in vivo circumstances by analyzing digital coronary and vascular arteriograms. A set of vascular segments was selected from 114 digital 512^2 angiographic images, being as diverse as possible, containing long and short, obstructed and non-obstructed, arterial segments. The selection was performed such that the resulting set of images represented a large variety in sizes, ranges and types.

In this study, the automatically detected contours obtained by the Wavecontour approach were compared to the contours that were drawn by an expert, which we use as a gold standard. The results are achieved by measuring the similarity between the contours using a threshold distance of 0.25 and 0.5 pixels, which corresponds to 0.05 - 0.1 mm, when taking an average pixel size of 0.2 mm. Furthermore, the variations in the contours as a result of the variation in start and endpoint that are user-defined were assessed. To that end, each analysis of these 114 patients was repeated 25 times automatically, each time with a slightly different start and endpoint. All 25 contour pairs were processed and the variations in the contours were measured. This is achieved by drawing 50 scanlines perpendicular to the straight line from proximal to distal point and measuring the standard deviation of the intersections of the contours with these scanlines. This is done for the previous algorithm (MCA) and our new Wavecontour.

Statistics

As a measure for the overall performance of the new Wavecontour, we use the accuracy, which is defined as the average signed difference between the measured value and true value, and the precision, which is defined as the standard deviation of these differences. These measures are calculated for each of the different measured tube diameters in the phantom study, and finally,

the overall accuracy and precision of the approach are calculated, which is the average accuracy and precision over all different measured tube diameters.

5.3 Results

5.3.1 Plexiglass phantom study

The results of the study with plexiglass phantoms are presented in Figure 5.5. The measured sizes of the phantoms are strongly correlated to the true sizes, with a correlation coefficient of 0.9994.

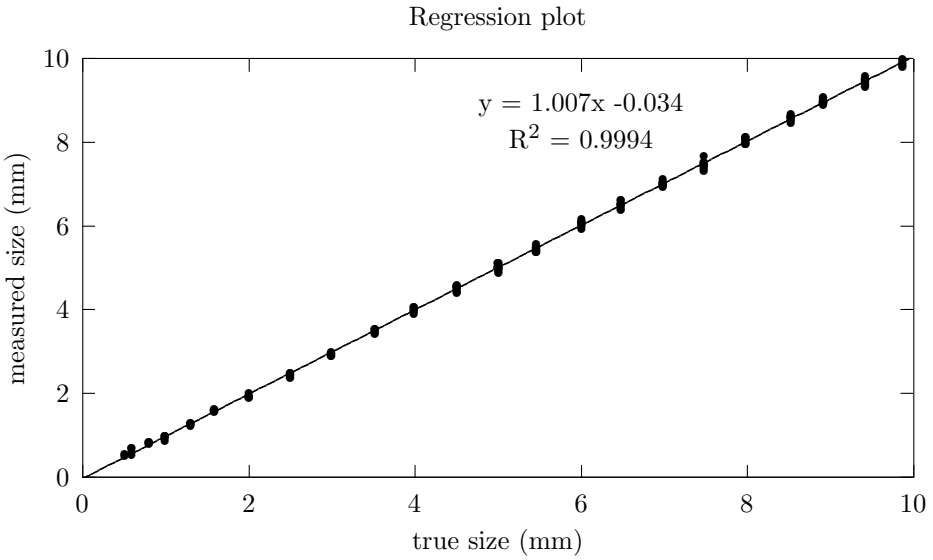


Figure 5.5: The measured size in mm against the true size of the phantoms in mm

In Figure 5.6, a Bland-Altman-plot is made, showing the error of the measured value in mm against the size of the tube in mm. Note that we only have a fixed number of tubes, which explains the non-continuous distribution along the x-axis. The dashed lines denote the minus and plus two times standard deviation boundaries. The vessel size measurements show an accuracy of 0.007 mm and a precision of 0.072 mm. It can also be seen that 82% of all measurements lie within the range of 0.1 mm relative to the baseline, 97% within the 0.2 mm range and the error never exceeds 0.3 mm. As is apparent from the figure, the error slightly increases with an increasing tube diameter; the major reason for that is that the images were acquired with an increasing pixel size, due to increasing image intensifier size.

The pooled standard deviation was 0.043 mm, which can be seen as a measure for the variation of the contour detection within a segment and was calculated over 100 points in each phantom segment. Figure 5.7 shows the error in pixels against the diameter of the tube, also measured in pixels. It can be seen that the error never exceeds 0.7 pixel for any measured

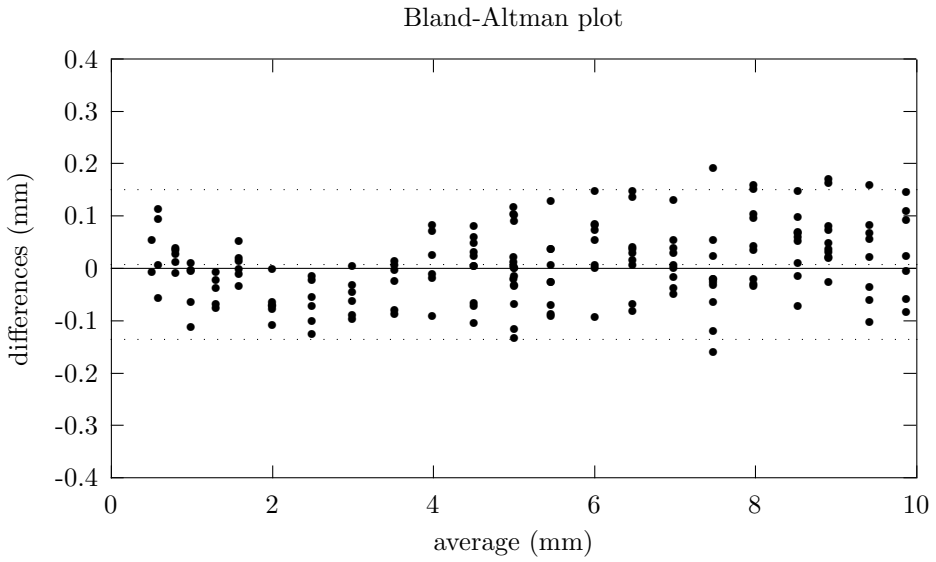


Figure 5.6: Bland-Altman plot in mm

phantom tube and is evenly distributed.

5.3.2 In Vivo study

The results of the study on clinical data, using expert contours, are shown in Table 5.1. To obtain these results, we measured the distance from the detected contour to the expert contour as well as the other way around, from the expert contour to the detected contour, and averaged these numbers. This is done, since in some extreme cases (for example where one of the contours makes a strong curve and the other one is more or less straight) these numbers can differ substantially.

Table 5.1: The similarity measurements for three different threshold-values.

threshold	0.25 pixel (0.05 mm)	0.5 pixel (0.1 mm)	1.0 pixel (0.2 mm)
similarity	51 %	81 %	93 %

Furthermore, the reproducibility of the Wavecontour was examined using the same clinical patient data set. The pathline and contours were calculated 25 times for each segment, while varying the proximal and distal point within a 7x7 matrix around the original points. The resulting contours were intersected with 50 scanlines perpendicular to the straight line from proximal to distal point, and the variation was calculated along these scanlines. This was done for the previous algorithm (MCA) as well as our new Wavecontour approach. The results are shown in Figure 5.8.

The experiments show that the contours are very robust and remain very stable in the middle part of the segment, which is the most important section. Typically, the variation is 0.6 pixel

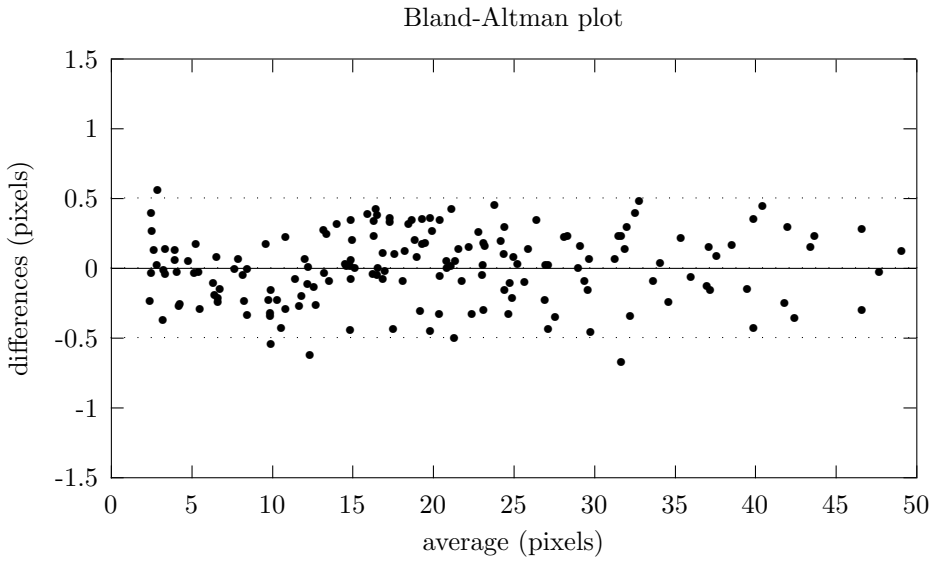


Figure 5.7: Bland-Altman plot in pixels

(0.03 mm) for the middle 60% of the contours. Only near the beginning and end of the segment some larger variabilities occur. This is demonstrated in two examples, shown in Figure 5.9.

Finally, the performance of the new contour detection approach was evaluated on difficult

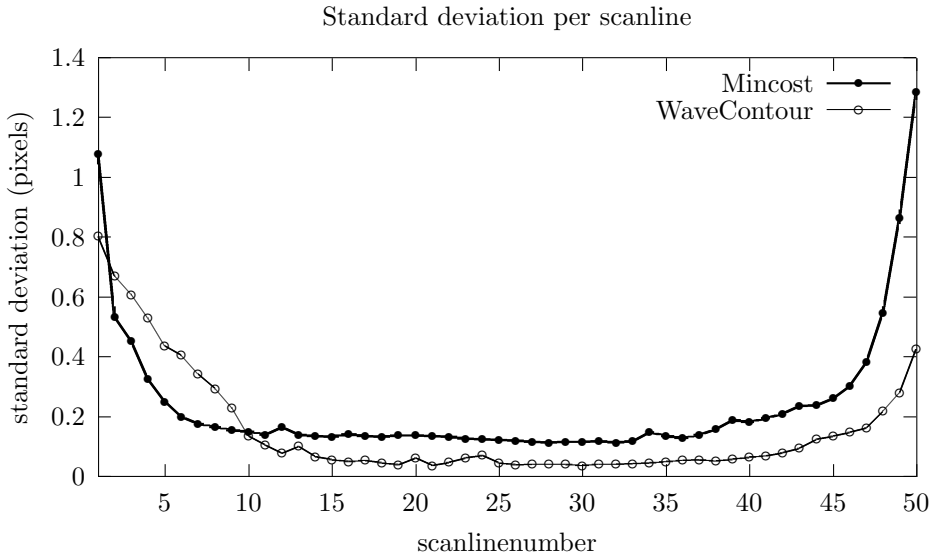
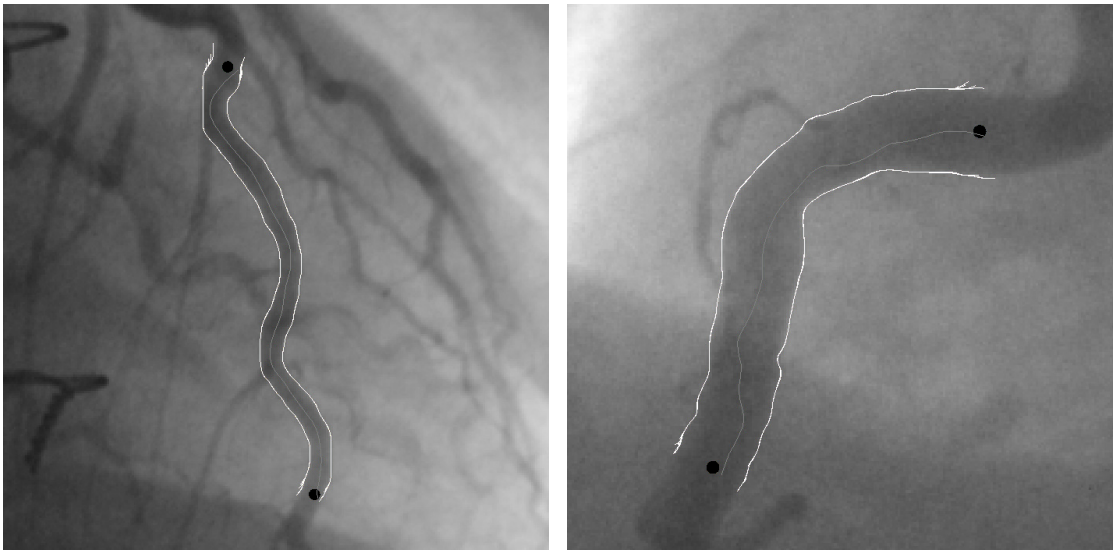


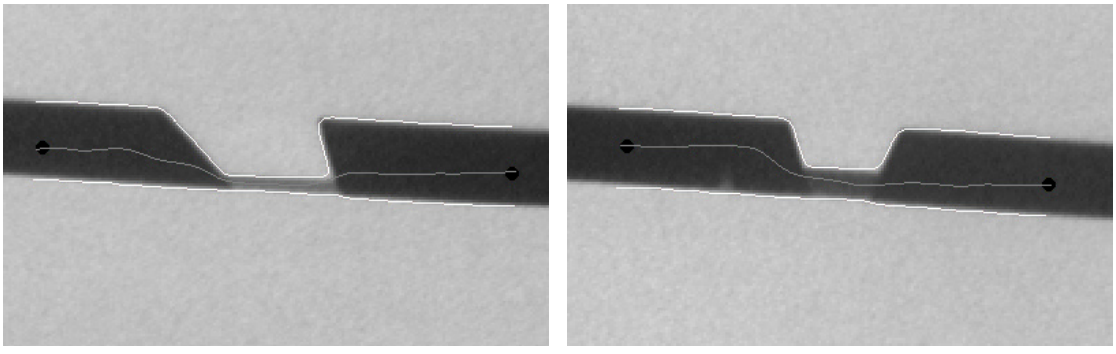
Figure 5.8: The variation in pixels of detected contours at the position of each scanline



(a) (b)

Figure 5.9: The detected contours for 25 different pairs of proximal- and distal points.

lesions with an overhang. For this experiment, a copper phantom is used, consisting of multiple segments with different diameters and different angles, which can be combined in order to create obstructed vessel phantoms with different stenosis morphologies and different stenosis degrees. The results show that the Wavecontour is indeed capable of following these sharp corners and is able to "go backwards" to follow the overhang. This can be obtained in Figure 5.10.



(a) (b)

Figure 5.10: The performance of the Wavecontour on difficult lesions and sharp angles.

5.4 Discussion and conclusion

We developed a new contour detection approach that is called the Wavecontour, and validated the approach on various phantom images as well as clinical patient data. The results show that an accurate measurement is achieved for the whole range of vessel sizes, and no significant systematic under- or overestimation occurs. The vessel size measurements demonstrate an accuracy of 0.007 mm and a standard deviation of 0.072 mm. The accuracy is slightly larger that the accuracy of the mincost algorithm, but the precision is lower, which means that the measurement is more reliable over the whole range of vessel segments. It is also shown that the contours in the clinical patient data show a good similarity to the contours that were drawn by an expert. More than 81% of the contours lie within a distance of 0.5 pixel from the expert-contour, and 93% within 1 pixel. Furthermore, it is shown that the approach is able to deal with complex lesions and sharp corners in the contours. Finally it is shown that the algorithm is robust and reproducible, since the approach shows virtually no change in the middle part of the detected contours due to variations in the user-defined proximal and distal markers.

The In Vivo study that is used to validate the contour detection approach was performed only on straight segments. We put effort in selecting different types of images and different types of vessels (with and without side-branches, straight and curved segments, high contrast and low contrast). However, no ostial and bifurcation segments were taken into account since no expert contours were available for these types of analysis. For further validating, it is necessary also to include these other vessel morphologies to be able to prove that the approach is suitable for all the analyses that can be performed in the vascular application.

The research as it is described in this paper, is a part of a broader research that aims at achieving a stable, more reproducible measurement of vascular lesions. In an earlier stage of the research, we have already developed the Wavepath approach, which has already proven to be a robust pathline detection algorithm. The Wavecontour approach subsequently provides robust and stable contours as is shown in this article. However, to achieve a robust and stable stenosis quantification, also a proper method for the measurement of the diameters of the vessel is needed, as well as a method for quantification of the lesion. This is a topic for future research.

CHAPTER 6

New approaches for the assessment of vessel sizes in quantitative (cardio-) vascular X-ray analysis

This chapter was published as:

Janssen JP, Rareş A, Tuinenburg JC, Koning G, Lansky AJ, Reiber JHC.
New approaches for the assessment of vessel sizes in
quantitative (cardio-)vascular X-ray analysis.
Int J Cardiovasc Imaging. 2010;26(3):259-271

Abstract

This paper presents new approaches for the assessment of the arterial and reference diameters in (cardio-)vascular X-ray images, designed to overcome the problems experienced in conventional quantitative coronary and vascular angiography approaches. In single or "straight" vessel segments, the arterial and reference diameter directions were made independent of each other in order to be able to measure the minimal lumen diameter (MLD) more accurately, especially in curved vessel segments. For ostial segments, an extension of this approach was used, to allow measurement of ostial lesions in sidebranches more proximal than using conventional methods. Furthermore, two new bifurcation approaches were developed.

The validation study shows that the straight segment approach results in significant smaller MLDs (on average 0.032 mm) and the ostial approach achieves on average an increase in %DS of 3.8% and an increase in lesion length of 0.59 mm due to loosening the directional constraint. The validation of our new bifurcation approaches in phantom data as well as clinical data shows only small differences between pre- and post-intervention measurements of the reference diameters outside the bifurcation core (errors smaller than 0.06 mm) and the bifurcation core area (errors smaller than 1.4% for phantom data).

In summary, these new approaches have led to further improvements in the quantitative analyses of (cardio-)vascular X-ray angiographies.

6.1 Introduction

Over the last several decades, Quantitative Coronary Angiography (QCA) has become the standard in the assessment of coronary artery stenosis. Its methods are widely used in hospitals and core laboratories all over the world to measure accurately the severity of coronary artery lesions and other clinically relevant parameters. Although the accuracy and precision of the system have been presented in many validation studies [115, 116, 117, 118, 96, 38, 36, 40], there is still room for further improvements especially for cases with extreme vessel morphologies such as highly curved vessels and complex-shaped lesions.

In addition, the treatment of the more complex vessel structures, such as bifurcations and sidebranches [101, 104, 105], has received a great deal of attention over the last few years. Since more and more interventions are performed in this field, there is an increasing demand for a system that can accurately measure all clinically relevant parameters in those particular cases. With that in mind, we developed a new pathline detection algorithm that is more robust and suitable for ostial and bifurcation vessel segments [84, 102]. Furthermore, we carried out research on a novel contour detection approach, the Wavecontour, designed to accurately detect the contours in a wide range of vessel sizes and different vessel morphologies [119].

In this publication, the focus is on the accurate and robust assessment of the vessel sizes in a wide range of morphologies and the proper estimation of the size and course of the original healthy vessels, which are denoted reference diameter functions and reference contours, respectively.

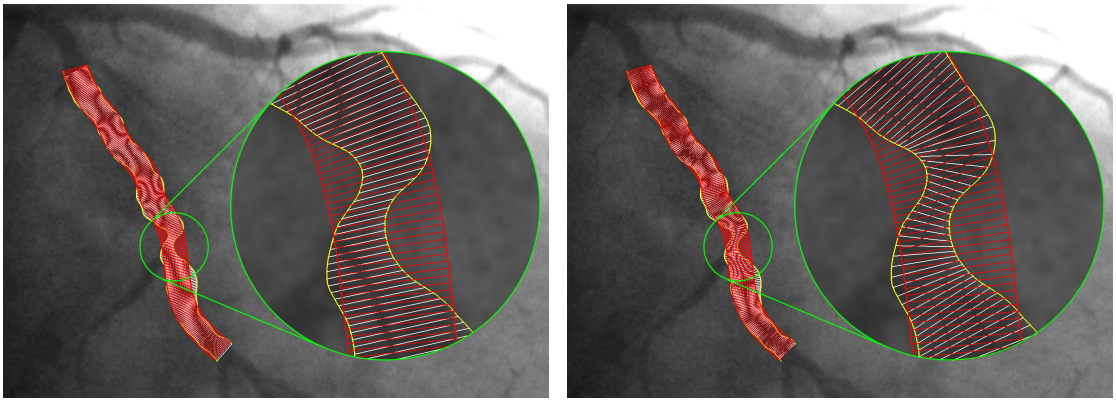
The organization of this manuscript is as follows: First, the new approach for the assessment of the arterial and reference diameters of a single segment is presented. Next, the approach is extended towards the analysis of (the ostium of) a sidebranch with its benefit clearly demonstrated. Thereafter, the latest bifurcation analysis approaches will be discussed. For all the mentioned approaches, validation studies have been carried out, of which the most important results will be presented. The manuscript is concluded by a discussion section and conclusions.

6.2 Methods and materials

6.2.1 The New Diameter Function

To quantify the degree of severity of a lesion accurately, the arterial diameters must be calculated reliably and a good estimation of the original healthy vessel size, hereinafter referred to as the "reference diameter function", must be available. This reference diameter function is an interpolated reference line based on the model of a constantly tapering vessel. Traditionally, the arterial and reference diameter values are measured at the same positions and in the same directions. This was required, since there had to be a one-to-one correspondence between the arterial and reference diameters. In most of the cases, the assumption that the actual vessel and the reconstructed vessel lie in approximately the same direction, holds. However, in cases where there is a lesion with a complex morphology or when the vessel is highly curved, this approximation may not be true, see Fig. 6.1(a).

To ensure the correct directions of the arterial diameters, the central lumen line through the vessel is used to calculate the arterial diameters. Since the direction of this centerline is



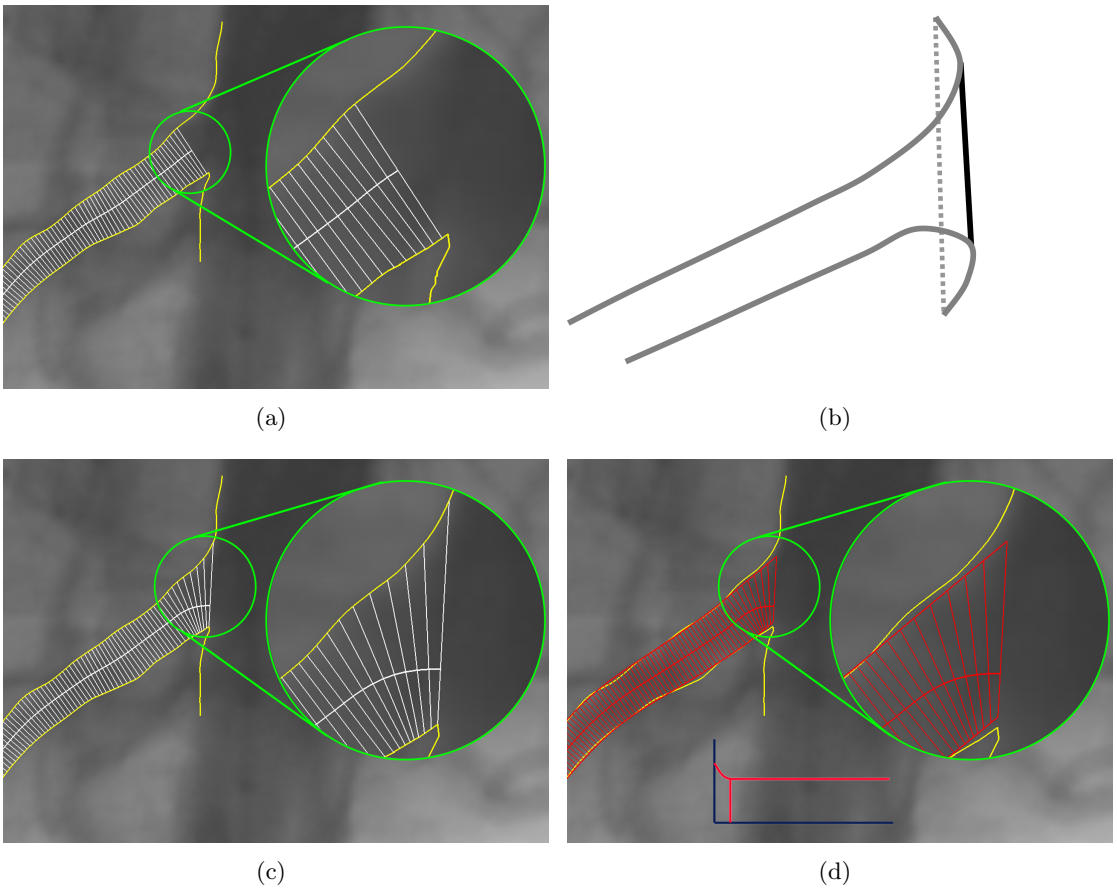
(a) (b)

Figure 6.1: An example where directions of arterial and reference diameters should be very different. The white lines represent the arterial diameters, while the red lines represent the reference diameters. a) Traditional measurement: direction of arterial diameters is not correct, b) the diameters with our new diameter method.

always locally perpendicular to the narrowest opening of a vessel, the arterial diameters, which are perpendicular to the centerline, should represent the shortest distance between the vessel walls. To assess the reference diameters, however, the global direction of the healthy vessel needs to be defined, which will result in a much smoother centerline. Therefore, the directions of the arterial diameters and the reference diameters must be relatively independent of each other. By doing that, a different correspondence needs to be defined between the arterial and reference diameters in order to be able to calculate the clinically relevant stenosis parameters.

The first step of our diameter calculation approach is the calculation of the arterial centerline using the two detected arterial contours as input. To this end, a medial axis is calculated between the two arterial contours using the wavefront propagation [80] and this medial axis is smoothed subsequently. The result is used as a centerline, with the diameters measured perpendicular to this centerline at positions sampled equidistantly along the centerline.

These diameter measurements are presented in a graph, denoted as the "arterial diameter function". From this arterial diameter function an interpolated reference diameter function is calculated using linear regression (see Reiber et al [115]). Next, the global direction of the vessel as it would have been in the healthy state is calculated, and this global direction results in the reference centerline. This reference centerline, along with the reference diameter function, is then used for the placement and orientation of the reference diameters. This is done in exactly the same way as the arterial diameters are positioned based on the arterial centerline: The reference diameters are calculated perpendicular to the reference centerline at positions equidistantly spaced along the reference centerline. Finally, the arterial diameters are linked with the reference diameters for a good correspondence.



(a) (b)

(c) (d)

Figure 6.2: Results of: a) the straight analysis, b) the ostium calculation, c) the new ostial arterial and d) the new ostial reference diameter calculations.

6.2.2 The New Ostial Analysis

When analyzing an ostial segment, we face a different problem: How to measure the diameters at the beginning of the ostium. When the sidebranch is not at a 90 degree angle to the main vessel, a single or straight segment analysis (as discussed above) isn't able to cover the ostium, as can be seen in Fig. 6.2(a).

In the most proximal part, the diameters could not be measured, because they intersected only with one of the two arterial contours. To solve this problem the direction of the diameters needs to be changed in such a way that the diameters turn towards the ostium of the vessel. In order to achieve this, the very first diameter of the sidebranch, the one that is touching (and in line with) the main vessel, needs to be found. This is not always simply the line that connects the two start points of the contours (see Fig. 6.2(b) dotted grey line). If the contours extend into the main vessel, as shown in Fig. 6.2(b), the common tangent of both contours is calculated and used as the first diameter (black line).

The rest of the diameters (between the first one in the ostium and the previously calculated

straight part) are fitted perpendicularly to a prolongation of the "straight" centerline. This centerline prolongation is achieved by means of a spline that starts perpendicularly to the first diameter and smoothly connects to the centerline that was previously calculated. Note that the spline part of the final centerline does not necessarily lie in the middle of the respective arterial diameters.

Similar to the straight segment arterial diameter calculation, the measured arterial diameters are put into an arterial diameter function graph and used to calculate the interpolated reference diameter function. However, the assumption of a constantly tapering vessel does not hold for the ostium of the segment. The morphology of the ostium makes the corresponding reference diameters increase, depending on the angle at which the sidebranch is connected to the main vessel (see Fig. 6.2(d)).

For the straight part of the segment, the reference diameter function and reference centerline are calculated in the normal way. However, for the ostium, we must estimate the reference diameters differently. The first reference diameter will be in the direction of the first arterial diameter. The following reference diameters will gradually fan towards the straight part, similar to the interpolation of the arterial diameters. The results of this method can be seen in Fig. 6.2(c) and 6.2(d).

6.2.3 The New Bifurcation Analysis

The bifurcations represent a different category in a vessel's anatomy. Their various morphologies make them challenging to analyze. For example, when analyzing bifurcation lesions by means of two straight segment analyses over the bifurcation, the interpolated reference diameter functions do not accurately predict the course of the healthy vessel segments, as shown by Lansky et al [120] and Goktekin et al [121]. When on the other hand measuring the proximal and the two distal vessel segments independently from each other by performing three straight segment analyses, lesions inside the bifurcation core cannot be measured and the procedure is very time consuming. To circumvent all these problems, we have developed new approaches for the special case of bifurcations.

Bifurcations can be divided into four building blocks, which are called segments, as shown in Fig. 6.3 and 6.5 by the different colored areas: the bifurcation core (the central part of the bifurcation which begins where the common vessel starts to split into two branches and ends at the carinal point), the proximal segment (the common part of the vessel before the bifurcation core), and the two distal segments, representing the branches. In order to analyze the various morphologies of the bifurcations properly, new methods were developed, that aim at covering the entire bifurcation and producing reliable reference estimations, without the drawback of several parts being analyzed twice. Two new types of bifurcation models were designed that cover the vast majority of bifurcation morphologies: a Y-shape and a T-shape model. Both models are combinations of the four previously defined segments.

The Y-shape Model

This model is used in case of a Y-shape bifurcation, where the distal branches have roughly the same size, roughly the same angle with the proximal vessel and a narrow angle between

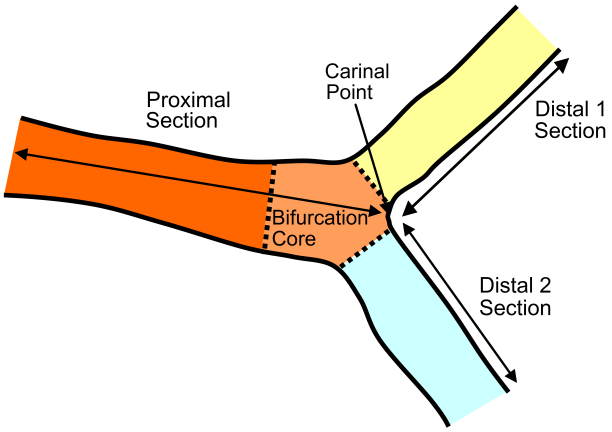
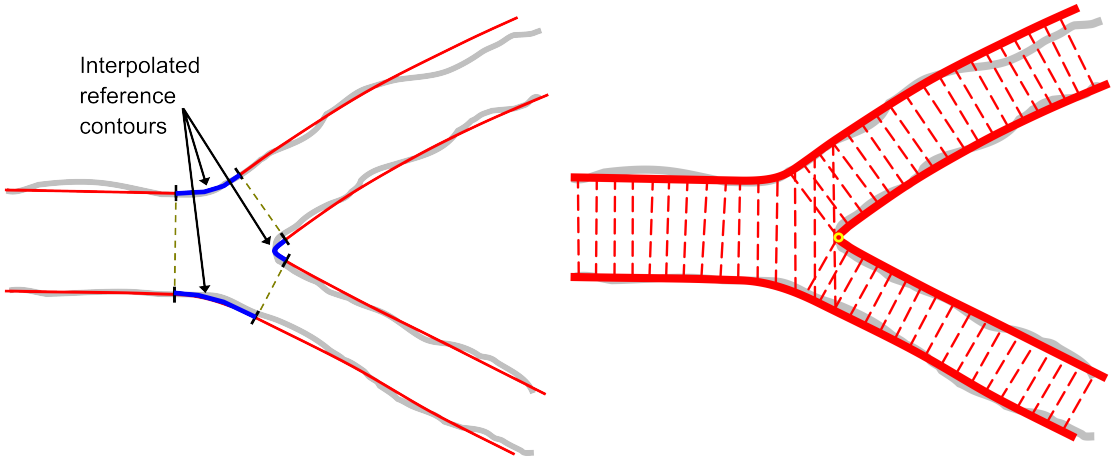


Figure 6.3: Partitioning of the bifurcation into three sections.

the two distal branches. In this model, the segment of analysis is divided into three sections: a proximal section and two distal sections. The proximal section of this model consists of the proximal segment extended with the bifurcation core, whereas the two distal sections consist of one distal segment each, as can be seen in Fig. 6.3.

As opposed to the straight and ostial approaches, the final reference diameters can only be calculated after the bifurcation's reference contours have been created. These contours are built upon the three pairs of reference contours coming from the three "straight" segments: proximal, distal 1 and distal 2, respectively. These six contours are subsequently connected two by two by means of splines, in order to create the three reference contours of the bifurcation, as shown in Fig. 6.4(a).



(a) (b)

Figure 6.4: Interpolation of the reference contours in the bifurcation core; and b) the reference diameters in the Y-shape analysis.

As already mentioned, for the two distal sections, classical straight analyses are carried out to calculate the arterial and reference diameters. In the proximal section, however, the bifurcation core violates the linear tapering assumption. Therefore, the reference diameters for the bifurcation core part are "passively" calculated based on the already calculated left and right reference contours of the bifurcation, see Fig. 6.4(b).

This model covers all vessel regions completely. There may be a small region of overlap between the proximal and distal sections, depending on the angle between them. This is required in order to always ensure a complete coverage of the bifurcation.

The T-shape Model

In this model, the segment of analysis consists of two sections: a main section and a side branch section that splits off, as shown in Fig. 6.5. This model is thereby used for bifurcations that are uneven, having one distal vessel much larger than the other one. It also covers the case where there is a wide angle between the distal branches and the case where one of the branches continues in the direction of the main vessel while the other one branches away at a steep angle with respect to the first one (a T-shape bifurcation). The main section consists of two parts: the proximal main subsection and the distal main subsection, where the proximal main subsection itself consists of the proximal segment and the bifurcation core. This division into two sections requires a virtual contour to define the boundary between them (explained later).

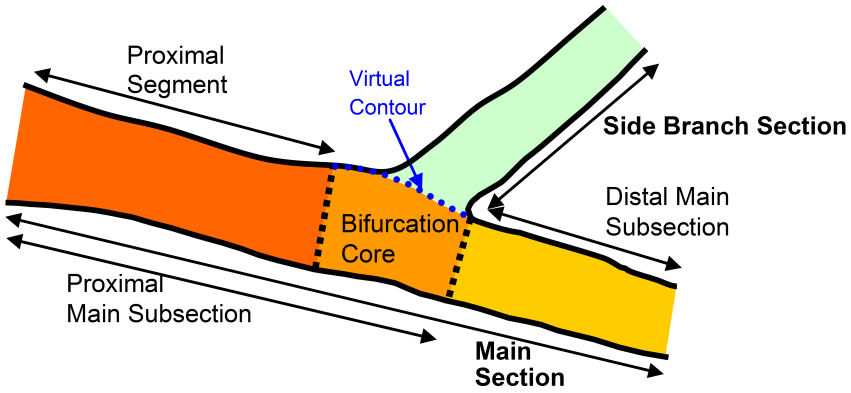


Figure 6.5: Partitioning of the bifurcation into two sections, the main section and the side branch section.

Analogous to the previously described Y-shape model, the reference contours are estimated before the reference diameters, by means of splines that connect the three pairs of "straight" reference contours computed outside the bifurcation core.

Analyzing the main section cannot be done by one single straight analysis since the proximal diameters are larger than the distal ones, the "step down phenomenon" [120], and therefore cannot be approximated by a linear interpolation. Therefore, the arterial and reference diameters are calculated for the proximal and distal segments separately by means of classical straight analyses. In the bifurcation core, the reference diameter function is linearly interpolated. This

can be seen as a transition area in the middle of the diameter function plot (see Fig. 6.6).

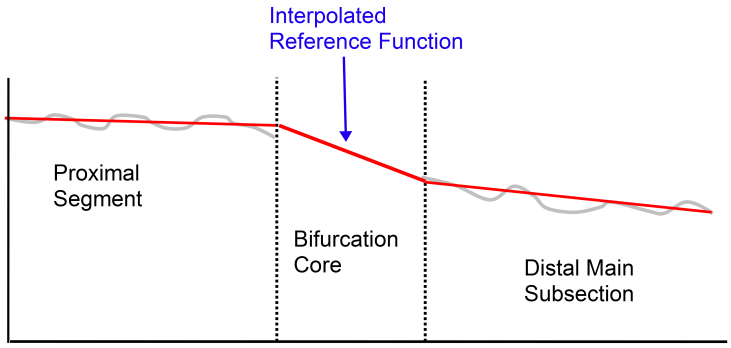


Figure 6.6: Reference diameter function of the Main Section.

By using the spline-based reference contours (see Fig. 6.4(a)) and the linearly interpolated reference diameters lengths (see Fig. 6.5), a virtual reference contour is created, which connects the proximal and distal main vessel contour inside the bifurcation core, and hereby separating the side branch from the main vessel (see Fig. 6.7(a)). Inside the bifurcation core, the reference diameters ensure a smooth connection between the proximal and the distal main subsection. The virtual reference contour is also used to delimit the arterial diameters in the bifurcation core. By keeping this contour equal for the arterial and reference diameters it is ensured that virtually any obstruction inside the bifurcation core is found opposite to the side branch. The obstructions lying on the other side will be covered by the side section.

The side section is automatically analyzed by means of an ostial model, starting from the interpolated contour that delineates the bifurcation core, and covering the rest of the side branch (see Fig. 6.7(b)). In this way, all vessel regions are completely covered and virtually no section overlap is generated.

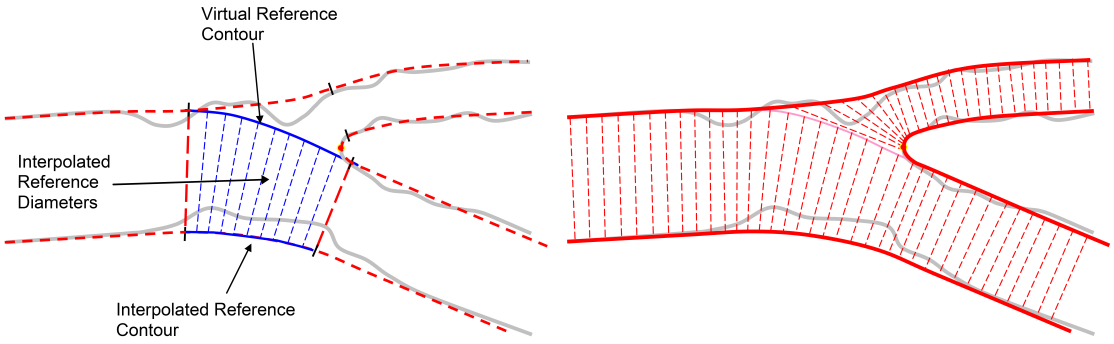


Figure 6.7: a) The virtual reference contour that bridges the sidebranch and b) the reference diameters in the T-shape analysis.

6.2.4 Validation Materials

Straight Analysis

To assess the performance of our new diameter function method for straight segments, a validation study was carried out and the earlier mentioned criterion was used: the algorithm must be able to measure the correct arterial diameters in cases with strange lesion morphologies or highly curved vessels. To that end, a routinely acquired data set of digital angiograms was composed, consisting of a wide variety of vessels, with lesions of various severities, curved and relatively straight vessels, coronary and vascular cases. This data set was used to carry out a comparison between the new and conventional diameter function approach by measuring the minimal lumen diameters (MLDs).

To show the additional value of our new method more clearly, the data set was divided into two different groups: one group with approximately straight vessels and another group with more curved vessels. This division was made by estimating the difference in direction of the arterial and reference vessel at the lesion position and taking a 10 degree threshold value into account. This was done for 46 coronary cases (29 straight and 17 curved) and 24 vascular cases (18 straight and 6 curved), resulting in four data sets. All analyses were performed by an experienced analyst using standard operating procedures (SOPs) for frame selection, segment selection and contour correction.

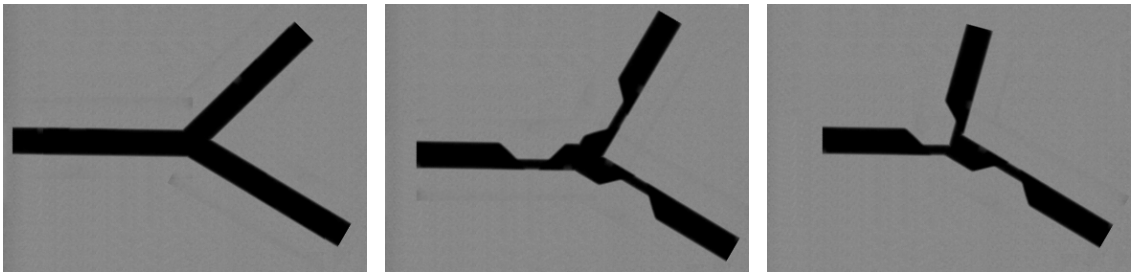
Ostial Analysis

To validate the new approach for diameter calculation in ostial segments, a similar study was carried out. The diameters distally in the vessel are calculated as a straight vessel, which means that the previously mentioned validation results of the straight vessel analysis also apply to ostial vessel segments with lesions outside the ostium. The new aspect of the ostial analysis approach is the measurement inside the ostium and therefore only vessel segments with proximal lesions are included.

For the validation, a set of 22 clinical cases was collected (9 coronary and 13 vascular) and the severity of the ostial lesions was calculated using the new and the conventional approach. The percentage diameter stenosis was used as a parameter to asses the performance of the ostial extension. It takes into account both arterial and reference diameters, which is important, since the new ostial analysis has an effect on both. Besides that, the length of the lesions was measured and compared as well. All analyses were once again performed by an experienced analyst using SOPs for frame selection, segment selection and contour correction.

Bifurcation Analysis

The performance of our new bifurcation approach was assessed using a set of artificial images and two sets of clinical data. The artificial images consisted of a set of twelve different bifurcation morphologies, showing four different angles between the two distal branches (60, 75, 90 and 105 degrees, with one branch fixed), each having a version without lesions, with separate lesions and with a combined lesion, as can be seen in Fig. 6.8. These artificial images were analyzed by an experienced analyst using the Y-shape analysis and the T-shape analysis models.



(a) (b) (c)

Figure 6.8: Examples of the artificial images: a) 75 degrees without lesions, b) 90 degrees with separate lesions, and c) 105 degrees with a combined lesion.

The clinical data that has been used consisted of two different coronary artery datasets. The first set contained ten cases, pre- and post-intervention, randomly selected from the Diverge trial, which uses the DEVAX stent, a self expanding carinal skirt stent [122]. These images were analyzed at the Cardiovascular Research Foundation (CRF) using the Y-shape model. The second set contained 9 cases, pre- and post-intervention, randomly selected from the TriReme medical TOP study, which uses stenting in the main branch with side branch conservation. These images were again analyzed at the CRF, this time using the T-shape analysis. In the DEVAX study, as well as the TriReme study, number of post-intervention analyses showed clearly the effects of an overdilated stent. Since this validation has the purpose to compare the reference and arterial results to a normal healthy vessel, the measured segments that showed an overdilation were excluded from the validation.

For the artificial images as well as the clinical data, the reference diameters just outside the bifurcation core were compared in the pre- and post-intervention analyses to prove the robustness of our reference diameter calculation in the straight segments that are influenced by the bifurcation. These diameters were measured in segments of 15 mm for the phantom data and 5 mm for the clinical data, located just distal of the bifurcation core. Furthermore, the arterial and reference diameters of the post- analysis were compared, at the same locations to assess the correctness of the reference estimation when there are no lesions.

Besides the measurements just outside the bifurcation core, the area of the bifurcation core itself was measured as well. The definition of the bifurcation core area is different for Y-shape and T-shape since in T-shape it is delimited by the virtual contour, as can be seen in Fig. 6.3 and 6.5. The value of the bifurcation core area can be calculated using the arterial contours and diameters, resulting in an arterial bifurcation core area, and using reference contours and diameters, resulting in a reference bifurcation core area. For the artificial images as well as the clinical data, the reference bifurcation core areas were compared in the pre- and post-intervention analyses to asses the robustness of the reference estimation inside the bifurcation. Finally, in the post-intervention analysis, the arterial and reference areas were compared to validate the correctness of the reference estimation.

Statistical Analysis

The measurements that have been done in the validation studies are comparisons between the new and the conventional methods or between the new method and a gold standard. In order to evaluate the comparisons, the differences are measured and the mean difference and the standard deviation of the differences are calculated, representing consecutively the systematic and random differences. Furthermore a paired T-Test is performed on the measurements, to calculate the p-values and determine the significance of the differences. A p-value smaller than 0.05 is considered a significant difference.

6.3 Results

6.3.1 Straight Analysis

The results of the MLD measurements for our novel diameter calculation method are shown in Fig. 6.9.

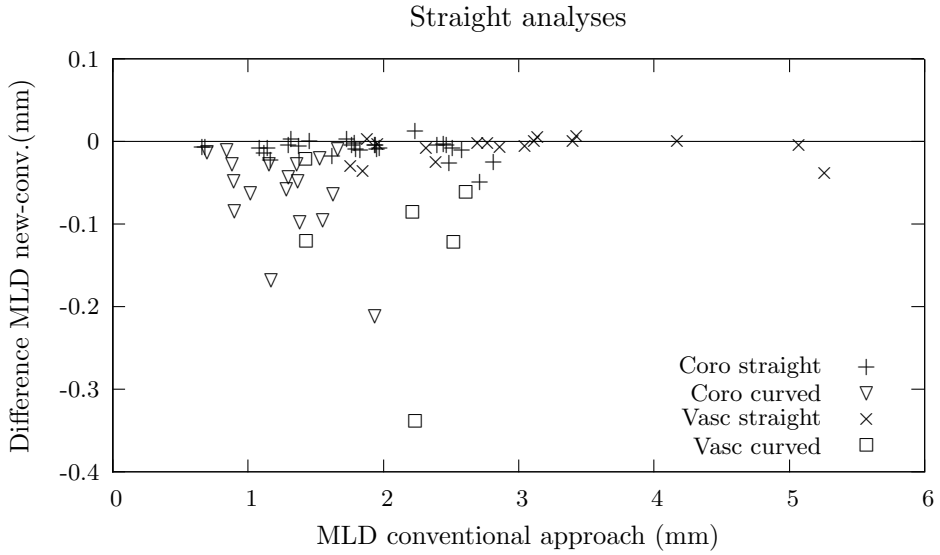


Figure 6.9: The differences in MLD between the new and the conventional approach, for curved (more than 10 degrees difference between arterial and reference diameter at the obstruction) and straight (less than 10 degrees difference) vessels, coronary and vascular.

As can be seen from Fig. 6.9 and Table 6.1, there is only very little difference (on average 0.009 mm), between the new and the conventional approach when measuring coronary or peripheral vessels that are approximately straight. Note that these small differences are significant. In curved vessels however, the new approach performs better, which is demonstrated by the smaller

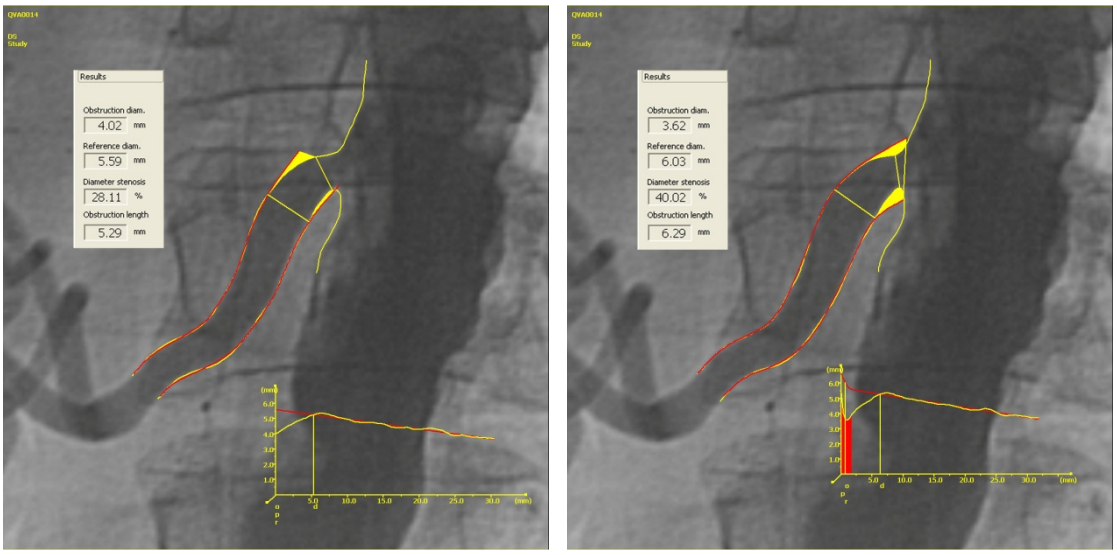
Table 6.1: The differences in MLD between the new and the conventional approach.

	Differences in MLD new - conv. (mm)		
	Systematic	Random	p-Value
Coronary straight	-0.009	0.011	**0.0002**
Coronary curved	-0.066	0.054	**0.0001**
Vascular straight	-0.009	0.014	**0.018**
Vascular curved	-0.125	0.111	**0.040**
Total	-0.032	0.056	**0.00001**

MLDs measured by the new approach. For coronary arteries this difference is on average 0.066 mm and for peripheral arteries 0.125 mm, both highly statistically significant.

6.3.2 Ostial Analysis

The validation results for our novel diameter measurement approach in ostial segments are best shown by an example (Fig. 6.10). As can be seen here, the measurement can be performed more proximal in the new analysis resulting in a larger percentage diameter stenosis and a longer lesion length. The overall results are shown in Table 6.2.



(a) (b)

Figure 6.10: An example of the a) straight segment measurements and b) the enhanced ostial measurements.

Overall, our new approach for measuring ostial lesions generally results in a higher percentage diameter stenosis (3.8 percent), and a slightly longer lesion length (0.59 mm) compared to the conventional straight analysis.

Table 6.2: The differences in percentage diameter stenosis and lesion length between the new and the conventional approach.

	Differences in %DS: new - conv.			Diff in lesion length: new - conv. (mm)		
	Systematic	Random	p-Value	Systematic	Random	p-Value
Coronary	2.3	4.2	0.13	0.65	0.66	**0.04**
Vascular	4.9	7.9	**0.05**	0.56	1.71	0.30
Total	3.8	6.6	**0.01**	0.59	1.37	0.08

6.3.3 Bifurcation Analysis

The validation results of the arterial and reference diameters of our new bifurcation approach just outside the bifurcation core can be seen in Table 6.3.

Table 6.3: The differences in reference values between the pre- and post-intervention analyses and the differences between the arterial and reference values in the post-intervention analyses, measured just outside the bifurcation core.

		Diff in reference: post - pre (mm)			Diff in post: ref - art (mm)		
	model	Systematic	Random	p-Value	Systematic	Random	p-Value
Phantom	Y-shape	0.016	0.031	**0.02**	0.002	0.008	0.48
N=16	T-shape	0.003	0.035	0.65	-0.019	0.104	0.61
Clinical	Y-shape	0.057	0.368	0.54	0.018	0.089	0.48
N=12	T-shape	0.041	0.246	0.49	-0.007	0.177	0.91

The differences in the reference measurements just distal of the bifurcation core are very small for both the artificial and the clinical images, although the difference is statistically significant for the Y-shape model in the artificial images. In the post-intervention analyses, the difference in arterial and reference measurements in the artificial images as well as the clinical data are very small.

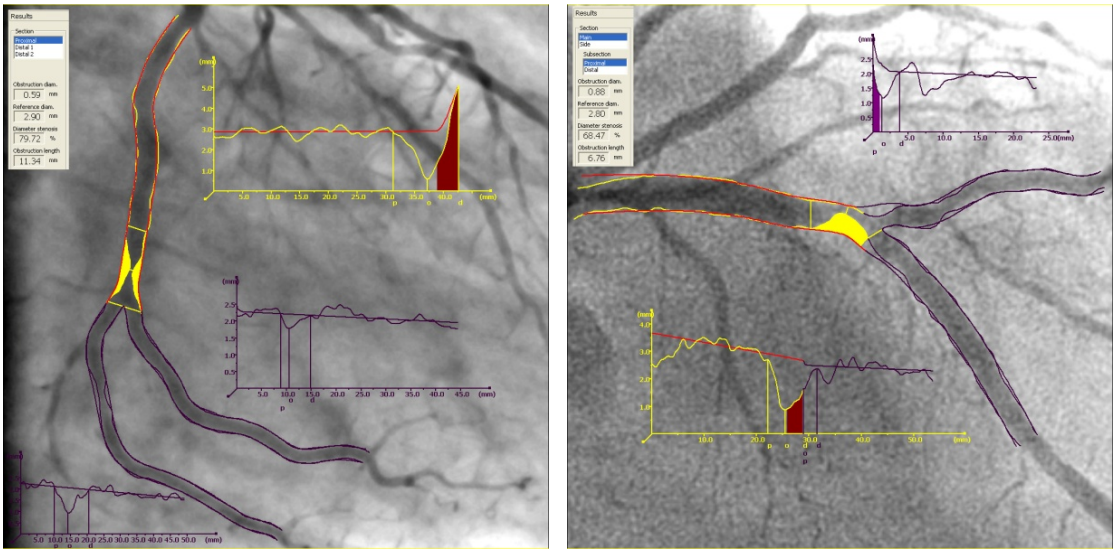
Furthermore, the measurements of the arterial and reference bifurcation core areas are shown in Table 6.4.

Table 6.4: The differences in reference bifurcation core areas between the pre- and post-intervention analyses and the differences between the arterial and reference bifurcation core areas in the post-intervention analyses.

		Diff in reference area: post - pre			Diff in area post: ref - art		
	model	Diff (mm^2)	Diff (%)	p-Value	Diff (mm^2)	Diff (%)	p-Value
Phantom	Y-shape	-0.45	-1.35	0.50	1.09	3.10	0.08
N=8	T-shape	0.18	0.53	0.50	1.36	4.60	**0.0003**
Clinical	Y-shape	2.49	13.89	**0.04**	-0.80	-5.73	0.28
N=6	T-shape	0.36	3.72	0.34	-0.90	-10.84	0.24

It shows that the differences between the reference bifurcation core areas in the pre- and post-intervention analyses are very small and not significant for the phantom and for the clinical

data, except the clinical Y-shape data (13.89%). The post-intervention analyses show reference bifurcation core areas that are slightly larger than the arterial areas for the phantom data (Y-shape 4.6% was significant) whereas the clinical data show reference areas that are smaller than the arterial areas (-5.73% and -10.84%). Note that the absolute differences in the phantoms are larger than in the clinical data, whereas the relative differences are smaller. This is due to the fact that the phantom is larger than the average vessel in the clinical images (5 mm and 2-3 mm respectively). An example of the final results of a Y-shape analysis can be seen in Fig. 6.11(a), and a T-shape analysis in Fig. 6.11(b).



(a) (b)

Figure 6.11: An example of a) the Y-shape and b) the T-shape analysis results.

6.4 Discussion

In this paper, our new approach for the measurement of arterial and reference diameters is presented. In case of straight vessel segments, the goal was to develop a robust method for measuring the obstruction diameter when the vessel is highly curved or has a complex shape. As can be seen in the validation data, the new approach achieves this goal and measures on average a smaller obstruction diameter than the conventional method. When only the "normal" vessel segments are taken into account, the measurements of the new and conventional approaches are very much comparable. For the more extreme cases, however, a significant difference of 0.08 mm is observed with the new approach which is more in line with one's expectation.

The method relies on removing the connection between the directions of the arterial and reference diameters, which makes sense especially when the local direction of the diseased vessel and the reference vessel differ much due to a high curvature or a complexly shaped lesion. Removing the connection means that it is possible to measure both arterial and reference di-

ameters in the correct directions; on the other hand, it introduces a problem of correspondence between the two. This is solved by resampling the arterial diameters at positions where the arterial centerline crosses the reference diameters.

As discussed earlier in section 2.2, the old ostial diameter measurement approach suffers from the fact that the diameters do not cover the entire proximal part (ostium) of the sidebranch. As can be derived from Fig. 6.2, this problem mainly holds for sidebranches that have a small angle with respect to the main vessel. The validation data shows that the new method allows better measurements of the minimal diameter and length of lesions proximal in sidebranches, which could not be achieved using the conventional method.

As can be seen in the validation data of the new bifurcation approaches, the reference diameters outside the bifurcation core show a very good correspondence between pre- and post-intervention (smaller than 0.06 mm). This means that the reference contours and diameters are very robust and that the references that were measured pre-intervention are a reliable estimation for the undiseased vessels. This holds for the artificial images as well as the clinical data. Furthermore, the results of the post-intervention analyses show only very small differences between the arterial and reference values for both artificial and clinical data. For the T-shape analyses, this data was only available for the main distal subsection, reducing the size of the dataset by a factor of two. To increase the number of measurements, also the images of the DEVAX-study were analyzed with the T-shape model and included in the dataset. For the sidebranch, an average value could not be measured in a similar way, but instead, the diameter was measured at one single location, the end of the ostium (5 mm after the bifurcation core), which showed similar results: a difference of 0.028 mm with a p-value of 0.67.

Also the reference bifurcation core areas show a very good correspondence between pre- and post-intervention in both the phantom images and the clinical T-shape data. Only the results of the Y-shape study in clinical data show a larger difference (13.89%) in reference bifurcation core area. This is due to the fact that although the cases with an overdilated stent had been excluded, two borderline cases were still present in the dataset. Since the analyzed sections were short, there was not enough normal vessel present, which caused the reference contours to follow the arterial contours and go too wide. Without the data of these two cases, this difference goes down to 8.9%, with a p-value of 0.23. In the post-intervention analyses of the phantom images, the reference bifurcation core areas are slightly larger than the arterial areas. This can be explained by the fact that our method interpolates the reference contours from the different sections in a smooth way, which is more likely in real clinical data. Since our artificial images show sharp angles between the segments, the reference bifurcation core area is slightly larger, which turns out to be a significant difference in T-shape (1.36 mm^2 or 4.60%) due to the small random errors in the measurements (0.15 mm^2). In the clinical cases, the bifurcation core areas show a slightly smaller reference area compared to the arterial area (not significant).

The new parameter that is introduced here, the bifurcation core area and more specifically the percentage bifurcation core area reduction, is an interesting parameter that quantifies the severity of lesions inside the bifurcation core, similar to the percentage diameter reduction that is used in the straight segments. It can be used to monitor the vessel over time or during an intervention, or to assess the results of the intervention procedure afterwards.

6.5 Conclusions

The new approach for measuring the arterial and reference diameters, presented in this paper, has proven to outperform the conventional QCA approaches. For the straight vessel segments, it was demonstrated that releasing the connection between the direction of the arterial and reference diameters results in a significantly better measurement of the obstruction diameter in highly curved parts of the vessel. For "normal" straight segments, no significant difference was found between the new and the conventional approach.

Our newly developed method for the analysis of ostial vessel segments has proven to achieve accurate measurements of diameters and lengths of proximal lesions in sidebranches, which could not be achieved using the conventional method. Furthermore, it was demonstrated that our two new bifurcation approaches achieve accurate results in the segments just outside the bifurcation core and produce reliable measurements of the arterial and reference bifurcation core areas.

In summary, a major step forward has been set in the quantitative analyses of coronary and vascular lesions from X-ray angiographies. These methodological improvements will provide accurate and robust solutions for all the clinical research angiographic QCA applications.

Acknowledgements

We would like to thank the Cardiovascular Research Foundation (CRF) in New York and in particular Alexandra Lansky, MD and Maria Corral for analyzing the clinical data and therefore helping us validating our new bifurcation approaches.

CHAPTER 7

Dedicated bifurcation analysis: basic principles

This chapter was published as:

Tuinenburg JC, Koning G, Rareş A, Janssen JP, Lansky AJ, Reiber JHC.
Dedicated bifurcation analysis: basic principles.
Int J Cardiovasc Imaging. 2011;27(2):167-174

Abstract

Over the last several years significant interest has arisen in bifurcation stenting, in particular stimulated by the European Bifurcation Club. Traditional straight vessel analysis by QCA does not satisfy the requirements for such complex morphologies anymore. To come up with practical solutions, we have developed two models, a Y-shape and a T-shape model, suitable for bifurcation QCA analysis depending on the specific anatomy of the coronary bifurcation. The principles of these models are described in this paper, as well as the results of validation studies carried out on clinical materials. It can be concluded that the accuracy, precision and applicability of these new bifurcation analyses are conform the general guidelines that have been set many years ago for conventional QCA-analyses.

7.1 Introduction

In interventional cardiology, Quantitative Coronary Arteriography (QCA) has been used for on-line vessel sizing for the selection of the interventional devices and the assessment of the efficacy of the individual procedures, for the on-line selection of patients to be included or excluded in clinical trials based on quantitative parameters (e.g. small vessel disease), and for training purposes. But, in particular, QCA has been applied worldwide in core laboratories and clinical research sites to study the efficacy of the procedures and devices in smaller and larger patient populations in off-line situations. Newer developments are directed towards the 3D reconstruction of the coronary arteries and the fusion with IVUS or OCT [123, 124, 125].

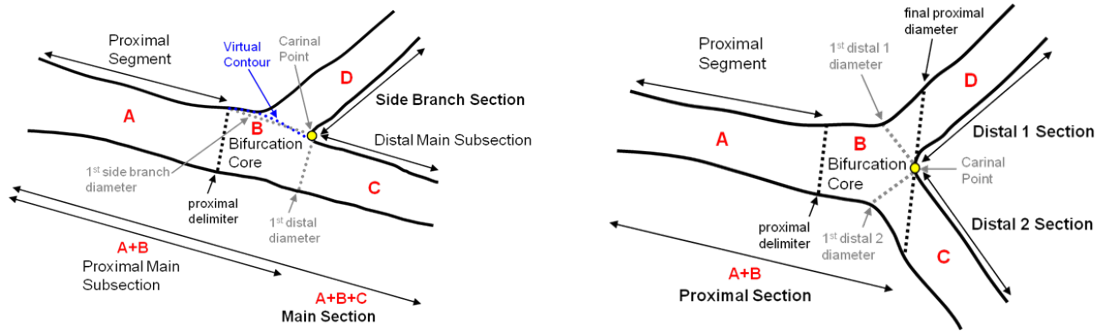
The goal of this paper is to provide a brief overview of the basic principles of a modern QCA software package, particularly on the field of coronary bifurcation analysis. This is best illustrated by the QAngio® XA package (Medis medical imaging systems bv, Leiden, the Netherlands).

7.2 Bifurcation analysis

With the expanding practice of stenting coronary bifurcation lesions worldwide [126], the need for reliable, standardized and reproducible quantitative bifurcation analyses became apparent. Hence, the QAngio XA version 7.2 bifurcation application was developed, which contains two bifurcation models: a T-shape bifurcation model (suitable for bifurcations with a standard side branch structure: Fig. 7.1(a)) and a Y-shape bifurcation model (suitable for bifurcations with distal branches of equal size: 7.1(b)). The particular advantage of these models is that they combine the proximal and two distal vessel segments with the bifurcation core, resulting in a total of two or three sections (depending on the model type), all derived from one analysis procedure, such that each of these sections has its own diameter function and associated parameter data.

To be able to start a bifurcation analysis, an analysis frame is chosen from the selected image run in which the target vessel is fully contrast-filled (usually second or third cardiac cycle following contrast injection) and in a "stable" position (preferably end-diastole), i.e. minimal motion with respect to neighboring frames to prevent motion blur [127, 128]. As a first step, the user selects three pathline points in the image to define the arterial bifurcation segment: a start point in the proximal segment and one end point in each of the two distal segments are required. Subsequently, independent of the model type, two pathlines through the bifurcation segment of interest are computed automatically (Fig. 7.2(a)) based on the wavefront propagation principle ('the wavepath approach') [84, 102], followed by the automated detection of the arterial contours of all three vessel segments at once (Fig. 7.2(b)).

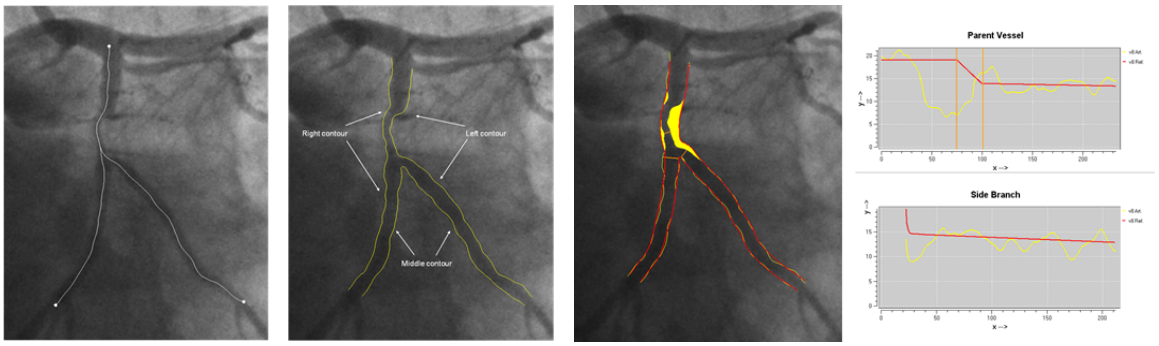
This arterial contour-detection procedure is carried out in two iterations relative to a model (here explained for a straight vessel, to keep things simple). In the first iteration, the pathline is used as the model (Fig. 7.3(a)). To detect the contours, scanlines are defined perpendicular to the model (Fig. 7.3(b)). For each point or pixel along such a scanline, the corresponding edge-strength value (local change in brightness level) is computed as the weighted sum of the corresponding values of the first- and second-derivative functions applied to the brightness values along these scanlines (Fig. 7.4). The resulting edge-strength values are input to the so-called minimum cost contour-detection algorithm (MCA) [36, 39, 129], which searches for an optimal



(a) (b)

Figure 7.1: Schemes of the a) T-shape model and b) Y-shape model, explaining the segments, proximal delimiter, interpolated contour and sections terminology. For each model, four segments that represent the building blocks of the models are generated by the software. a) Using the T-shape model, the arterial and reference diameters of the ostium of the side branch and the whole main section (including the transition within the bifurcation core) can be accurately determined. b) Using the Y-shape model, the arterial and reference diameters up to the carinal point and in the distal 1 and 2 sections can be determined accurately.

contour path along the entire segment (Fig. 7.3(c)). The individual left and right vessel contours, detected in the first iteration, now serve as models for the MCA procedure in the second iteration, resulting in the initially detected arterial contours (Fig. 7.3(d)). If the operator does not agree with one or more parts of the initially detected contours, these can be edited/corrected in various ways. In a similar manner, the arterial contours are detected for the bifurcation analysis, resulting in three contours: the left, right and middle contour (Fig. 7.2(b)).



(a) (b) (c)

Figure 7.2: An example of the T-shape model bifurcation analysis. a) The three pathline points with the two detected bifurcation pathlines. b) The three detected arterial contours. c) The final analysis contours, plaque filling and the two corresponding diameter functions of the main and side branch sections.

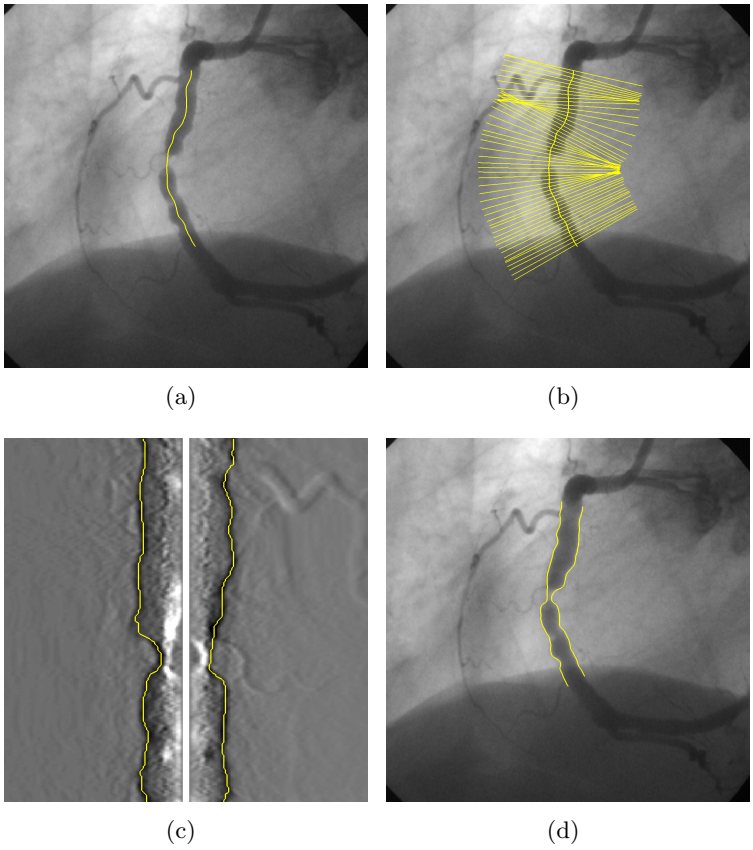


Figure 7.3: Basic principles of the minimum cost contour-detection algorithm (MCA). a) Initial segment with pathline, b) scanlines defined, c) straightened for analysis; contours calculated, d) contours returned to initial image.

The bifurcation core of the T-shape model is defined as the area between the automatically determined proximal delimiter in the proximal main subsection (of which the position is independent of the presence of a lesion) and the carinal point, which is flanked at one side by the first diameter of the distal main subsection (identical to the distal main segment) and at the other side by the interpolated (virtual) contour between the proximal and distal main segments (Fig. 7.1(a)). From the arterial contours and the interpolated contour, two sections are defined: the main section (i.e. the proximal main, distal main and bifurcation core segments merged) and the side branch section (identical to the side branch segment) (Fig. 7.1(a)). From the left- and right-hand contours of the main section, an arterial diameter function is calculated following the conventional straight analysis approach (Fig. 7.5(a), yellow graph), while for the side branch section the ostial analysis approach is followed [130], making sure that the arterial diameters at the ostium of the side branch are measured properly (Fig. 7.5(b), yellow graph).

The most widely used parameter to describe the severity of an obstruction is the percentage of diameter stenosis. Calculation of this parameter requires that a reference diameter value is

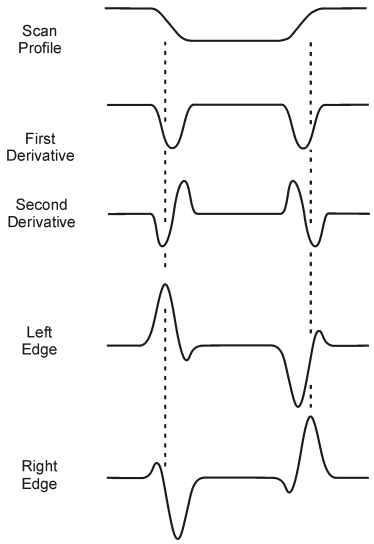


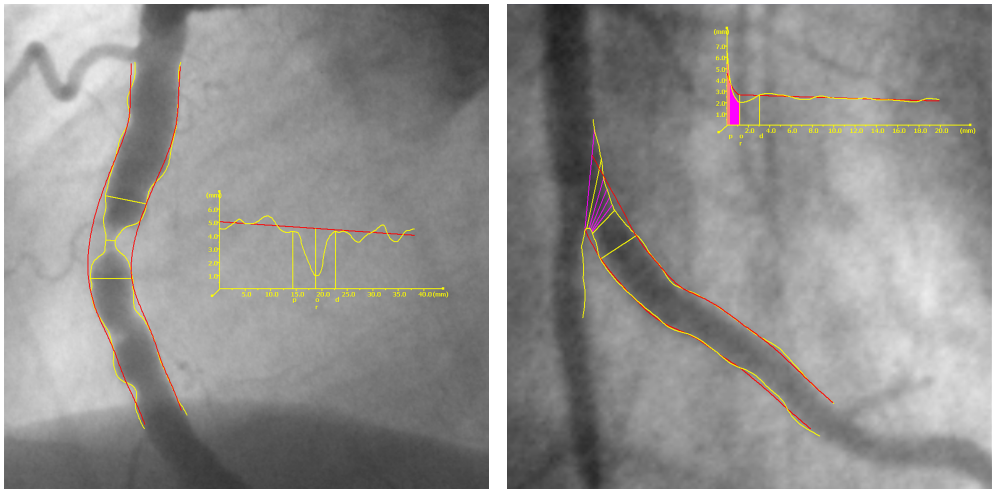
Figure 7.4: The edge-strength values along a scanline. Schematic presentation of the brightness profile of an arterial vessel assessed along a scanline perpendicular to the local pathline direction and the computed 1st-derivative, 2nd-derivative, and the combinations of these 1st- and 2nd-derivative function; the maximal values of the last functions determine the edge positions.

computed, for which two options are available: (1) a user-defined reference diameter as positioned by the user at a so-called "normal" portion of the vessel, and (2) the automated or interpolated reference diameter value. In practice, this last approach is preferred because it requires no user interaction and takes care of any tapering of the vessel. For a conventional straight analysis, a reference diameter function is calculated by an iterative regression technique (excluding the influence of any obstructive or ectatic area) and displayed in the diameter function as a (slightly tapering) horizontal straight line (Fig. 7.5(a), red line), which represents the best approximation of the vessel size before the occurrence of a focal narrowing. Now that the reference diameter function is known, reference contours can be reconstructed around the actual vessel segment, representing the original size and shape of the vessel before any disease occurred. The value of the reference diameter function at the location of the obstruction diameter equals the reference diameter, so that neither overestimation nor underestimation occurs. Finally, from the reference diameter and the obstruction diameter, the percent diameter stenosis is calculated.

However, due to the "step down" phenomenon caused by the bifurcating vessels, it is not a trivial task to derive a suitable reference diameter function for the entire main section [120]. Therefore, the calculation of the reference diameter function is based on each of the three segments separately. By this approach, it is assured that both the proximal and distal main (interpolated) reference diameter functions are only based on the arterial diameters outside the bifurcation core. Finally, the reference diameter function of the bifurcation core is based on the reconstruction of a smooth transition between the proximal and distal vessel diameters. As a result, the reference diameter function graph of the entire main section will be displayed as one function, which is composed of three different straight reference lines that are linked together

(Fig. 7.2(c), right above). For the side branch section an "ostial" reference diameter function calculation is used (Fig. 7.5(b), red line) [130], which is displayed as one function, which is straight and slightly curved proximally (Fig. 7.2(c), right under).

The bifurcation core of the Y-shape model is defined as the area between the automatically



(a) (b)

Figure 7.5: Examples of the a) straight analysis and b) ostial analysis, each with their own contours and specific diameter function (graph).

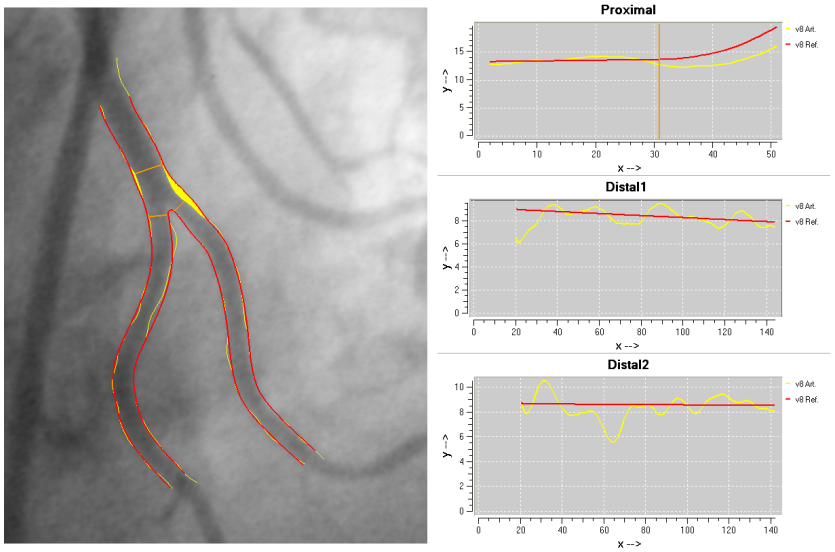
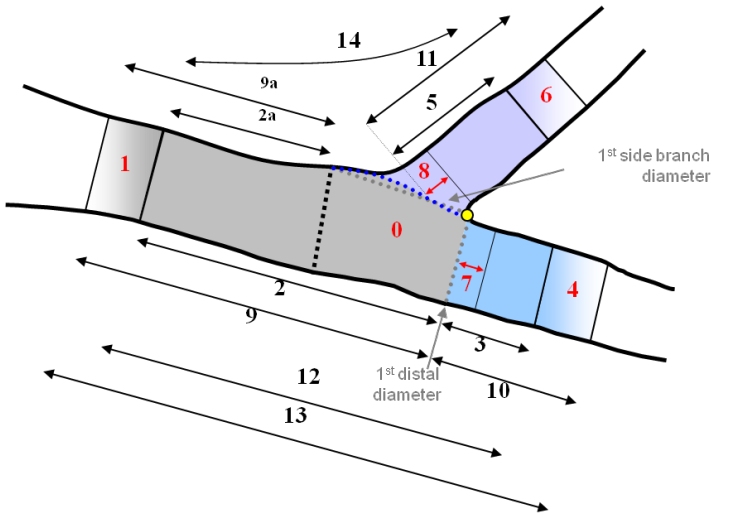


Figure 7.6: An example of the Y-shape model bifurcation analysis. The final analysis contours, plaque filling and the three corresponding diameter functions of the proximal, distal 1 and distal 2 sections, respectively.

determined proximal delimiter in the proximal section and the carinal point (Fig. 7.1(b)). From the arterial contours and by using the carinal point, three sections are defined: the proximal section (i.e. the proximal and bifurcation core segments merged), the distal 1 section and the distal 2 section (Fig. 7.1(b)). For each of these sections the corresponding arterial diameter functions are calculated following the conventional straight analysis approach [130]. This method guarantees that within the bifurcation core the arterial diameters are measured in their fullest extent (e.g. important for skirt stenting).

In order to derive a suitable reference diameter function for each section, again the calculation of the reference diameter function is based on each of the segments separately. The reference diameter function of the bifurcation core itself is based on reconstructed reference contours between the proximal segment and two distal sections. As a result, the reference diameter function graph of the entire proximal section will be displayed as one function, which is straight for the proximal segment and curved in the bifurcation core. The two reference diameter functions of the distal sections will each be displayed as one function and are straight (Fig. 7.6).

The reported bifurcation analysis results of all sections (both models) will be a complete listing of the angiographic parameters similar to the conventional straight QCA, including the obstruction, reference, minimum, maximum, and mean diameters and areas, the percent diameter and area stenosis as well as the vessel and lesion lengths. Additionally, an option for



0 – Bif Core	7 – Ostium Distal Main (3 or 5 mm)
1 – Edge Proximal	8 – Ostium Side Branch (3 or 5mm)
2 – Stented Proximal Main	9 – Analyzed Proximal Main
2a – Stented Proximal Segment	9a – Analyzed Proximal Segment
3 – Stented Distal Main	10 – Analyzed Distal Main
4 – Edge Distal Main	11 – Analyzed Side Branch
5 – Stented Side Branch	12 – Stented Main
6 – Edge Side Branch	13 – Analyzed Main
	14 – Stented Proximal-Side Branch

Figure 7.7: A schematic overview of the edge segment analysis for the bifurcation's T-shape analysis model.

edge segment analysis over the bifurcation (both models) will be available for the assessment of (drug eluting) stent segments and the corresponding stent- and ostial edge segments (Fig. 7.7; T-shape). For each of these (sub)segments the complete parameter set including some edge specific parameters (e.g. MLD position relative to the stent boundary or segment start position, etc.) will be reported, to allow to study the regression and progression of the bifurcation lesion to the fullest.

7.3 Validation

Whichever QCA analytical software package is being used, it will always produce numbers describing the morphology of the coronary segment analyzed. However, validation studies must demonstrate the true strengths and weaknesses, as well as the clinical validity of such analytical package.

For a QCA technique to be acceptable, guidelines for systematic and random error (a.k.a. accuracy and precision) values of absolute vessel dimensions have been established. These guidelines are shown in Table 7.1 [118]. Over the years we have carried out many validation studies, which all have been presented in the international literature (e.g.: [118, 131, 47]).

Table 7.1: Guidelines for systematic and random errors of a state-of-the-art QCA System.

Type of study	Systematic error (mm)	Random error (mm)	
		Guidelines	Result ranges
Plexiglass phantom, off patient	<0.10	0.10 - 0.13	0.06 - 0.12
Plexiglass phantom, on patient	<0.10	0.10 - 0.13	0.10 - 0.11
		Guidelines	D_{obs} D_{ref}
Intra-observer variabilities		0.10 - 0.15	0.10 0.13
Inter-observer variabilities		0.10 - 0.15	0.11 0.13
Short-term variabilities		0.15 - 0.25	0.19 0.22
Medium-term variabilities		0.20 - 0.30	0.18 0.34
Inter-core lab variability			0.14 0.15

Table 7.2: The intra-observer differences (Mean ± StDev) of the obstruction and reference diameters, for both the T-and Y-shape models. All values are very low, demonstrating the high reproducibility of the analyses with both models, including lesions at the bifurcation core.

		Prox Main (incl bif core)	Dist Main	Side Branch
T-shaped model (n=18)	D_{obs} (mm)	0.01 ± 0.03	-0.01 ± 0.04	0.01 ± 0.05
	D_{ref} (mm)	0.08 ± 0.10	0.01 ± 0.08	0.04 ± 0.10
Y-shaped model (n=18)	D_{obs} (mm)	0.00 ± 0.03	0.02 ± 0.08	-0.01 ± 0.06
	D_{ref} (mm)	0.03 ± 0.11	-0.03 ± 0.09	0.02 ± 0.10

Considering the bifurcation analysis, the most relevant bifurcation validation studies are of the bifurcation's diameter functions [132] and the intra-observer variability of the T- and Y-

shape models (see Table 7.2). All values are very low, demonstrating the high reproducibility of the analyses with both models, including lesions at the bifurcation core.

7.4 Conclusion

Semi-automated segmentation techniques are able to detect the luminal boundaries of coronary arteries from two-dimensional digital X-ray arteriograms after minimal user interaction. QCA can be used in an off-line mode for clinical research studies and in an on-line mode during the interventional procedure to support the clinical decision-making process. New approaches have become available for more extensive analyses such as the coronary bifurcation analysis.

CHAPTER 8

Clinical validation of the new T- and Y-shaped models for the quantitative analysis of coronary bifurcations: An inter-observer variability study

This chapter was accepted for publication as:

Tuinenburg JC, Janssen JP, Kooistra R, Koning G, Corral MD, Lansky AJ, et al.
Clinical validation of the new T- and Y-shape models for the quantitative analysis of coronary bifurcations: An inter-observer variability study.
Cathet Cardiovasc Interv. 2012

Abstract

Objectives: This paper presents the results of an inter-observer validation study of our new T- and Y-shape bifurcation models including their edge segment analyses.

Background: Over the last years, the coronary artery intervention procedures have been developed more and more towards bifurcation stenting. Since traditional straight vessel QCA is not sufficient for these measurements, the need has grown for new bifurcation analysis methods.

Methods: In this paper, our two new bifurcation analysis models are presented, the Y-shape and T-shape model. These models were designed for the accurate measurement of the clinically relevant parameters of a coronary bifurcation, for different morphologies and intervention strategies and include an edge segment analysis, to accurately measure (drug-eluting) stent, stent edge and ostial segment parameters.

Results: The results of an inter-observer validation study of our T-shape and Y-shape analyses are presented, both containing the pre- and post-intervention analyses of each 10 cases. These results are associated with only small systematic and random errors, in the majority of the cases compliant with the QCA guidelines for straight analyses. The results for the edge segment analyses are also very good, with almost all the values within the margins that have been set by our brachytherapy directive.

Conclusions: Our new bifurcation approaches including their edge segment analyses are very robust and reproducible, and therefore a great extension to the field of quantitative coronary angiography.

8.1 Introduction

Since the late 1970s, Quantitative Coronary Arteriography (QCA) has become the standard method for hospitals and core laboratories to quantify the effects of pharmacological agents and interventional devices on the regression and progression of coronary artery disease [133]. In the past, the emphasis has always been on the so-called straight vessel, for which conventional QCA has demonstrated to be a robust technique for the accurate and reliable assessment of the arterial dimensions (lesions and other clinically relevant parameters). However, in the last decade the interventional armaments for coronary and peripheral artery lesions have expanded significantly (e.g., with drug-eluting stents and bifurcation stents). Especially with the increasing interest in the quantification of bifurcating arterial vessels and their lesions, it became clear that conventional QCA did not meet the requirements anymore for a standardized and accurate quantification of the bifurcating vessel. In particular issues regarding the determination of the correct reference diameter per vessel segment, the resulting over- and underestimations of the percentage diameter stenosis of the bifurcation lesion, and the bifurcation lesion length became apparent [120]. To overcome these problems, a special bifurcation analysis option needed to be developed. The first approach that we developed was the so-called three-section bifurcation analysis model, which became commercially available with the release of QVA-CMS® V6.0 in 2005 and its successor QAngio XA V7.0® in 2006 (both Medis medical imaging systems BV, Leiden, The Netherlands). The particular advantage of this three-section model was that it combined the proximal and two distal artery segments (fragments) with the central fragment of the bifurcation, resulting in three separate analyses (sections) each with its own set of parameters, all derived in one analysis procedure. The accuracy and precision of the bifurcation analysis results for each of the three sections was conform or better than the conventional straight QCA analysis results [134, 135, 121], so that useful information about the bifurcating vessel and the extent and severity of the bifurcation lesion was provided for the various clinical studies in which this technique was employed [136, 137, 122, 138].

However, based on further discussions with key opinion leaders and practical experiences regarding the optimal derivation of clinically relevant parameters, a new QAngio XA software package (Version 7.2, Medis medical imaging systems BV, Leiden, The Netherlands) was developed with two new models for the bifurcation analysis option. These two new models were developed in order to provide optimal bifurcation data for the specific bifurcation morphology at hand, and such that these models follow the widely accepted Medina classification [120, 139, 140]. As a result, there is now a two-section model for the T-shaped bifurcation (a main vessel being a proximal vessel that continues in the same direction into a distal vessel, and a side branch at an acute angle) and a three-section model for the Y-shaped bifurcation (a proximal vessel with two distal branches that are approximately equal in size and split off at similar angles). Both new models are based upon a typical combination of the proximal and two distal vessel segments with the bifurcation core, but now resulting in two or three sections (depending on the model type), respectively, such that each of these sections has its own diameter function and associated parameter set.

The advantages (including decreased analysis time) and accuracy of the bifurcation analysis mentioned in previous studies on its comparison with conventional straight analyses [2,3], holds for the new bifurcation models as well [17,18] due to the fact that the models are based on the

same principles, composed of similar building blocks, and use the same underlying algorithm for the straight parts.

The two bifurcation models are mainly based upon vessel anatomy, which can be automatically determined by the software. However, practice shows that the applied intervention (e.g. provisional T-stenting or skirt stenting) mainly defines the bifurcation model type, due to the available model type specific parameter set (see further on). Therefore, for a selected stent study, the model type can be fixed in advance by the user, to allow simple comparison of the study data.

Similar to the QCA developments for straight vessel stenting, the bifurcation analysis required the ability to deal with drug-eluting stent (DES) analysis as well. Therefore, both bifurcation analysis models are extended (optional) with an edge segments analysis. The segment numbering (see below) is achieved in collaboration with and based upon the methodology proposed by Lansky et al. [120]. The goal of this paper is to present the two new bifurcation models, the edge segments analysis and their accompanying inter-observer variability data. With these validation data we want to prove that the two new bifurcation analysis models are very reproducible in use.

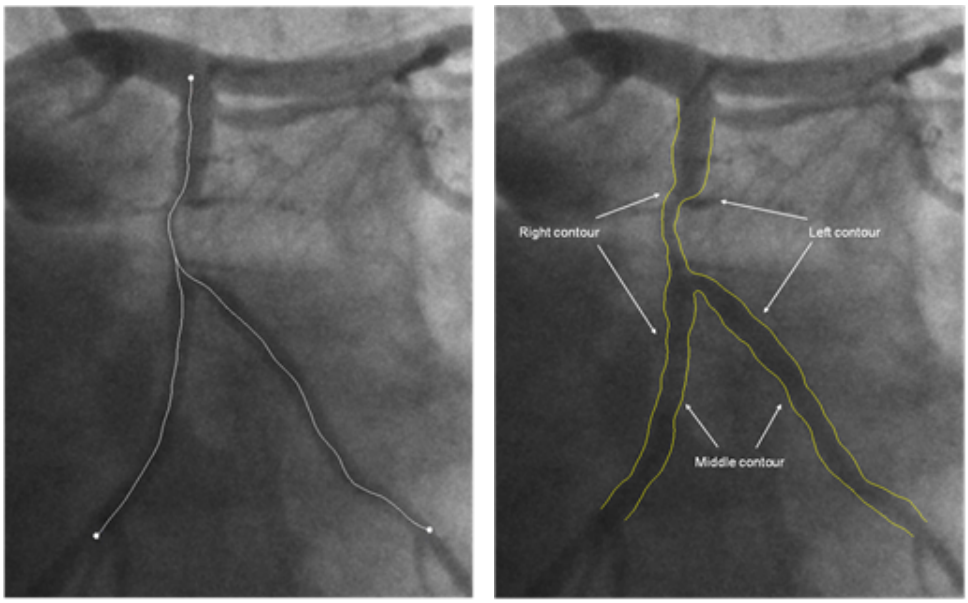
8.2 Material and Methods

8.2.1 Methods

The basic principles of the coronary bifurcation analyses of the T-shape and Y-shape models can be summarized as follows: As a first step, the user places three pathline points to define the bifurcating vessel segment of analysis: a start point in the proximal vessel and one end point in each of the two distal vessels. Subsequently, independent of the model type, two wavepath pathlines are detected (Figure 8.1(a)) [84, 102] followed by the automated detection of the arterial contours of all three vessel segments at once using the minimum cost algorithm (MCA) (Figure 8.1(b)) [39, 129]. When the QCA operator does not agree with one or more specific parts of the initially detected contours, the operator can edit the contours by choosing the automatic (attraction point) or manual contour correction option, similar to the conventional and established QCA approach for straight vessels [129, 141, 115].

In addition to the arterial contours, the initial position of the carinal point (split point of the two distal vessels) on the arterial middle contour is automatically determined as well. In case the operator finds the local arterial middle contour at the carinal point or the position of the carinal point itself being improperly detected, the position of the carinal point can be edited by manually dragging the carinal point to a different position. Subsequently, the MCA algorithm searches again for the contours, based on the available image information and the modified carinal point (that serves as a support point).

In the next step, the position of the proximal delimiter of the bifurcation core is automatically determined. This position is independent of the presence of lesions, with the advantage of having a similar position throughout Pre, Post and FU analyses. The positions of the proximal delimiter and the carinal point serve to define the four building blocks of the two bifurcation models. In the following paragraphs, the differences between the two models will be described.



(a) (b)

Figure 8.1: An example of a bifurcation analysis with: a) the three pathline points and the two detected bifurcation pathlines which are coinciding in the proximal segment; and b) the three detected arterial contours.

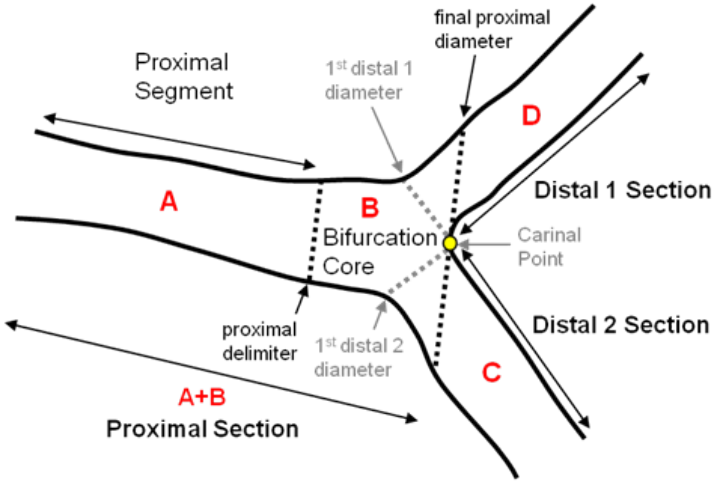


Figure 8.2: Scheme of the Y-shape model, explaining the segments, proximal delimiter and sections terminology. The partitioning of the bifurcation segment is into three sections: the proximal section, the distal 1 section and the distal 2 section. Using this model, the arterial and reference diameters up to the carina point and the distal 1 and 2 sections can be determined accurately.

The Y-shape model

The bifurcation core of the Y-shape model is defined as the area between the automatically determined proximal delimiter and the carinal point. Based on the arterial contours and the carinal point, three sections are defined (the proximal section, the distal 1 section and the distal 2 section: Figure 8.2) and their corresponding arterial diameter functions are calculated following the conventional straight analysis approach [115]. This method guarantees that within the bifurcation core the arterial diameters are measured to their fullest extent.

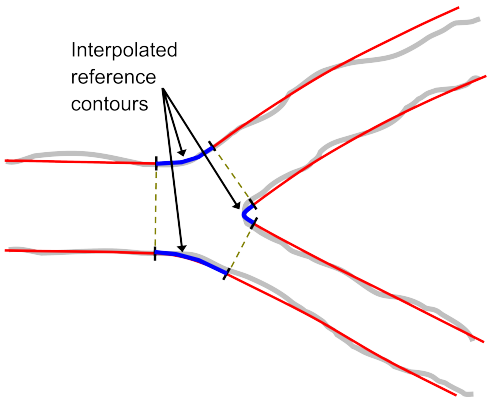


Figure 8.3: The interpolation of the reference contours in the bifurcation core.

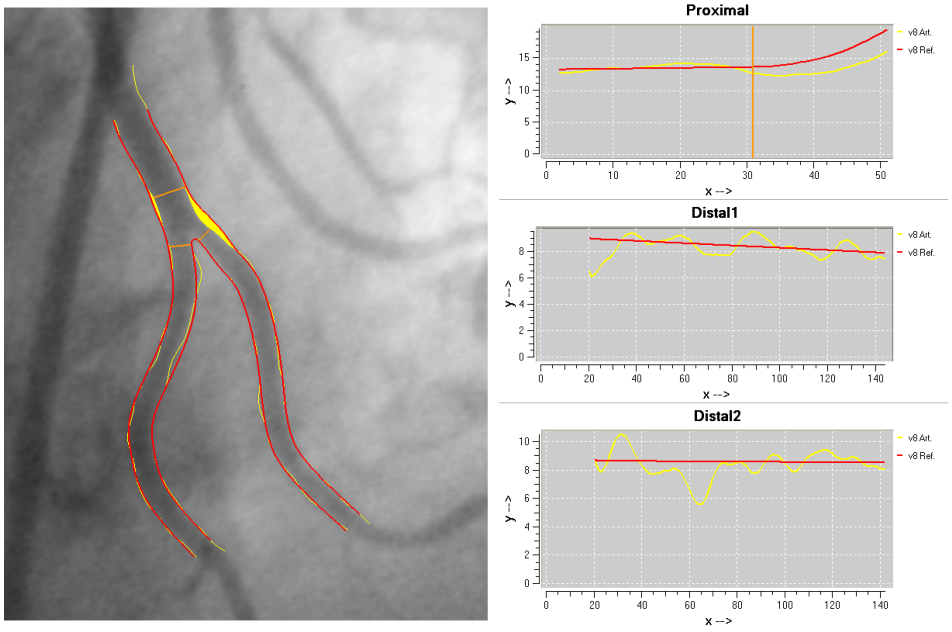


Figure 8.4: An example of a bifurcation analysis using the Y-shape model, showing the final arterial and reference contours, plaque filling and the three separate diameter functions of the three sections.

It is well known, that it is not a simple task to obtain an appropriate reference diameter function for the entire bifurcating vessel segment, due to the "step down" phenomenon [120]. To obtain a suitable and automatically derived reference diameter function for each section, the calculation of the reference diameter function is based on each of the vessel segments separately (so excluding the bifurcation core). In practice this means that from the arterial diameter functions of the proximal and two distal vessel segments the corresponding interpolated reference diameter functions are derived separately by an iterative regression technique [115]. In this way, it is assured that these reference diameter functions are only based on the arterial diameters outside of the bifurcation core. The reference diameter function of the bifurcation core itself is mainly based on two interpolated reference contours (spline-based), reconstructing a smooth transition between the reference diameters of the proximal and the two distal vessel segments [132] (Figure 8.3). As a result, the reference diameter function graph of the proximal section will be displayed as one function, which is straight for the proximal segment and curved in the bifurcation core (Figure 8.4). The two reference diameter functions of the distal sections are straight and will each be displayed as one function (Figure 8.4).

The T-shape model

The bifurcation core of the T-shape model is defined as the area between the proximal delimiter and the carinal point, delimited at one side by the first diameter of the distal main subsection and at the other side by a virtual contour between the proximal segment and the distal main subsection (Figure 8.5). This virtual contour, which separates the side branch from the main vessel, is created by making use of the interpolated reference contours (see text above) and the linearly interpolated reference diameters of the bifurcation core (see text below) [132]. Based on the arterial contours and the virtual contour, two sections are defined: the combination of the proximal segment, distal main subsection and the bifurcation core defines the first section (i.e. main section), while the side branch forms the second section (Figure 8.5). For the entire main section the arterial diameter function is continuously calculated following the conventional Medis straight analysis approach, while the Medis ostial analysis approach is followed for the side branch section, to assure that the arterial diameters at the ostium of the side branch are measured properly [115, 132].

Similar to the Y-shape model, the T-shape model deals with the "step down" phenomenon in a partly comparable manner. This means that from the arterial diameter functions of the proximal segment and distal main subsection, the corresponding interpolated reference diameter functions are derived separately. In the bifurcation core, the reference diameters are linearly interpolated (by means of a straight reference diameter function; red line [see Figure 8.6(a)]), reconstructing a transition between the proximal and distal main reference diameters. By using the interpolated reference contour opposite to the side branch ostium and the linearly interpolated reference diameters, a virtual contour is created (see Figure 8.6(b)).

It should be noted that besides being the virtual contour for the reference diameters, this contour is used to delimit the arterial diameters in the bifurcation core as well. Note that the arterial diameters inside the virtual reference contour are left unchanged, so only the diameters at the actual side branch crossing are clipped. By keeping the virtual contour equal for the arterial and reference diameters crossing the actual side branch ostium, means that in essence

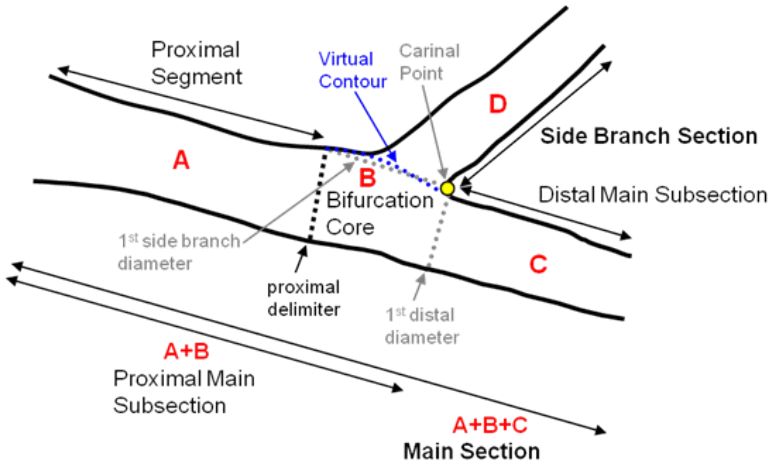
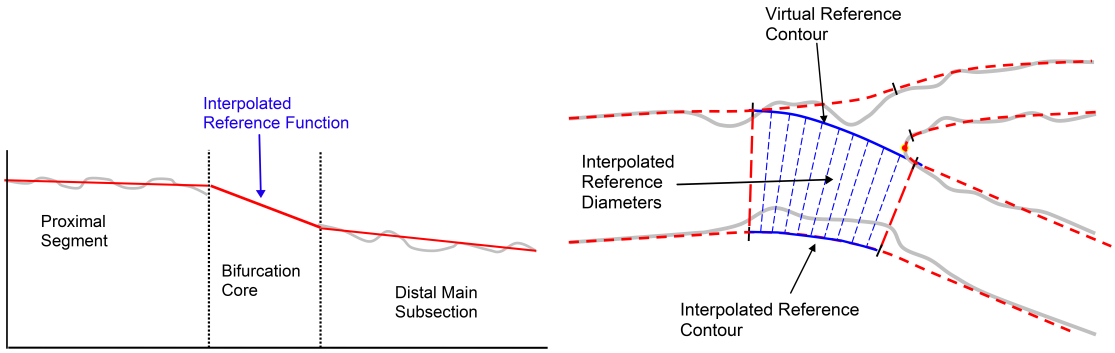


Figure 8.5: Scheme of the T-shape model, explaining the segments, proximal delimiter, virtual contour and sections terminology. The partitioning of the bifurcation into two sections: the main section and the side branch section. Using this model, the arterial and reference diameters of the ostium of the side branch and the whole main section can be accurately determined.



(a) (b)

Figure 8.6: a) The virtual reference contour that bridges the sidebranch and b) the reference diameters in the T-shape analysis.

any obstruction of the main section at the location of the side branch is found opposite to the side branch [132]. As a final result, the reference diameter function graph of the entire main section will be displayed as one continuous function, which is composed of three different straight reference lines that are linked together (Figure 8.7). One additional advantage of this continuous diameter function for the main section is the possibility to detect and calculate parameters of a so-called "combined lesion" (i.e. the total main section lesion). This is a bifurcation lesion that starts in the proximal main subsection and extents into the distal main subsection. Previously, such a lesion was: 1) split up into two separate straight analyses (a proximal and distal segment of analysis), with each having its own lesion and leaving to the user to determine what the

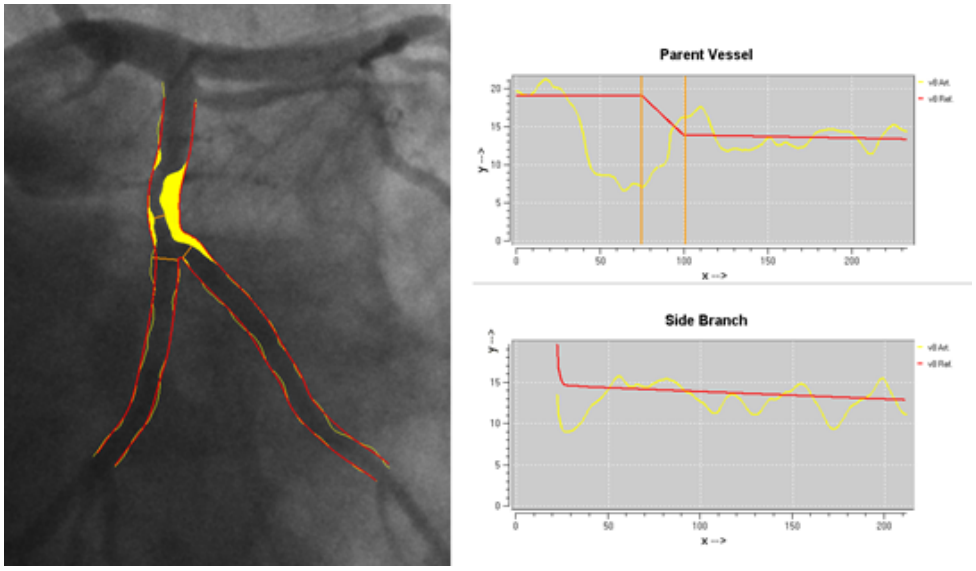


Figure 8.7: An example of a bifurcation analysis using the T-shape model, showing the final arterial and reference contours, plaque filling and the two separate diameter functions of the two sections.

actual obstruction diameter and total lesion length is; or 2) detected as one lesion, with an over- or under-estimations of the %DS and lesion length, in case of a single straight analysis "over the bifurcation core". However, the "combined lesion" does take into account the "step down" phenomenon [120] and provides the accurate lesion parameters for one single lesion. For the side branch section an "ostial" reference diameter function calculation is used [115, 132]. This will result in a reference diameter graph of the side branch section that will be displayed as one function, which is straight for the most part and slightly curved proximally (Figure 8.7).

Edge segments

For the assessment of (drug eluting) stent segments, an edge segment analysis option was created, providing a set of 9 suitable parameters for each of the segments as defined in Figure 8.8 (for Y-shape) and Figure 8.9 (for T-shape). This edge segment analysis allows studying the regression and progression of the bifurcation lesion more accurate, by including some extra parameters; the MLD position relative to the stent boundary (in stent edge segments) and the (sub-) segment start positions.

It should be noted that segment 14 of the T-shape edge segments (stented segment from proximal - over the bifurcation core - into the side branch) and segments 12 and 14 of the Y-shape edge segments (stented segments from proximal - over the bifurcation core - into the either distal branches) are not continuous in the bifurcation core (i.e., this trajectory consists of two separate diameter functions) and therefore the full parameter set cannot be calculated. The segment length (in this case representing the stented length) is the only value that can be calculated for these segments.

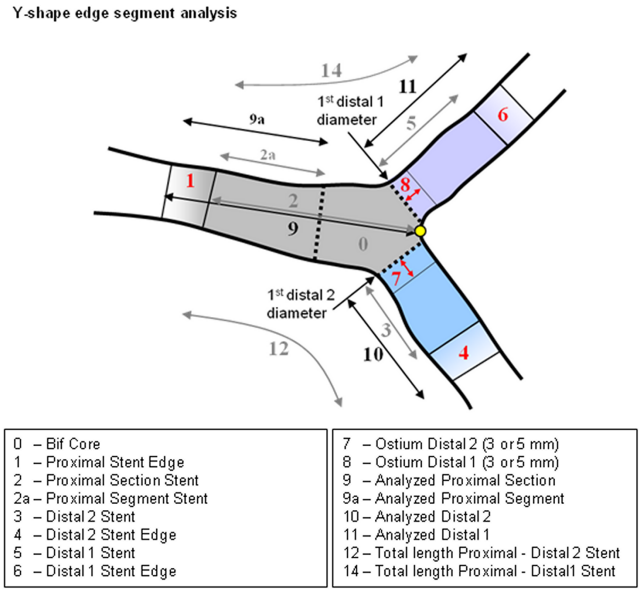


Figure 8.8: A schematic overview of the segments of the Y-shape bifurcation analysis with edge segments.

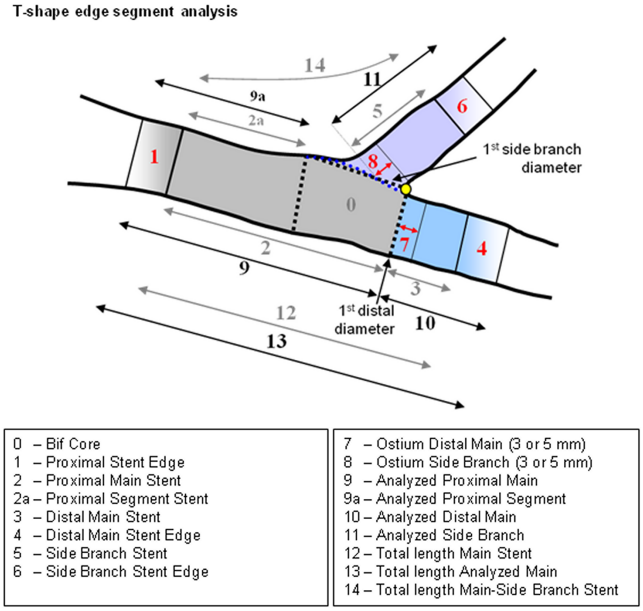


Figure 8.9: A schematic overview of the segments of the T-shape bifurcation analysis with edge segments.

8.3 Material

For this validation study 20 patient cases were selected at the Cardiovascular Research Foundation (CRF, New York, NY, USA). Ten cases were randomly selected from the cohort of the Diverge trial. This study is making use of the self-expanding DEVAX stent, which is a carinal skirt stent. These cases were analyzed with the Y-shape bifurcation model, specifically designed for the optimal stent length and diameter measurements up to the carinal point. Another 10 cases were randomly selected from the TriReme medical TOP study. This study is making use of main branch stenting (so, crossing the bifurcation core) with side branch preservation. In consequence of expansion of the stent body, an ostial crown (designed of ca. 2 mm long struts) automatically deploys into the ostium of the side branch. These cases were analyzed with the T-shape bifurcation model, specifically designed for the optimal (total) stent length and diameter measurements, while crossing the bifurcation core and optimal diameter measurement of the side branch ostium.

For each of these 20 patient cases the pre- and post-intervention analyses (n=40) were carried out with the two bifurcation analysis models of QAngio XA V7.2. The analyses were performed by two different QCA analysts, and according to QCA standard operating procedures (SOPs) [48]. Some specifics of the used analysis SOPs were: 1) bifurcation analyses started with the post-intervention case to define the bifurcation segment of analysis; 2) the bifurcation segment of analysis was defined by the length of the implemented stent(s) plus at least an additional 5 mm or a nearby landmark (e.g. side branch); 3) in case the initial interpolated reference diameter function was wrongly or too much tapered, flagging was primarily used for editing; 4) for pre-intervention analysis the same bifurcation segment of analysis was used as in the post-intervention analysis; and 5) in case a user-defined reference diameter was needed for the analysis, it was positioned in an approximately normal region of the vessel segment (or when applicable outside the stent).

8.3.1 Statistics

The four most relevant parameters for the bifurcation analysis that were studied are: the obstruction diameter (mm), reference diameter (mm), diameter stenosis (%), and obstruction length (mm). These parameters were studied per section and are expressed in terms of systematic and random errors (inter-observer variability).

For the bifurcation analysis with edge segments, the following three relevant parameters were studied: the mean diameter (mm), obstruction diameter (mm) and the diameter stenosis (%). These parameters were studied per segment (i.e., segment 1 to 11, see Figure 8.8 and 8.9) and are expressed in terms of systematic and random errors. Additionally, the stented length (mm) for segment 12 to 14 was studied in a similar manner. The systematic error is defined by the average value of the signed differences between measurement 1 and 2. The random error is defined by the standard deviation of the signed differences between measurement 1 and 2. The student's paired t-test was used to determine the significance of the differences (which hypothetically are equal to zero) between the repeated measurements. Level of significance $\alpha = 0.05$.

8.4 Results

The guidelines and results from previous publications presenting straight QCA inter-observer variability values are used to evaluate the performance of the two bifurcation models. This is done in the first place because of the lack of suitable bifurcation analysis references, and secondly because the bifurcation and straight analyses quality should be very similar.

The standard bifurcation analysis is compared to the QCA guidelines for straight analyses [115, 132, 48, 118] and study data of a previous publication [39], showing an inter-observer variability range of 0.10-0.15mm for the obstruction and reference diameter, 5.64% for the diameter stenosis and 1.46mm for the lesion length.

The bifurcation analysis with edge segments results is compared with the data of a straight brachytherapy analysis study [142]. The inter-observer variability data of the brachytherapy's injured segment (based on balloon and stent markers) was used for comparison with the bifurcation's stented segment (both determined by manually positioned markers). The brachytherapy inter-observer variability results (further on called the brachytherapy directive) show a slightly larger inter-observer difference (0.08 ± 0.17mm for the obstruction diameter) than conventional straight QCA (see above), due to the manual positioning of the markers (additional user variability).

Table 8.1: Inter-observer variability data of the Y-shaped bifurcation analysis model. The 10 pre- and 10 post-intervention cases used, were selected from the Diverge Trial.

n=20 (pre + post cases)	Proximal Section sys err	Proximal Section rand err	Distal 1 Section sys err	Distal 1 Section rand err	Distal 2 Section sys err	Distal 2 Section rand err
Obstruction Diameter (mm)	0.06	0.16	-0.05	0.08*	-0.03	0.07
Reference Diameter (mm)	-0.05	0.24	0.00	0.10*	-0.01	0.09
Diameter Stenosis (%)	-1.9	4.6	2.1	4.2	0.8	3.3
Lesion Length (mm)	-0.49	1.44	0.63	1.02*	-0.37	1.12

* statistically significant difference

In Table 8.1, the inter-observer differences of the 10 pre and 10 post intervention cases analyzed with the Y-shape analysis model are presented for the four most relevant parameters.

Most values are well within the boundaries defined by the QCA guidelines for straight vessel analyses. Only the random errors of the obstruction and reference diameters in the proximal section are a bit larger and all the differences (except for the reference diameter) in the distal 1 section are statistically significant (although within the boundaries of the QCA guidelines). The inter-observer differences for the analyses using the T-shape analysis model (10 pre and 10 post intervention cases as well) are presented in Table 8.2. Again, all values are within the boundaries of the QCA guidelines, except for the side branch section, where the difference of the obstruction diameter is a bit larger (statistically significant) and the percentage diameter stenosis shows a statistically significant difference (although within the boundaries of the QCA guidelines).

In Table 8.3, the inter-observer differences of the edge segment analysis using the Y-shape model (10 post intervention cases) are presented. In the segments 0, 2 and 9, an absolute positioning of the MLD is used instead of the relative one. The reason for this is that all the data for

Table 8.2: Inter-observer variability data of the T-shaped bifurcation analysis model. The 10 pre- and 10 post-intervention cases used, were selected from the TriReme Study.

n=20 (pre + post cases)	Proximal Section sys err	rand err	Distal Main Section sys err	rand err	Side Section sys err	rand err
Obstruction Diameter (mm)	0.01	± 0.11	0.04	± 0.15	0.09	± 0.12*
Reference Diameter (mm)	-0.01	± 0.13	0.01	± 0.14	0.01	± 0.15
Diameter Stenosis (%)	-0.4	± 4.3	-1.1	± 5.3	-3.0	± 4.2*
Lesion Length (mm)	-0.53	± 1.70	0.13	± 0.87	-0.28	± 0.93

* statistically significant difference

the edge segment analyses come from POST analyses, which do not really have lesions (percentage diameter stenosis smaller than 24%). This means that the obstruction position is influenced heavily by noise, since there is no obvious obstruction. Especially in the bifurcation core, which is a transition area that widens severely, a small difference in the percentage diameter stenosis can result in a large shift of the obstruction position due to the relative MLD calculation. Considering the tapering of the bifurcation core this can result in very different obstruction diameters. Therefore, the obstruction diameter found in a relative way is not a representative measure. This holds mainly for segment 0, 2 and 9 (all containing the bifurcation core) in the Y-shape edge segment analysis. Therefore, for these three segments, the absolute obstruction position was studied.

Table 8.3: Inter-observer variability data of the Y-shaped bifurcation's edge segment analysis. The 10 post-intervention cases used, were selected from the Diverge trial.

	n=10 POST Segment	Mean diam (mm) sys err	rand err	Obstr diam (mm) sys err	rand err	Diam stenosis (%) sys err	rand err	Stenth length(mm) sys err	rand err
0	Bifurcation Core	-0.08	± 0.12	-0.05	± 0.15	2.4	± 5.5		
1	Edge Prox	0.07	± 0.10	-0.07	± 0.13	3.5	± 3.9*		
2	Stented Prox	-0.02	± 0.06	-0.07	± 0.10	1.3	± 5.0		
2a	Stented Prox	-0.01	± 0.06	-0.06	± 0.10	3.0	± 4.6		
3	Stented D2	-0.01	± 0.04	0.05	± 0.17	-1.0	± 1.8		
4	Edge D2	-0.06	± 0.11	0.02	± 0.10	-0.3	± 3.8		
5	Stented D1	0.01	± 0.02	0.03	± 0.06	1.3	± 2.4		
6	Edge D1	0.02	± 0.11	0.04	± 0.14	-0.1	± 4.8		
7	Ostium D2	0.01	± 0.04	0.03	± 0.09	0.0	± 2.5		
8	Ostium D1	-0.02	± 0.06	0.00	± 0.05	0.7	± 2.9		
9	Analyzed Prox	-0.04	± 0.05	-0.10	± 0.10*	2.5	± 4.5		
9a	Analyzed Prox	-0.03	± 0.06	-0.08	± 0.11*	3.7	± 4.1*		
10	Analyzed D2	-0.01	± 0.04	0.05	± 0.17	-0.8	± 3.6		
11	Analyzed D1	0.02	± 0.05	0.04	± 0.12	-0.1	± 4.9		
12	Stented Prox-D2							0.30	± 0.51
14	Stented Prox-D1							0.28	± 0.28

* statistically significant difference

Most of the inter-observer values are smaller than the values specified by the brachytherapy directive. We see, however, some deviations in the proximal segments; a slightly larger obstruction diameter error in segment 9 and significant differences in the obstruction diameters of segments 9 and 9a and in the percentage diameter stenosis of segments 1 and 9a.

Finally, the results of the inter-observer validation of the edge segment analysis using the

T-shape model (10 post intervention cases) are presented in Table 8.4. The majority of the measured inter-observer variabilities are smaller than the values specified by the brachytherapy directive. In the proximal section, the mean diameter of segment 2a is statistically significantly different (although within the boundaries of the guideline). In the distal main section, somewhat larger random errors can be seen for the lesion diameter (segment 3, 7, 10, 12) and percentage diameter stenosis (segment 3 and 7). In the side branch section, a slightly larger systematic error for the obstruction diameters of segment 5 and 8 (in segment 8 statistically significant), and for the mean diameter of segment 8 are found.

Table 8.4: Inter-observer variability data of the T-shaped bifurcation's edge segment analysis. The 10 post-intervention cases used, were selected from the TriReme Study.

	n=10 POST	Mean diam (mm)	Obstr diam (mm)	Diam stenosis (%)	Stenth length(mm)
	Segment	sys err rand err	sys err rand err	sys err rand err	sys err rand err
0	Bifurcation Core	-0.07 ± 0.18	-0.05 ± 0.14	-0.1 ± 5.2	
1	Edge Prox	0.02 ± 0.06	-0.01 ± 0.06	-0.5 ± 2.1	
2	Stented Prox	-0.02 ± 0.05	-0.02 ± 0.05	-0.6 ± 2.1	
2a	Stented Prox	-0.01 ± 0.02*	-0.01 ± 0.07	-0.8 ± 2.3	
3	Stented Dist	-0.01 ± 0.10	0.05 ± 0.23	-1.2 ± 7.0	
4	Edge Dist	-0.01 ± 0.06	0.02 ± 0.15	-0.9 ± 3.8	
5	Stented Side	-0.06 ± 0.06	-0.10 ± 0.11	3.4 ± 5.7	
6	Edge Side	0.07 ± 0.12	0.05 ± 0.10	-2.6 ± 4.9	
7	Ostium Dist	-0.01 ± 0.14	0.01 ± 0.28	-0.2 ± 9.5	
8	Ostium Side	-0.11 ± 0.15	-0.10 ± 0.12*	3.5 ± 5.5	
9	Analyzed Prox	-0.01 ± 0.04	-0.02 ± 0.05	-0.5 ± 2.0	
9a	Analyzed Prox	0.00 ± 0.02	-0.01 ± 0.07	-0.7 ± 2.2	
10	Analyzed Dist	-0.01 ± 0.06	-0.05 ± 0.22	0.7 ± 4.3	
11	Analyzed Side	-0.04 ± 0.05	-0.02 ± 0.09	3.5 ± 3.8	
12	Stented Main	-0.02 ± 0.05	0.01 ± 0.25	-0.2 ± 2.4	-0.23 ± 0.64
13	Analyzed Main	-0.01 ± 0.04	-0.04 ± 0.17	0.0 ± 3.2	-0.23 ± 0.64
14	Stented Prox-Side				-0.29 ± 0.26

* statistically significant difference

8.5 Discussion

In this article we describe the results of an inter-observer variability study performed with the new Y- and T-shape bifurcation analysis models of QAngio XA V7.2. A validation study like this is essential to determine whether the bifurcation analyses performed are reproducible, given the fact that the analyses are performed at different moments in time (without previous obtained knowledge), by two QCA analysts (introducing a subjectivity level), and by using the same analysis SOPs.

Looking at the inter-observer analysis data of the Y-shape analysis model, the results are very good and comparable to the values known from previous publications and the QCA guidelines for straight analyses [39, 115, 118], which are very precise. Only in a few cases the random error shows a slightly larger value. The first very slightly diverging value is the variability in the proximal section's obstruction diameter (0.16 mm vs. 0.15 mm of the QCA guidelines). It turned out that this is caused by the minor variations in the arterial contours, caused by manual edits of the two analysts. When this is the case at the lesion site, this greatly influences the value

of the obstruction diameter. Therefore, we strongly recommend not to edit the lesion sites. Nevertheless, sometimes one cannot fully avoid it, for example, when: a) using the automatic correction points, which might have a slight influence further along the contour; b) the lesion is very irregular due to complexity or poor edges and requires manual editing, or c) because of a small vessel that overlaps or a side branch crossover that requires correction. Unfortunately, all these situations were present in our study cases, which is a random sample of practice.

Furthermore, the variability in the reference diameter in the proximal section is a bit larger as well (0.24 mm), which is indirectly caused by the variation in arterial contours between the two analysts, as discussed above. Differences in arterial contours can lead to different automatic reference diameter functions and because of that slightly different (relative) obstruction positions (based upon the maximum percentage diameter stenosis), which in turn has its influence on the corresponding reference diameter value. Besides that, a second cause might have been the editing of the reference diameter function itself. Of course an analysis SOP was used to do this, but small difference in the proximal or distal sections can have an influence on the reference diameter function of the bifurcation core as well, mainly due to the significant tapering in this area. Besides these random errors, we see some statistical differences (p-value <0.05) for the obstruction, diameter stenosis and lesion length of the distal1 section (see Table 8.1). However, looking at the corresponding systematic and random errors, these values are not large at all. The random errors are much smaller than mentioned in the QCA guidelines and literature, which causes the found differences to be significant. Besides that, clinically speaking, systematic error values of this magnitude do not have any influence on the clinical decision making process or meaning for study outcomes, in other words: they're clinically not relevant [143, 144, 145].

The validation data of the T-shape analysis model looks very good as well; the random errors of the obstruction and reference diameter are similar to the inter-observer variability data previously published [39] and the percentage diameter stenosis is even smaller than these published values. Only the systematic error of the obstruction diameter in the side branch is a bit large (0.09 mm) and statistically significant. Splitting up the side branch data in lesions in the straight part and ostial part of the side branch section, it turned out that the ostial lesions are the cause of this systematic difference (n=10; 0.13 $\pm$ 0.15 mm, p-value 0.004 compared to n=10; 0.04 $\pm$ 0.07 mm, p-value 0.09). This significant difference is probably caused by small differences in the manual editing of the carinal point by the two analysts. As a result of this, the middle arterial contour can shift slightly, causing differences in arterial diameters that are positioned proximally in the distal branches. In that perspective, both branches are oppositely influenced. In combination with an ostial lesion this might slightly influence the size of the obstruction diameter. In these cases, the main reason for editing the carinal point was poor contrast and poor edges in that region of the image, resulting in slightly subjective editing differences. Therefore, we recommend not to edit the carinal point too easily. Furthermore, only the diameter stenosis of the side branch section shows a statistical significant difference. Again the relatively small random errors are the cause for this. Clinically these differences are not relevant [143, 144].

Finally, the random error for the obstruction length of the proximal section is somewhat larger than published before (1.70mm vs. 1.46mm) [39]. This is mainly due to small differences in the arterial contours, causing a small shift in the positioning of the proximal and/or distal lesion markers. Nevertheless, the inter-observer variability value remains so small that it will

not have any influence on the clinical decision making process. As can be expected, these small shifts in the proximal and distal lesion marker positions have a comparable (slightly enlarging) influence on the random errors of the "combined lesion" length (2.21 mm, p >0.05; n=6!) as well. The inter-observer variability for the percentage diameter stenosis of the "combined lesion" (5.22%, p >0.05) is very comparable to the value mentioned before (5.64%) [39]. Given the fact that these variations have clinically no relevance, it does indicate that the "combined lesion" data can be used very well.

8.5.1 Edge segments

In general, the inter-observer data for the bifurcation analysis with edge segments of both models are good and consistent with the results that were previously published [142]. In fact, most of the data is even within the ranges defined by the QCA guidelines for straight analyses and a previous publication [39, 115, 118].

For the Y-shape edge segments, Table 8.3 shows that only a few diverging values are present in the proximal segments, which is similar to the conventional Y-shape bifurcation analysis. The segment results for the two distal sections are considered to be similar. The statistically significant differences found are due to the relatively small random errors, and are considering the size of the systematic error not clinically relevant [143, 144, 145]. The only exception is segment 9, the obstruction diameter, for which the systematic error is a bit large (-0.10 mm) as well. According to the conventional bifurcation analysis this can be traced back to the differences in manual edits of the analysts (see size mean diameter segment 0 and 1 as well). Because segment 9 is composed of segment 0, 1 and 2a, differences are accumulated here the most.

As can be seen in Table 8.4, the T-shape edge segments show very good inter-observer values in the proximal segments, only segment 2a shows a statistically significant difference (due to the very small random error), which has clinically no relevant meaning (-0.01 mm) [144, 145]. Similar to the conventional T-shape bifurcation analysis is the influence of the manual repositioning of the carina point, which has caused slightly larger systematic and random errors for the obstruction diameter and percentage diameter stenosis in (particularly) the ostial segments (7 and 8) and the segments (3, 5, 10 and 12) containing these ostial segments.

For both models, the systematic errors of the stent lengths of segment 12, 13 (only T-shape) and 14 are very comparable to the values in the brachytherapy directive, but the random errors are very small compared to the brachytherapy directive. As a result, the manual positioning of the stent markers and with that the definition of the edge segments are very reproducible. One should however notice that this accuracy will be influenced by the visibility of the stent struts or stent markers and the preciseness of the analyst when placing the stent markers.

In general, the results of this bifurcation analysis (with edge segments) inter-observer variability study are very good, although one must recognize the influence of the manual contour edits. Probably due to the fact that this type of analysis has become very complex, the edits, especially the ones around the bifurcation core (the most complex part) have a slightly larger influence on the results than one is used to for straight analysis. Looking at the results of the intra-observer variability study, performed on exactly the same dataset [146], it will be noticed that for the T- and Y-shape model the systematic- and random errors of the obstruction and reference diameter are very low (random errors $\leq$ 0.11 mm!). This demonstrates the possibil-

ity of a high reproducibility of the bifurcation analysis with both models and the influence of the subjective differences caused by the manual contour edits. In other words, it is possible to obtain even better inter-observer variability data when: 1) less contour edits are needed (clear vessel edges, optimal bifurcation viewing angle, etc), and/or 2) the analysts are editing more alike. Because the arterial contours are the basis of every type of QCA analysis, we want to emphasize (once more) the importance of highly precisely and unambiguously written Standard Operating Procedures (SOPs) for the analyses, which will help the analysts to accomplish good and reproducible analysis results.

8.6 Conclusion

The inter-observer variability data of the T- and Y-shape bifurcation analysis models show a robust and very good reproducibility for both models. The data for the bifurcation analysis with edge segments (both models) is very good as well, although in some segments a slightly larger random error might be evident. In general, the inter-observer variability data shows that the T- and Y-shape models of the bifurcation analysis (with edge segments) is a great improvement in the field of quantitative coronary angiography.

CHAPTER 9

Discussion

9.1 Objective

The main objective of the research presented in this thesis was to improve the quality of QCA-analyses. This means improving the reliability and reproducibility of the analyses, reducing the inter- and intra-observer variability, reducing the time and amount of interaction that is needed by the users to perform an analysis and extending the possibilities of the current analyses. To achieve this, a number of new algorithms and methods were presented in this thesis.

9.2 Wavepath

In Chapters 3 and 4, the novel Wavepath approach was presented and compared to the pathline methods that were available at that time in the QCA-software. The validation studies have demonstrated that the Wavepath reduces the variability between repeated measurements substantially and as a result increases the reproducibility of the pathline detection. Furthermore, because of the robustness of the algorithm, it performs well on a wide variety of images and coronary morphologies. Because of the positive results of the validation study, the Wavepath algorithm was integrated into the Medis QAngio XA software and performs very well (according to experienced users), with less user corrections needed, for both coronary and peripheral analyses. In our opinion, it is fair to conclude that the Wavepath algorithm contributes to a better quality of the QCA-analyses.

9.3 Wavecontour

In Chapter 5, our novel contour detection method was introduced: the Wavecontour. As demonstrated in the validation study, it reduces the variability and the systematic errors in the contour definition, mainly because it does not use scanlines to resample the image. In combination with the Wavepath algorithm, it results in contours that are virtually independent of the user-defined

start- and endpoint. However, the ability of the Wavecontour to follow edges with the correct intensity profile (e.g. bright to dark) in any direction, meaning not only perpendicular to the pathline, also causes problems while crossing sidebranches that the user does not want to take into account in the analysis. This, combined with the fact that the method was rather time-consuming compared to the existing MCA-algorithm, was the main reason that the Wavecontour was not (yet) incorporated in the commercial software package, despite the good accuracy demonstrated in the validation study. To make the Wavecontour more applicable and more likely to be used in future QAngio XA versions, some improvements have to be made, particularly related to the sidebranch crossing of the algorithm. Although the global position of a sidebranch can already be detected, finding the exact location where the algorithm must not follow the edge information anymore but should cross the sidebranch instead, remains a challenge. The performance however is not likely to be a problem anymore, since computer power has significantly increased over the last few years.

A different approach could be to adjust the usage of our method: not using it for the entire contour, but only in the regions where it is needed the most, being the sharp bends and the lesion itself. In this way, a combination of the two methods would be feasible, where MCA is used in the normal parts of the vessel (as it is used now to the satisfaction of most users) and the Wavecontour where the high precision is the most important factor and the MCA cannot follow the correct contours. The most difficult part in such a combination is of course how to decide precisely where to switch from one algorithm to the other, which can be a source of variation again. To increase the reproducibility of the combined method, this should be done automatically. This forces the method into a two-stage approach: First, the traditional MCA is used to calculate the contours and a preliminary diameter function, which would be used to determine the position of the lesion in the vessel. Sharp bends can be found by analyzing the curvature of the MCA-contours or of the pathline. In the second stage, the Wavecontour will be used to modify the contours in these "difficult areas", increasing the accuracy of the total approach.

It can be concluded that our novel approach has a lot of potential, but it was not ready yet to be incorporated into the commercial software. It would still be very useful to do so, most likely in a combined form as described above, or incorporate only parts of the approach, such as the optimal filtering or the advanced smoothing.

9.4 Diameter Function

The next step in achieving more reliable and more robust QCA-measurements, is presented in chapter 6, where our new approach for the calculation of vessel diameters is discussed. The main idea behind this approach is that the requirement that the arterial and reference diameters are measured is the same direction, is released. This means that the arterial diameters can now be assessed separately from the reference diameters and that these arterial diameters are perpendicular to the central lumen line, the centerline. This avoids overestimated MLD measurements in curved vessel segments. Whether this approach achieves the correct diameters in every part of the vessel could be a point of discussion. The arterial centerline definition is slightly different from the line that represents the blood flow, since the blood flow tends to follow the outside of

the curves, whereas our centerline is pulled inwards at the curves to achieve a slightly shorter centerline and a smoother curve. In our opinion, the way our method defines the centerline and measures the diameters perpendicular to it is the most clinically relevant way, and the MLD (which is clinically the most important diameter) is measured smaller than using the traditional approach.

Still there are some points where the approach could be improved in the definition of the arterial diameters. In extremely sharp curves for example, it is sometimes unavoidable that the diameter chords intersect with each other in the inside curve, which is not necessarily wrong, but may appear to be strange to the user. Whether the diameters should be perpendicular to the centerline in all cases could be argued. For example, in case of an asymmetric stenosis, this will create a minor overshoot just before and just after the stenosis. Furthermore in the bifurcation analysis, the direction of the diameters in the ostia of the distal branches is often a point of discussion. In our method the first diameter starts in the direction of the main vessel and then turns into the side branch. However, the interpretation of these diameters, which are showing an increase in the ostium, is not trivial.

The difficult part in taking different directions for the arterial and reference diameters is the correspondence between the two. At a certain location, we still want to compare a specific arterial diameter with the corresponding reference diameter that represents the healthy vessel size at that point best. We dealt with this problem by resampling the arterial diameters and centerline at positions where the arterial centerline intersects with the reference diameters. This creates a one-to-one correspondence that is needed in order to calculate a percentage diameter stenosis. The length of the vessel segment should be measured along the reference centerline, since this one is more reliable and stable than the arterial centerline, especially when comparing pre- and post-intervention analyses.

Overall we may conclude that our new diameter measurement approach allows a better and more realistic measurement of the minimal lumen diameter in curved segments and also more accurate diameter measurements in bifurcating vessel segments than was possible before.

9.5 Overall QCA

All these new methods presented in this thesis contribute to more accurate, more robust and much more versatile QCA measurements. Despite all the improvements, the measurements will never be perfect and there is always room for even further improvements. As already discussed above, the contour detection could be improved by merging the MCA with our newly developed Wavecontour method and the diameter calculation in the ostium of the branches in the bifurcation analysis could be improved too.

Furthermore, the next step in the bifurcation analysis would be not only calculating the relation between the reference diameters proximal and distal of a bifurcation (using the relation of Finet or Murray's law), but also automatically adjust the reference diameter functions to comply with these relations. This would give a more realistic estimation of normal vessels that are undiseased.

Apart from that, there are some more improvements that could be made to achieve the ideal measurements: for example the selection of the segment under study could be done automati-

cally, especially for the single segments, by detecting the pathlines for the whole coronary tree, analyzing all segments that are available and finding the most severe lesion that is present. This would make the analysis even more reproducible since it would take out the variability of the definition of the segment. This would be quite a challenging task to develop and also, it is not always the most severe lesion that is of interest to the user. One could think of another option, selecting the segment of interest by means of one point in the lesion instead of two points as a start and end of the segment. This also would make the analysis more reproducible, since it would take out the variation in finding the start and end points of the segment that is analyzed.

9.6 External developments

In the field of automatic coronary angiography analysis systems, there are three groups worldwide playing a significant role: Pie Medical Imaging, bv and Paieon Medical Ltd., and Medis medical imaging systems, bv.

Paieon concentrates its efforts on 3-D reconstructions of coronary segments from biplane images and not strictly on the accurate 2D measurements, so it is difficult to obtain a quantitative comparison between the Paieon software and the Medis software. For the 'traditional" 2D measurement of coronary artery disease, there are two different solutions available on the market, QAngio XA from Medis and CAAS II from Pie Medical. There are no recent studies that assess the accuracy and precision in straight vessel analysis of the two packages and which would allow an objective comparison between these. Therefore the older validation data of the packages at the time they were released, is considered the best we have currently, but may be entirely out-of-date. On the other hand, it is not likely that the core algorithms changed significantly over these years. According to the validation by Haase et al [147], the CAAS II system measured the MLD in vitro with an accuracy of 0.00 mm and precision of 0.11 mm and in vivo with an accuracy of -0.01 mm and precision of 0.18 mm. The QAngio XA system achieved an accuracy of 0.00 mm and precision of 0.08 mm over the whole range of phantoms and an accuracy of 0.02 mm and precision of 0.15 mm for the in vivo measurements. Statistically, the methods perform similarly; however the difference between the two methods is mainly in the workflow, the user interaction and above all, the determination of reference values.

Over the last several years, the same two groups have developed methods to analyze coronary bifurcations in 2D. Both use a slightly different approach of determining the boundaries of the bifurcation area, the determination of the diameters in and around the bifurcation and in constructing the reference contours. According to a recently performed comparison-study by Girasis [148], the two packages perform quite similarly when measuring the dedicated bifurcation phantom he developed for this purpose. The CAAS II system of Pie Medical seemed to perform slightly better that QAngio XA V7.2, although this was not statistically significant, mainly because the inner contours had a very smooth transition (at the carina) which does not mimic the reality very well, and because the phantom had severe stenoses in the area of the carina, which contradicts the assumption of QAngio XA that the carina in general is disease-free. Aside from that issue, the two packages perform very similarly. Differences include the fact that QAngio XA determines the reference contours differently, and that QAngio XA V7.2 has two different models (Y-shape and T-shape), which makes it much more applicable to certain interventions

and core lab studies.

The 3D QCA is still under development at Medis (see below in the following paragraphs), whereas Pie Medical and Paieon do have versions on the market (CAAS 5 and CardiOp-B, respectively.). According to a comparison study by Ramcharitar [149], the CAAS system performs better than the CardiOp-B system, with a higher accuracy (mean difference 0.01 vs. 0.03mm) and a higher precision (standard deviation 0.09 vs. 0.23mm)

9.7 Future of QCA

The question remains: What is the future of x-ray angiography in the presence of the newer 3D imaging modalities such as CTA and MRA? It is a fact that there are many new developments in CTA and MRA which will increase the resolution, decrease the imaging time and for CT decrease the dose of radiation. CTA in particular (its resolution is higher than MRA) is used more and more for diagnostic purposes and it is expected to eventually take over the diagnostic role of x-ray angiography.

Nevertheless, the x-ray system will not disappear from the hospitals in the near future because of one very specific property of the x-ray system: its ability to be used during an intervention. As long as no other imaging technique can be used to guide an intervention, there is always a role for the x-ray angiography and doctors and scientists will continue to use QCA to determine the severity of a lesion in the coronary arteries, and the objective results of the interventions.

Furthermore, the x-ray system itself can be used to extract 3D information by recording two different angiographic images from two different angles that are at least 25 degrees apart, either a biplane or two monoplane acquisitions. Software has been developed lately to calculate the optimal viewing angles for a selected coronary segment without the need to 3D-reconstruct the entire coronary tree [123, 150]. The system starts with standard QCA in two selected angiographic views and the correction of angiographic system distortions. In a next step, the segment of interest is reconstructed in 3D and optimal viewing angles associated with minimal foreshortening are proposed. For each viewing angle, the possible overlap with other parts of the coronary tree is assessed resulting in the final optimal viewing angle. This angle should then be used for further interventions on that particular segment. Biplane (or two monoplane acquisitions) can also be used to reconstruct the whole coronary tree (or a part of it) in 3D in order to correct the measurements that were performed in a single QCA-analysis afterwards. Especially the length measurements can be inaccurate due to foreshortening [124].

With 3D reconstruction, an elliptical vessel shape is assumed, restricting the possibilities of analyzing complex lesions. To accurately reconstruct such complex morphologies, more than two projections are needed. This can actually be done with the same X-ray tube by a technique that is called rotational angiography. This technique rotates the X-ray tube around the patient resulting in a whole set of projections that can be reconstructed into a 3D image with a very high resolution. This procedure has to be performed ECG-triggered to avoid the effects of the movement of the heart in the cardiac cycle.

Nowadays, the combination of different imaging modalities is a promising research topic. Two other imaging techniques that are often used to assess the extent and composition of coronary

lesions are intravascular ultrasound (IVUS) and optical coherence tomography (OCT). IVUS has been used for a long time to assess the composition of the plaque. OCT is a relatively new technique and is now used mainly for the assessment of the malapposition of the stent struts. It is expected that it may also play a role in determining the composition of the plaque.

The fusion of QCA and IVUS/OCT is such a new development that combines the best of both worlds: the detailed cross-sectional viewing of IVUS/OCT and the 3D overview of the x-ray angiography (XA) [125]. When an IVUS/OCT pullback is performed, the interventional cardiologist uses these images to plan the intervention and decide where the stent can be positioned optimally. However, the IVUS/OCT catheter has to be removed during the stent deployment and therefore, XA is the only imaging tool available for guidance, meaning that the planned stent position has to be mapped from IVUS/OCT to XA images. This is where the co-registration of XA and IVUS/OCT helps out: when the segment of interest is reconstructed in 3D, the XA and IVUS/OCT images can be aligned using only one landmark that is visible in both data sets. This means that for each position in the IVUS/OCT dataset, the corresponding position in the X-ray images can be determined. Next, the position of the planned stent can be transferred to the X-ray images, meaning that the stent can be positioned with great accuracy. Furthermore, the measurements of the QCA and the IVUS/OCT are quite complementary: In IVUS, the composition of the plaque, the position of a stent and the cross-sectional area can be assessed accurately whereas the length measurements can be quite unreliable for some pullback devices. This measurement can be performed accurately in the 3D-QCA and in this way we get reliable numbers for all measurements.

9.8 In Conclusion

Concerning the QCA software developed in our group, it can be stated that the 2D single segment Quantitative Coronary Angiography still holds as a golden standard in this field and by achieving a similar accuracy/precision and workflow in the bifurcation analysis methods, it is expected that the bifurcation package will be regarded as a standard in its field too. For this moment, our newly developed bifurcation software performed equally in a comparison phantom study with the other 2D-bifurcation package on the market, but further validation studies with real patient data will indicate which bifurcation analysis approach achieves the best and most reliable results and is best usable in clinical practice. Our mission is to continue this research and new developments to extend the good reputation, accuracy and reliability of our 2D QCA methods also into the field of the 3D QCA and in the fusion with OCT and IVUS.

Summary and Conclusion

Over the last decades, several methods have been developed for the assessment of coronary artery stenoses in X-ray angiograms. Although quantification methods have proven to increase the reproducibility of stenosis measurements, the majority of the X-ray angiograms is still assessed visually by the interventionalist for decision making purposes. However, the development of new interventional devices and techniques, such as bifurcation stenting, have called for new quantitative methods to accurately measure the vessels dimensions and stenosis parameters to facilitate planning of the intervention and the choice of the proper intervention devices. Furthermore, the continuous development of new types of stents has lead to clinical trials, which require accurate, reproducible analysis software to prove the value, applicability and limitations of the various devices. This is all part of the paradigm of evidence-based medicine.

The main objective of this thesis is to develop new, accurate and reproducible automated methods for the detection and quantification of coronary and peripheral artery lesions, which make it possible to extend the straight segment analysis to analyses of sidebranches and bifurcations.

In **chapter 1** a general introduction to this thesis is presented, describing the field of coronary arteriography, its history and its developments towards quantification of lesion parameters. Furthermore, the current state and usage of the QCA-software is discussed.

Chapter 2 presents a general inventory of contour detection techniques that have been applied within medical applications. The most important methods are described and their advantages and disadvantages are discussed, which formed the basis of our research towards a new contour detection method. Due to the requirements of reproducibility and speed, the fastmarching levelset method based on the edge information in the image was chosen as the most promising method for the new contour detection in our application.

Chapter 3 introduces the Wavepath, our new approach for detecting pathlines in coronary angiograms. This novel method is also based on the fastmarching levelset method (wavefront propagation) and was developed to increase the reproducibility of the detected pathlines and decrease the amount of user interaction that is needed to achieve a proper pathline. Due to its reproducibility, the Wavepath is very suitable for detecting pathlines, not only in straight

segments, but also in different morphologies, such as bifurcations and side-branches, providing a very stable and reproducible separation point for the bifurcation and ostial analyses. This was demonstrated in the validation study that was performed on coronary angiograms, containing straight as well as bifurcation and ostial segments.

In **chapter 4** the application of the Wavepath method in peripheral vessel analyses is described, showing the value of our pathline method in vessels other than the coronaries. An extensive validation study was performed using a large variety of images, with different image characteristics, different image intensifiers, different morphologies and covering the whole range of vessel sizes. In this validation study, the Wavepath has once again proven its reliability and reproducibility, showing only minor variations when varying the start- and endpoints.

Chapter 5 introduces and discusses the Wavecontour, our new approach for the detection of arterial contours in X-ray angiograms. As a result of the inventory of contour detection methods presented in chapter 2, the contour detection method is based on a wavefront propagation that uses the directional edge information in the image as input. The algorithm is implemented as a two stage approach so that an estimate of the vessel size can be incorporated in the second stage of the process in order to use a matched filter approach. This new approach was designed mainly to overcome the problems encountered with other contour detection techniques, such as under- and oversampling in sharp bends and the proper detection of complex lesions. In the validation study that was carried out on phantom data as well as in vivo patient data, the Wavecontour demonstrated the improvement in accuracy and reproducibility showing no systematic errors and only little variation in the repeated measurements. However, the accurate crossing of side branches with this method still remains a challenge.

Chapter 6 presents our new approach for the measurement of the diameters of the vessels and the estimate of the reference diameters. The main objective for this new method was to overcome the problems that were encountered with the current diameter measurement method regarding the direction of the diameters in case of complex lesions and sharp bends. Furthermore, the new method includes a specific approach for the measurement of the vessel diameters in the proximal part of a sidebranch, the ostium, as well as the definition of reference diameters in that section of the vessel. The validation study shows an improvement in the accuracy of the lesion measurements, caused by the ability of this new approach to measure the true minimal diameter. Next to the straight segment and ostial segment approach, our new method also defines two new bifurcation models in order to accurately measure the diameters and lesion parameters of an entire bifurcation. We introduce the Y-shape and T-shape bifurcation models which correspond to different intervention techniques and together cover the whole range of bifurcation morphologies. These models provide data for the proximal and distal parts and the bifurcation core itself, which was not possible with other measurement methods so far. In the validation study, the high accuracy and precision are demonstrated using bifurcation phantom images.

Chapter 7 presents an overview of all the steps used in the bifurcation analysis including the newly introduced edge segment analysis. This edge segment analysis divides the entire analyzed bifurcation into segments according to stent placements. It provides data for stent segments and the corresponding stent- and ostial edge segments. Furthermore, in this chapter the results of the first bifurcation validation study on patient data are presented, demonstrating low intra-observer variability, proving a high reproducibility of our new bifurcation analysis methods.

Chapter 8 describes an extensive validation study for the bifurcation analysis that was performed on clinical data. This validation study assesses the inter- and intra-observer variability on pre- and post-intervention data using both the Y-shape and the T-shape bifurcation model. The results show a good reproducibility for both of our newly developed bifurcation analysis methods.

In **chapter 9** each of our newly developed methods presented in the previous chapters are discussed. For each method it is determined to what extend our goals have been met and what is still open for further research. Furthermore, the performance of our methods in comparison to other commercially available packages is evaluated. The outcome is that the accuracy and precision of our software are very similar to the ones obtained by competing products, for the straight segment analysis as well as for the bifurcation analysis. The difference is in the workflow, the user interaction and above all, the determination of reference values, which favors our package due to more possibilities in calculating these references. In addition, our vision on the future of QCA is presented: I believe that analysis techniques that combine different modalities will become very important, such as the fusion of QCA and IVUS/OCT.

Finally, an overall conclusion is presented, considering the goals of the entire research: our 2D QCA software is still regarded as a standard in the field and the bifurcation package is expected to become a standard as well. We can conclude that our goal of improving the QCA analysis and extend it towards the new morphologies and new intervention techniques has been met.

Samenvatting en Conclusie

In de afgelopen decennia zijn verschillende methoden ontwikkeld voor de beoordeling van coronaire stenoses in röntgen angiogrammen. Hoewel kwantificatie methoden hebben bewezen de reproduceerbaarheid van stenose metingen te verhogen, wordt de meerderheid van de röntgen angiogrammen nog steeds visueel beoordeeld door de interventionalist voor het nemen van beslissingen over de te volgen behandeling. Echter, de ontwikkeling van nieuwe interventie hulpmiddelen en technieken zoals bifurcatie stenting, hebben aangezet tot nieuwe kwantitatieve methoden om nauwkeurig de afmetingen van het bloedvat en de stenose parameters te kunnen meten om de planning van de interventie en de keuze van de juiste interventie hulpmiddelen te vergemakkelijken. Bovendien heeft de voortdurende ontwikkeling van nieuwe soorten en typen stents geleid tot klinische studies, waarvoor nauwkeurige en reproduceerbare analysesoftware nodig is om de waarde, de toepasbaarheid en de beperkingen ervan te bewijzen. Dit maakt allemaal deel uit van het paradigma van evidence-based medicine.

Het belangrijkste doel van dit proefschrift is om nieuwe, nauwkeurige en reproduceerbare geautomatiseerde methoden te ontwikkelen voor de detectie en kwantificatie van coronaire en perifere slagader laesies, die het mogelijk maken om de standaard rechte-segment analyse uit te breiden tot analyses van zijtakken en bifurcaties.

In **hoofdstuk 1** wordt een algemene inleiding tot dit proefschrift gepresenteerd, met een beschrijving van het werkgebied van coronaire arteriografie, de geschiedenis en de ontwikkelingen in de richting van de kwantificatie van laesie parameters. Verder wordt de huidige status en het gebruik van de QCA-software besproken.

Hoofdstuk 2 bevat een algemene inventarisatie van contourdetectie technieken die zijn toegepast binnen de medische toepassingen. De belangrijkste methoden worden beschreven en hun voordelen en nadelen besproken, wat de basis vormt voor ons onderzoek naar een nieuwe contourdetectie methode. Door de eisen van reproduceerbaarheid en snelheid, werd de fastmarching levelset methode gebaseerd op de rand informatie in het beeld gekozen als de meest veelbelovende methode voor de nieuwe contourdetectie in onze applicatie.

Hoofdstuk 3 introduceert de Wavepath, onze nieuwe aanpak voor het detecteren van padlijnen in coronaire angiogrammen. Deze nieuwe methode is gebaseerd op de fastmarching levelset

methode (wavefront propagatie) en is ontwikkeld om de reproduceerbaarheid van de gedetecteerde padlijnen te verhogen en het aantal interacties van de gebruiker dat nodig is om een goede padlijn te verkrijgen, te verlagen. Dankzij de reproduceerbaarheid is de Wavepath zeer geschikt voor het detecteren van padlijnen niet alleen in rechte segmenten, maar ook in andere morfologiën, zoals bifurcaties en zijtakken, waarbij dit een zeer stabiel en reproduceerbaar splitsingspunt voor de bifurcatie en ostiale analyses oplevert. Dit is aangetoond in de validatiestudie die werd uitgevoerd op coronaire angiogrammen die zowel rechte segmenten, als bifurcaties en ostial segmenten bevatten.

In **hoofdstuk 4** wordt de toepassing van de Wavepath methode in perifere bloedvat analyses beschreven, en de waarde van onze padlijn methode in andere bloedvaten dan de kransslagaders getoond. Een uitgebreide validatie studie is uitgevoerd, gebruik makend van een grote verscheidenheid aan beelden, met verschillende beeldkenmerken, verschillende beeldversterkers, verschillende morfologiën en de hele range van bloedvat afmetingen. In deze validatie studie, heeft de Wavepath nogmaals haar betrouwbaarheid en reproduceerbaarheid bewezen; er waren slechts kleine variaties te zien wanneer de start- en eindpunten werden gevarieerd.

Hoofdstuk 5 introduceert en bespreekt de Wavecontour, onze nieuwe aanpak voor het detecteren van arteriële contouren in röntgen angiogrammen. Naar aanleiding van de inventarisatie van contourdetectie methoden gepresenteerd in hoofdstuk 2, is de contourdetectie methode gebaseerd op een wavefront propagatie die gebruik maakt van directionele rand-informatie in het beeld. Het algoritme is geïmplementeerd als een twee-fasen methode, zodat een schatting van de grootte van het bloedvat kan worden meegenomen in de tweede fase van het proces om een matched-filter-benadering te hanteren. Deze nieuwe aanpak is ontworpen voornamelijk om de problemen die bestaan met andere contour detectietechnieken, zoals onder- en oversampling in scherpe bochten en de juiste detectie van complexe laesies, op te lossen. In de validatiestudie die werd uitgevoerd op zowel fantoomdata als in vivo patiëntendata, heeft de Wavecontour de verbetering in nauwkeurigheid en reproduceerbaarheid aangetoond, waarbij geen systematische fouten en slechts weinig variatie in de herhaalde metingen te zien waren. De nauwkeurige oversteek van zijtakken met deze methode blijft echter nog steeds een uitdaging.

Hoofdstuk 6 presenteert onze nieuwe aanpak voor de meting van de diameters van de bloedvaten en de schatting van de referentie diameters. Het belangrijkste doel voor deze nieuwe methode was het oplossen van de problemen die werden ondervonden met de huidige diameter meetmethode met betrekking tot de richting van de diameters in complexe laesies en in scherpe bochten. Bovendien bevat de nieuwe methode een specifieke aanpak voor de meting van de vaatdiameters in het proximale deel van een zijtak, het ostium, evenals de definitie van referentie diameters in die sectie van het bloedvat. De validatie studie toont een verbetering in de nauwkeurigheid van de metingen van de laesie, doordat deze nieuwe aanpak de ware minimale diameter kan meten. Naast de rechte-segment en ostiale segment benadering, definieert onze nieuwe methode ook twee nieuwe bifurcatie modellen voor het nauwkeurig meten van de diameters en laesie parameters van een hele bifurcatie. We introduceren de Y-shape en T-shape bifurcatie modellen die overeenkomen met verschillende interventietechnieken en samen het hele scala aan bifurcatie morfologiën omvatten. Deze modellen bieden gegevens voor het proximale, het distale en het centrale deel van de bifurcatie (birfurcation core), wat tot nu toe niet mogelijk was met andere meetmethoden. In de validatiestudie, worden de hoge nauwkeurigheid en precisie aangetoond door middel van bifurcatie fantoom beelden.

Hoofdstuk 7 geeft een overzicht van alle stappen die in de bifurcatie analyse worden gebruikt met inbegrip van de onlangs ingevoerde 'edge segment' analyse. Deze edge segment analyse verdeelt de hele geanalyseerde bifurcatie in subsegmenten aan de hand van stent plaatsingen. Het biedt gegevens voor stent segmenten en de bijbehorende stent- en ostiale rand-segmenten. Daarnaast worden in dit hoofdstuk de resultaten van het eerste bifurcatie validatieonderzoek op patiëntgegevens gepresenteerd, die een lage intra-observer variabiliteit laten zien, wat een hoge reproduceerbaarheid van onze nieuwe bifurcatie analysemethoden impliceert.

Hoofdstuk 8 beschrijft een uitgebreide validatiestudie voor de bifurcatie-analyse die op klinische gegevens is uitgevoerd. Deze validatiestudie analyseert de inter- en intra-observer variabiliteit op pre- en post-interventie beeld data met behulp van zowel het Y-shape als het T-shape bifurcatie model. De resultaten tonen een goede reproduceerbaarheid voor beide van onze nieuw ontwikkelde bifurcatie analysemethoden.

In **hoofdstuk 9** worden elk van onze nieuw ontwikkelde methoden, gepresenteerd in de voorafgaande hoofdstukken, besproken. Voor elke methode wordt geëvalueerd in welke mate aan onze doelstellingen is voldaan en wat nog open staat voor verder onderzoek. Verder worden de prestaties van onze methoden in vergelijking met andere commercieel beschikbare pakketten geëvalueerd. De nauwkeurigheid en precisie van onze software zijn zeer vergelijkbaar met die van concurrerende producten, voor zowel de rechte-segment analyse als de bifurcatie-analyse. Het verschil zit in de workflow, de gebruikersinteractie en voornamelijk de bepaling van de referentie waardes, wat ons pakket een voordeel geeft vanwege de verschillende mogelijkheden voor de berekening van deze referenties. Daarnaast wordt onze visie op de toekomst van QCA uiteengezet: ik denk dat de analysetechnieken die verschillende modaliteiten combineren zeer belangrijk zullen worden, zoals de fusie van QCA en IVUS/OCT.

Tot slot wordt een algemene conclusie gepresenteerd, waarbij de doelstellingen van het gehele onderzoek in acht worden genomen: onze 2D QCA software wordt nog steeds beschouwd als een standaard en naar verwachting gaat het bifurcatie-pakket een vergelijkbare standaard worden. We kunnen concluderen dat ons doel om de QCA analyse te verbeteren en uit te breiden met nieuwe morfologiën en nieuwe interventie technieken is gehaald.

References

[1] Heart Disease and Stroke Statistics - 2005 Update. Dallas, Tex.;. Available from: http://www.americanheart.org.

[2] European Heart Network;. Available from: http://www.ehnheart.org.

[3] World Health Organization;. Available from: http://www.who.int.

[4] Bruschke AVG, Sheldon WC, Shirey EK, Proudfit WL. A Half Century of Selective Coronary Arteriography. J Am Coll Cardiol. 2009;54(23):2139–2144.

[5] Rontgen WC. On a new kind of rays. Nature. 1896;53(41):274–277.

[6] Rontgen WC. On a new kind of rays. Science (New York, NY). 1896;3(59):227–231.

[7] Sones FMJ, Shirey EK. Cine coronary arteriography. Modern concepts of cardiovascular disease. 1962;31:735–738.

[8] Castellanos A GA Pereiras R. La angio-cardiografia radio-opaca. Arch Soc de Estudios Clin De Habana. 1937;31:523–596.

[9] Arnulf G, Buffard P. Die Arteriographie der Koronarien mittels Azetylcholin. Fortschr Rontgenstr. 1960;92(02):115–129.

[10] Judkins MP. Selective Coronary Arteriography: A Percutaneous Transfemoral Technic. Radiology. 1967;89(5):815–824.

[11] Amplatz K, Anderson R. Angiographic appearance of myocardial bridging of the coronary artery. Invest Radiol. 1968;3(3):213–215.

[12] Ludwig JW, Bruschke AV. Improvement of Diagnostic Accuracy of Coronary Arteriogram By Unconventional Projections. Circulation. 1973;48(4):193–193.

[13] Glagov S, Weisenberg E, Zarins CK, Stankunavicius R, Kolettis GJ. Compensatory Enlargement of Human Atherosclerotic Coronary-arteries. N Engl J Med. 1987;316(22):1371–1375.

[14] Achenbach S. Cardiac CT: state of the art for the detection of coronary arterial stenosis. Journal of cardiovascular computed tomography. 2007;1(1):3–20.

[15] Schuijf JD, Delgado V, van Werkhoven JM, de Graaf FR, van Velzen JE, Boogers MM, et al. Novel clinical applications of state-of-the-art multi-slice computed tomography. Int J Cardiovasc Imaging. 2009;25:241–254.

[16] Leber AW, Knez A, von Ziegler F, Becker A, Nikolaou K, Paul S, et al. Quantification of obstructive and nonobstructive coronary lesions by 64-slice computed tomography - A comparative study with quantitative coronary angiography and intravascular ultrasound. J Am Coll Cardiol. 2005;46(1):147–154.

[17] Leber AW, Becker A, Knez A, von Ziegler F, Sirol M, Nikolaou K, et al. Accuracy of 64-slice computed tomography to classify and quantify plaque volumes in the proximal coronary system - A comparative study using intravascular ultrasound. J Am Coll Cardiol. 2006;47(3):672–677.

[18] Otsuka M, Bruining N, Van Pelt NC, Mollet NR, Ligthart JMR, Vourvouri E, et al. Quantification of coronary plaque by 64-slice computed tomography: A comparison with quantitative intracoronary ultrasound. Invest Radiol. 2008;43(5):314–321.

[19] Marquering HA, Dijkstra J, de Koning PJH, Stoel BC, Reiber JHC. Towards quantitative analysis of coronary CTA. Int J Cardiovasc Imaging. 2005;21(1):73–84.

[20] Bruining N, Roelandt JRTC, Palumbo A, La Grutta L, Cademartiri F, de Feijter PJ, et al. Reproducible coronary plaque quantification by multislice computed tomography. Cathet Cardiovasc Interv. 2007;69(6):857–865.

[21] Kopp AF, Schroeder S, Baumbach A, Kuettner A, Georg C, Ohnesorge B, et al. Non-invasive characterisation of coronary lesion morphology and composition by multislice CT: first results in comparison with intracoronary ultrasound. Eur Radiol. 2001;11(9):1607–1611.

[22] Leber AW, Knez A, Becker A, Becker C, von Ziegler F, Nikolaou K, et al. Accuracy of multidetector spiral computed tomography in identifying and differentiating the composition of coronary atherosclerotic plaques - A comparative study with intracoronary ultrasound. J Am Coll Cardiol. 2004;43(7):1241–1247.

[23] Schroeder S, Kopp AF, Baumbach A, Meisner C, Kuettner A, Georg C, et al. Noninvasive detection and evaluation of atherosclerotic coronary plaques with multislice computed tomography. J Am Coll Cardiol. 2001;37(5):1430–1435.

[24] Kim TH, Hur J, Kim SJ, Kim HS, Choi BW, Choe KO, et al. Two-phase reconstruction for the assessment of left ventricular volume and function using retrospective ECG-gated MDCT: Comparison with echocardiography. American Journal of Roentgenology. 2005;185(2):319–325.

[25] Henneman MM, Schuijf JD, Jukema JW, Holman ER, Lamb HJ, de Roos A, et al. Assessment of global and regional left ventricular function and volumes with 64-slice MSCT: A comparison with 2D echocardiography. J Nucl Cardiol. 2006;13(4):480–487.

[26] Wua YW, Tadamura E, Yamamuro M, Kanao S, Okayama S, Ozasa N, et al. Estimation of global and regional cardiac function using 64-slice computed tomography: A comparison study with echocardiography, gated-SPECT and cardiovascular magnetic resonance. Int J Cardiol. 2008;128(1):69–76.

[27] Jassal DS, Shapiro MD, Neilan TG, Chaithiraphan V, Ferencik M, Teague SD, et al. 64-slice multidetector computed tomography (MDCT) for detection of aortic regurgitation and quantification of severity. Invest Radiol. 2007;42(7):507–512.

[28] Messika-Zeitoun D, Serfaty JM, Laissy JP, Berhili M, Brochet E, Iung B, et al. Assessment of the mitral valve area in patients with mitral stenosis by multislice computed tomography. J Am Coll Cardiol. 2006;48(2):411–413.

[29] Pouleur AC, de Waroux JB, Pasquet A, Vanoverschelde JLJ, Gerber BL. Aortic valve area assessment: Multidetector CT compared with cine MR imaging and transthoracic and transesophageal echocardiography. Radiology. 2007;244(3):745–754.

[30] de Koning PJH, Schaap JA, Janssen JP, Westenberg JJM, van der Geest RJ, Reiber JHC. Automated segmentation and analysis of vascular structures in magnetic resonance angiographic images. Magn Reson Med. 2003;50(6):1189–1198.

[31] Kim DY, Park JW. Computerized quantification of carotid artery stenosis using MRA axial images. Magn Reson Imaging. 2004;22(3):353–359.

[32] Saam T, Ferguson MS, Yarnykh VL, Takaya N, Xu D, Polissar NL, et al. Quantitative evaluation of carotid plaque composition by in vivo MRI. Arteriosclerosis Thrombosis and Vascular Biology. 2005;25(1):234–239.

[33] Adame IM, van der Geest RJ, Wasserman BA, Mohamed MA, Reiber JHC, Lelieveldt BPF. Automatic segmentation and plaque characterization in atherosclerotic carotid artery MR images. Magnetic Resonance Materials In Physics Biology and Medicine. 2004;16(5):227–234.

[34] Kim WY, Stuber M, Bornert P, Kissinger KV, Manning WJ, Botnar RM. Three-dimensional black-blood cardiac magnetic resonance coronary vessel wall imaging detects positive arterial remodeling in patients with nonsignificant coronary artery disease. Circulation. 2002;106(3):296–299.

[35] Adame IM, de Koning PJH, Lelieveldt BPF, Wasserman BA, Reiber JHC, van der Geest RJ. An integrated automated analysis method for quantifying vessel stenosis and plaque burden from carotid MRI images - Combined postprocessing of MRA and vessel wall MR. Stroke. 2006;37(8):2162–2164.

[36] Reiber JHC, Serruys PW, Kooijman CJ, Wijns W, Slager CJ, Gerbrands JJ, et al. Assessment of Short-term, Medium-term, and Long-term Variations In Arterial Dimensions From Computer-assisted Quantitation of Coronary Cineangiograms. Circulation. 1985;71(2):280–288.

[37] Reiber JHC, Serruys PW. Quantitative coronary arteriography. Dordrecht: Kluwer Academic Publishers; 1991.

[38] Reiber JHC, van der Zwet PMJ, Land CDv. Quantitative coronary arteriography: equipment and technical requirements. In: Reiber JHC, Serruys PW, editors. Advances in Quantitative coronary arteriography. Dordrecht: Kluwer Academic Publishers; 1992. p. 75–111.

[39] Reiber JHC, van der Zwet PMJ, Koning G, Vonland CD, Vanmeurs B, Gerbrands JJ, et al. Accuracy and Precision of Quantitative Digital Coronary Arteriography - Observer-term, Short-term, and Medium-term Variabilities. Cathet Cardiovasc Diagn. 1993;28(3):187–198.

[40] van der Zwet PMJ, von Land CD, Loois G, Gerbrands JJ, Reiber JHC. An on-line system for the quantitative analysis of coronary arterial segments. In: Proceedings of Computers in Cardiology; 1989. p. 157–160.

[41] Marcus ML, Wilson RF, White CW. Methods of Measurement of Myocardial Blood-flow In Patients - A Critical-review. Circulation. 1987;76(2):245–253.

[42] Hoffman JIE. Maximal Coronary Flow and the Concept of Coronary Vascular Reserve. Circulation. 1984;70(2):153–159.

[43] Pijls NHJ, Vanson JAM, Kirkeeide RL, Debruyne B, Gould KL. Experimental Basis of Determining Maximum Coronary, Myocardial, and Collateral Blood-flow By Pressure Measurements For Assessing Functional Stenosis Severity Before and After Percutaneous Transluminal Coronary Angioplasty. Circulation. 1993;87(4):1354–1367.

[44] Debruyne B, Baudhuin T, Melin JA, Pijls NHJ, Sys SU, Bol A, et al. Coronary Flow Reserve Calculated From Pressure Measurements In Humans - Validation With Positron Emission Tomography. Circulation. 1994;89(3):1013–1022.

[45] Pijls NHJ, van Gelder B, van der Voort P, Peels K, Bracke FALE, Bonnier HJRM, et al. Fractional Flow Reserve - A Useful Index To Evaluate the Influence of An Epicardial Coronary Stenosis On Myocardial Blood-flow. Circulation. 1995;92(11):3183–3193.

[46] Pijls NHJ, de Bruyne B, Peels K, van der Voort PH, Bonnier HJRM, Bartunek J, et al. Measurement of fractional flow reserve to assess the functional severity of coronary-artery stenoses. N Engl J Med. 1996;334(26):1703–1708.

[47] Beauman GJ, Reiber JHC, Koning G, van Houdt RCM, Vogel RA. Angiographic core laboratory analyses of arterial phantom images: Comparative evaluations of accuracy and precision. In: Reiber JHC, Serruys PW, editors. Progress in Quantitative Coronary Arteriography. Dordrecht: Kluwer Academic Publishers; 1994. p. 87–104.

[48] Tuinenburg JC, Koning G, Hekking E, Desjardins C, Harel F, Bilodeau L, et al. One core laboratory at two international sites, is that feasible? An inter-core laboratory and intra-observer variability study. Cathet Cardiovasc Interv. 2002;56(3):333–340.

[49] Greenspan H, Laifenfeld M, Einav S, Barnea O. Evaluation of center-line extraction algorithms in quantitative coronary angiography. IEEE Trans Med Imaging. 2001;20(9):928–941.

[50] van der Zwet PMJ, Reiber JHC. A New Approach For the Quantification of Complex Lesion Morphology - the Gradient Field Transform - Basic Principles and Validation Results. J Am Coll Cardiol. 1994;24(1):216–224.

[51] Eichel PH, Delp EJ, Koral K, Buda AJ. A Method For A Fully-automatic Definition of Coronary Arterial Edges From Cineangiograms. IEEE Trans Med Imaging. 1988;7(4):313–320.

[52] Sun Y. Automated identification of vessel contours in coronary arteriograms by an adaptive tracking algorithm. IEEE Trans Med Imaging. 1989;8(1):78–88.

[53] Reiber JH, Kooijman CJ, Slager CJ, Gerbrands JJ, Schuurbiers JC, Den Boer A, et al. Coronary artery dimensions from cineangiograms methodology and validation of a computer-assisted analysis procedure. IEEE Trans Med Imaging. 1984;3(3):131–141.

[54] van der Zwet PMJ, Reiber JHC. A new algorithm to detect irregular coronary boundaries: the gradient field transform. In: Proceedings of Computers in Cardiology; 1992. p. 107 –110.

[55] Sonka M, Winniford MD, Collins SM. Robust Simultaneous Detection of Coronary Borders In Complex Images. IEEE Trans Med Imaging. 1995;14(1):151–161.

[56] Sonka M, Reddy GK, Winniford MD, Collins SM. Adaptive approach to accurate analysis of small-diameter vessels in cineangiograms. IEEE Trans Med Imaging. 1997;16(1):87–95.

[57] Chan RC, Karl WC, Lee RS. A new model-based technique for enhanced small-vessel measurements in X-ray cine-angiograms. IEEE Trans Med Imaging. 2000;19(3):243–255.

[58] Reiber JHC, Slager CJ, Schuurbiers JCH, den Boer A, Gerbrands JJ, Troost GJ, et al. Transfer functions of the x ray cine video chain applied to digital processing of coronary cineangiograms. In: Heintzen PH, Brennecke R, editors. Digital Imaging in cardiovascular radiology. Dordrecht: George Thieme Verlag; 1983. p. 89–104.

[59] Miles FP, Nuttall AL. Matched-filter Estimation of Serial Blood-vessel Diameters From Video Images. IEEE Trans Med Imaging. 1993;12(2):147–152.

[60] van der Zwet PMJ, Nettesheim M, Gerbrands JJ, Reiber JHC. Derivation of optimal filters for the detection of coronary arteries. IEEE Trans Med Imaging. 1998;17(1):108–120.

[61] Jalali S, Boyce JF. Determination of Optimal General Edge Detectors By Global Minimization of A Cost Function. Image and Vision Computing. 1995;13(9):683–693.

[62] Petrou M, Kittler J. Optimal Edge Detectors For Ramp Edges. IEEE Trans Pattern Anal Mach Intell. 1991;13(5):483–491.

[63] Canny J. A Computational Approach To Edge-detection. IEEE Trans Pattern Anal Mach Intell. 1986;8(6):679–698.

[64] Figueiredo MAT, Leitao JMN. A Nonsmoothing Approach To the Estimation of Vessel Contours In Angiograms. IEEE Trans Med Imaging. 1995;14(1):162–172.

[65] Kass M, Witkin A, Terzopoulos D. Snakes - Active Contour Models. International Journal of Computer Vision. 1987;1(4):321–331.

[66] Staib LH, Duncan JS. Boundary Finding With Parametrically Deformable Models. IEEE Trans Pattern Anal Mach Intell. 1992;14(11):1061–1075.

[67] Metaxas DN. Physics-Based Deformable Models. Dordrecht: Kluwer Academic Publishers; 1996.

[68] Eviatar H, Somorjai RL. A fast, simple active contour algorithm for biomedical images. Pattern Recognition Letters. 1996;17(9):969–974.

[69] Huang X, Metaxas D, Chen T. MetaMorphs: Deformable shape and texture models. In: Proceedings of IEEE Conf. on Computer Vision and Pattern Recognition. vol. 1; 2004. p. I–496 – I–503 Vol.1.

[70] Klein AK, Lee F, Amini AA. Quantitative coronary angiography with deformable spline models. IEEE Trans Med Imaging. 1997;16(5):468–482.

[71] Klein A, Egglin TK, Pollak JS, Lee F, Amini AA. Identifying vascular features with orientation specific filters and B-spline snakes. In: Proceedings of Computers in Cardiology; 1994. p. 113 –116.

[72] Xu CY, Prince JL. Snakes, shapes, and gradient vector flow. IEEE Trans Image Process. 1998;7(3):359–369.

[73] Xu CY, Prince JL. Generalized gradient vector flow external forces for active contours. Signal Processing. 1998;71(2):131–139.

[74] McInerney T, Terzopoulos D. T-snakes: Topology adaptive snakes. Medical Image Analysis. 2000;4(2):73–91.

[75] Ji LL, Yan H. Attractable snakes based on the greedy algorithm for contour extraction. Pattern Recognition. 2002;35(4):791–806.

[76] Caselles V, Kimmel R, Sapiro G. Geodesic active contours. International Journal of Computer Vision. 1997;22(1):61–79.

[77] Malladi R, Sethian JA, Vemuri BC. Shape Modeling With Front Propagation - A Level Set Approach. IEEE Trans Pattern Anal Mach Intell. 1995;17(2):158–175.

[78] Vese LA, Chan TF. A multiphase level set framework for image segmentation using the Mumford and Shah model. International Journal of Computer Vision. 2002;50(3):271–293.

[79] Paragios N, Deriche R. Geodesic active regions and level set methods for supervised texture segmentation. International Journal of Computer Vision. 2002;46(3):223–247.

[80] Adalsteinsson D, Sethian JA. A Fast Level Set Method For Propagating Interfaces. Journal of Computational Physics. 1995;118(2):269–277.

[81] Sethian JA. A fast marching level set method for monotonically advancing fronts. Proc Natl Acad Sci U S A. 1996;93(4):1591–1595.

[82] Quek FKH, Kirbas C. Vessel extraction in medical images by wave-propagation and traceback. IEEE Trans Med Imaging. 2001;20(2):117–131.

[83] Deschamps T, Cohen LD. Fast extraction of minimal paths in 3D images and applications to virtual endoscopy. Medical Image Analysis. 2001;5(4):281–299.

[84] Janssen JP, Koning G, de Koning PJH, Tuinenburg JC, Reiber JHC. A novel approach for the detection of pathlines in X-ray angiograms: the wavefront propagation algorithm. Int J Cardiovasc Imaging. 2002;18(5):317–324.

[85] Vincent L, Soille P. Watersheds In Digital Spaces - An Efficient Algorithm Based On Immersion Simulations. IEEE Trans Pattern Anal Mach Intell. 1991;13(6):583–598.

[86] Wang DM. A multiscale gradient algorithm for image segmentation using watersheds. Pattern Recognition. 1997;30(12):2043–2052.

[87] Manjunath BS, Chellappa R. Unsupervised Texture Segmentation Using Markov Random Field Models. IEEE Trans Pattern Anal Mach Intell. 1991;13(5):478–482.

[88] Shi JB, Malik J. Normalized cuts and image segmentation. IEEE Trans Pattern Anal Mach Intell. 2000;22(8):888–905.

[89] Boykov Y, Veksler O, Zabih R. Fast approximate energy minimization via graph cuts. IEEE Trans Pattern Anal Mach Intell. 2001;23(11):1222–1239.

[90] Xu N, Ahuja N, Bansal R. Object segmentation using graph cuts based active contours. Computer Vision and Image Understanding. 2007;107(3):210–224.

[91] Cootes TF, Taylor CJ, Cooper DH, Graham J. Active Shape Models - Their Training and Application. Computer Vision and Image Understanding. 1995;61(1):38–59.

[92] Mitchell SC, Lelieveldt BPF, van der Geest RJ, Bosch HG, Reiber JHC, Sonka M. Multistage hybrid active appearance model matching: Segmentation of left and right ventricles in cardiac MR images. IEEE Trans Med Imaging. 2001;20(5):415–423.

[93] Mitchell SC, Bosch JG, Lelieveldt BPF, van der Geest RJ, Reiber JHC, Sonka M. 3-D active appearance models: Segmentation of cardiac MR and ultrasound images. IEEE Trans Med Imaging. 2002;21(9):1167–1178.

[94] Bosch JG, Mitchell SC, Lelieveldt BPF, Nijland F, Kamp O, Sonka M, et al. Automatic segmentation of echocardiographic sequences by active appearance motion models. IEEE Trans Med Imaging. 2002;21(11):1374–1383.

[95] van der Geest RJ, Lelieveldt BPF, Angelie E, Danilouchkine M, Swingen C, Sonka M, et al. Evaluation of a new method for automated detection of left ventricular boundaries in time series of magnetic resonance images using an active appearance motion model. Journal of Cardiovascular Magnetic Resonance. 2004;6(3):609–617.

[96] Reiber JHC, Serruys PW. Quantitative coronary arteriography. In: Marcus ML, Skorton DJ, Schelbert HR, Wolf GL, editors. Cardiac Imaging. Philidelphia: Saunders; 1991. p. 211–281.

[97] van der Zwet PM, Pinto IM, Serruys PW, Reiber JH. A new approach for the automated definition of path lines in digitized coronary angiograms. Int J Card Imaging. 1990;5(2-3):75–83.

[98] Tommasini G, Rubartelli P, Piaggio M. A deterministic approach to automated stenosis quantification. Cathet Cardiovasc Interv. 1999;48(4):435–445.

[99] Barrett WA, Mortensen EN. Interactive live-wire boundary extraction. Medical image analysis. 1997;1(4):331–341.

[100] Privat C, Ravel A, Chirossel P, Borson O, Perez N, Bourlet P, et al. Endovascular Doppler guide wire in renal arteries - Correlation with angiography in 20 patients. Invest Radiol. 1999;34(8):530–535.

[101] van Assen HC, Vasbinder GBC, Stoel BC, Putter H, van Engelshoven JMA, Reiber JHC. Quantitative assessment of the morphology of renal arteries from X-ray images - Quantitative vascular analysis. Invest Radiol. 2004;39(6):365–373.

[102] Janssen JP, Koning G, de Koning PJH, Tuinenburg JC, Reiber JHC. Validation of a new method for the detection of pathlines in vascular x-ray images. Invest Radiol. 2004;39(9):524–530.

[103] Leiner T, Kessels AGH, Schurink GW, Kitslaar PJEHM, de Haan MW, Tordoir JHM, et al. Comparison of contrast-enhanced magnetic resonance angiography and digital subtraction angiography in patients with chronic critical ischemia and tissue loss. Invest Radiol. 2004;39(7):435–444.

[104] Lefevre T, Louvard Y, Morice MC, Dumas P, Loubeyre C, Benslimane A, et al. Stenting of bifurcation lesions: Classification, treatments, and results. Cathet Cardiovasc Interv. 2000;49(3):274–283.

[105] Louvard Y, Lefevre T, Morice MC. Percutaneous coronary intervention for bifurcation coronary disease. Heart. 2004;90(6):713–722.

[106] Haase J, Dimario C, Slager CJ, van der Giessen WJ, Denboer A, Defeyter PJ, et al. Invivo Validation of Online and Off-line Geometric Coronary Measurements Using Insertion of Stenosis Phantoms In Porcine Coronary-arteries. Cathet Cardiovasc Diagn. 1992;27(1):16–27.

[107] Kirkeeide RL, Fung P, Smalling RW, Gould KL. Automated evaluation of vessel diameter from arteriograms. In: Proceedings of Computers in Cardiology; 1982. p. 215 – 218.

[108] Kruger RA. Estimation of the Diameter of and Iodine Concentration Within Blood-vessels Using Digital Radiography Devices. Med Phys. 1981;8(5):652–658.

[109] Simons MA, Kruger RA, Power RLB. Cross-sectional Area Measurements By Digital Subtraction Videodensitometry. Invest Radiol. 1986;21(8):637–644.

[110] Westenberg JJM, van der Geest RJ, Wasser MNJM, van der Linden EL, van Walsum T, van Assen HC, et al. Vessel diameter measurements in gadolinium contrast-enhanced three-dimensional MRA of peripheral arteries. Magn Reson Imaging. 2000;18(1):13–22.

[111] Testi D, Zannoni C, Cappello A, Viceconti M. Border-tracing algorithm implementation for the femoral geometry reconstruction. Comput Methods Programs Biomed. 2001;65(3):175–182.

[112] Weber DM. Absolute Diameter Measurements of Coronary-arteries Based On the 1st Zero Crossing of the Fourier Spectrum. Med Phys. 1989;16(2):188–196.

[113] Hoffmann KR, Nazareth DP, Miskolczi L, Gopal A, Wang Z, Rudin S, et al. Vessel size measurements in angiograms: A comparison of techniques. Med Phys. 2002;29(7):1622–1633.

[114] Shen YZ, Barner KE. Fuzzy vector median-based surface smoothing. IEEE Transactions on Visualization and Computer Graphics. 2004;10(3):252–265.

[115] Reiber JHC, Tuinenburg JC, Koning G, Janssen JP, Rareş A, Lansky AJ, et al. Quantitative Coronary Arteriography. In: Oudkerk M, Reiser MF, editors. Coronary Radiology. 2nd ed. Medical Radiology. Dordrecht: Springer-Verlag; 2009. p. 41–65. Sub-series: Diagnostic Imaging, Baert, A.L. and Knauth, M. and Sartor, K. (eds).

[116] Reiber JHC, Schiemanck LR, van der Zwet PMJ, Goedhart B, Koning G, Lammertsma M, et al. State of the Art in Quantitative Coronary Arteriography as of 1996. In: Reiber JHC, Serruys PW, editors. Cardiovascular Imaging. Dordrecht: Kluwer Academic Publishers; 1996. p. 39–56.

[117] Tuinenburg JC, Koning G, Seppenwoolde Y, Reiber JHC. Is there an effect of flat-panel-based imaging systems on quantitative coronary and vascular angiography? Cathet Cardiovasc Interv. 2006;68(4):561–566.

[118] Reiber JHC, Koning G, von Land CD, van der Zwet PMJ. Why and how should QCA systems be validated? In: Reiber JHC, Serruys PW, editors. Progress in Quantitative Coronary Arteriography. Dordrecht: Kluwer Academic Publishers; 1994. p. 33–48.

[119] Janssen JP, Koning G, de Koning PJH, Bosch JG, Tuinenburg JC, Reiber JHC. A new approach to contour detection in X-ray arteriograms - The Wavecontour. Invest Radiol. 2005;40(8):514–520.

[120] Lansky A, Tuinenburg J, Costa M, Maeng M, Koning G, Popma J, et al. Quantitative Angiographic Methods for Bifurcation Lesions: A Consensus Statement from the European Bifurcation Group. Cathet Cardiovasc Interv. 2009;73(2):258–266.

[121] Goktekin O, Kaplan S, Dimopoulos K, Barlis P, Tanigawa J, Vatankulu MA, et al. A new quantitative analysis system for the evaluation of coronary bifurcation lesions: Comparison with current conventional methods. Cathet Cardiovasc Interv. 2007;69(2):172–180.

[122] Verheye S, Agostoni P, Dubois CL, Dens J, Ormiston J, Worthley S, et al. 9-Month Clinical, Angiographic, and Intravascular Ultrasound Results of a Prospective Evaluation of the Axxess Self-Expanding Biolimus A9-Eluting Stent in Coronary Bifurcation Lesions. J Am Coll Cardiol. 2009;53(12):1031–1039.

[123] Tu S, Koning G, Jukema W, Reiber JHC. Assessment of obstruction length and optimal viewing angle from biplane X-ray angiograms. Int J Cardiovasc Imaging. 2010;26(1):5–17.

[124] Tu S, Huang Z, Koning G, Cui K, Reiber JHC. A Novel Three-Dimensional Quantitative Coronary Angiography System: In-Vivo Comparison With Intravascular Ultrasound for Assessing Arterial Segment Length. Cathet Cardiovasc Interv. 2010;76(2):291–298.

[125] Tu S, Holm NR, Koning G, Huang Z, Reiber JHC. Fusion of 3D QCA and IVUS/OCT. Int J Cardiovasc Imaging. 2011;27(2):197–207.

[126] Lefevre T, Louvard Y, Morice MC, Loubeyre C, Piechaud JF, Dumas P. Stenting of bifurcation lesions: a rational approach. Journal of interventional cardiology. 2001;14(6):573–585.

[127] Lespérance J, Bilodeau L, Reiber JHC, Koning G, Hudon G, Bourassa M. Issues in the performance of quantitative coronary angiography in clinical research trials. In: Reiber JHC, van der Wall EE, editors. What's new in Cardiovascular Imaging? Dordrecht: Kluwer Academic Publishers; 1998. p. 31–46.

[128] Beleslin B, Ostojic M, Nedeljkovic M, et al. Assessment of the reproducibility of the basic parameters obtained from quantitative coronary arteriography analyses. In: European Heart Journal. vol. 16(abstract Suppl); 1995. p. 296.

[129] Reiber JHC, Koning G, Dijkstra J, Wahle A, Goedhart B, Sheehan FH, et al. Angiography and intravascular ultrasound. In: Sonka M, Fitzpatrick JM, editors. Handbook of Medical Imaging: Medical image processing and analysis. vol. 2. Belligham WA: SPIE Press; 2001. p. 711–808.

[130] Reiber JHC, Tuinenburg JC, Koning G, Janssen JP, Lansky A, Goedhart B. Quantitative Coronary Arteriography. In: Oudkerk M, Reiser MF, editors. Coronary Radiology Revised 2nd Edition. Medical Radiology, Diagnostic Imaging, Baert, A.L. and Knauth, M. and Sartor, K.. Berlin/Heidelberg/NewYork: Springer-Verlag; 2008. p. 41–65.

[131] Reiber JHC, von Land CD, Koning G, van der Zwet PMJ, van Houdt RCM, Schalij MJ, et al. Comparison of accuracy and precision of quantitative coronary arterial analysis between cinefilm and digital systems. In: Reiber JHC, Serruys PW, editors. Progress in Quantitative Coronary Arteriography. Dordrecht: Kluwer Academic Publishers; 1994. p. 67–85.

[132] Janssen JP, Rareş A, Tuinenburg JC, Koning G, Lansky AJ, Reiber JHC. New approaches for the assessment of vessel sizes in quantitative (cardio-)vascular X-ray analysis. Int J Cardiovasc Imaging. 2010;26(3):259–271.

[133] Reiber JHC, Booman F, Tan H, Slager CJ, Schuurbiers JC, Gerbrands JJ, et al. A cardiac image analysis system. Objective quantitative processing of angiocardiograms. In: Proceedings of Computers in Cardiology; 1978. p. 239–242.

[134] Tuinenburg JC, Koning G, Rareş A, Janssen JP, Louvard Y, Pattenier H, et al. A novel method for the analysis of bifurcation lesions in cardiovascular angiograms. Eur Heart J. 2005;26(1):478. 27th Congress of the European-Society-of-Cardiology, Stockholm, SWEDEN, SEP 03-07, 2005.

[135] Koning G, Louvard Y, Tuinenburg JC, Rareş A, Reiber JHC. A novel quantitative method for the analysis of bifurcation lesions in cardiovascular angiograms. Am J Cardiol. 2006;98(8A, S):138M. 18th Annual Transcatheter Cardiovascular Therapeutics Symposium, Washington, DC, OCT 22-27, 2006.

[136] Steigen TK, Maeng M, Wiseth R, Erglis A, Kumsars I, Narbute I, et al. Randomized study on simple versus complex stenting of coronary artery bifurcation lesions - The Nordic Bifurcation study. Circulation. 2006;114(18):1955–1961.

[137] Erglis A, Kumsars I, Niemela M, Kervinen K, Maeng M, Lassen JF, et al. Randomized Comparison of Coronary Bifurcation Stenting With the Crush Versus the Culotte Technique Using Sirolimus Eluting Stents The Nordic Stent Technique Study. Circulation-cardiovascular Interventions. 2009;2(1):27–34.

[138] Holm NR, Hojdahl H, Lassen JF, Thuesen L, Maeng M. Quantitative coronary analysis in the Nordic Bifurcation studies. Int J Cardiovasc Imaging. 2011;27(2):175–180.

[139] Medina A, de Lezo JS, Pan M. A new classification of coronary bifurcation lesions. Rev Esp Cardiol. 2006;59(2):183.

[140] Louvard Y, Thomas M, Dzavik V, Hildick-Smith D, Galassi AR, Pan M, et al. Classification of coronary artery bifurcation lesions and treatments: Time for a consensus! Cathet Cardiovasc Interv. 2008;71(2):175–183.

[141] Tuinenburg JC, Koning G, Reiber JHC. Quantitative Coronary and Vascular Angiography. In: Mario D, Dangas, Barlis, editors. Interventional Cardiology: Principal and practice. Oxford: Wiley-Blackwell; 2010. p. 90–99.

[142] Koning G, Tuinenburg JC, Hekking E, Peelen J, van Weert AWM, Bergkamp D, et al. A novel measurement technique to assess the effects of coronary brachytherapy in clinical trials. IEEE Trans Med Imaging. 2002;21(10):1254–1263.

[143] Waters D, Craven TE, Lesperance J. Prognostic-significance of Progression of Coronary Atherosclerosis. Circulation. 1993;87(4):1067–1075.

[144] Lansky AJ, Desai K, Leon MB. Quantitative coronary angiography in regression trials: A review of methodologic considerations, endpoint selection, and limitations. American Journal of Cardiology. 2002;89(4A):4B–9B.

[145] Jukema JW, Bruschke AVG, Vanboven AJ, Reiber JHC, Bal ET, Zwinderman AH, et al. Effects of Lipid-lowering By Pravastatin On Progression and Regression of Coronary-artery Disease In Symptomatic Men With Normal To Moderately Elevated Serum-cholesterol Levels - the Regression Growth Evaluation Statin Study (REGRESS). Circulation. 1995;91(10):2528–2540.

[146] Tuinenburg JC, Koning G, Rareş A, Janssen JP, Lansky AJ, Reiber JHC. Dedicated bifurcation analysis: basic principles. Int J Cardiovasc Imaging. 2011;27(2):167–174.

[147] Haase J, Escaned J, van Swijndregt EM, Ozaki Y, Gronenschild E, Slager CJ, et al. Experimental Validation of Geometric and Densitometric Coronary Measurements On the New-generation Cardiovascular Angiography Analysis System (caas-ii). Cathet Cardiovasc Diagn. 1993;30(2):104–114.

[148] Girasis C, van Geuns RJ, Onuma Y, Serruys PW. Essentials of quantitative angiography for bifurcation lesions. Eurointervention. 2010;6:J36–J43.

[149] Ramcharitar S, Daeman J, Patterson M, van Guens RJ, Boersma E, Serruys PW, et al. First direct in vivo comparison of two commercially available three-dimensional quantitative coronary angiography systems. Cathet Cardiovasc Interv. 2008;71(1):44–50.

[150] Tu S, Hao P, Koning G, Wei X, Song X, Chen A, et al. In vivo assessment of optimal viewing angles from X-ray coronary angiography. Eurointervention. 2011;7(1):112–120.

Acknowledgements

Dit proefschrift beschrijft het onderzoek dat gedaan is in een periode van 12 jaar bij het Laboratorium van Klinische en Experimentele Beeldverwerking onder begeleiding van prof. dr. ir. J.H.C. Reiber en ir. G. Koning. Hierbij wil ik hen bedanken voor het geven van de mogelijkheid om dit onderzoek en deze promotie compleet te maken.

Uiteraard wil ik mijn huidige collega's en niet te vergeten ook de oud-collega's van LKEB bedanken. Het zijn er teveel geweest in al die jaren om iedereen persoonlijk te noemen, maar jullie hebben er een groot aandeel in dat ik nog steeds elke dag met veel plezier naar het werk kom. Jullie zijn wat LKEB echt bijzonder maakt: iedereen is altijd bereid om te helpen, mee te denken en te discussiëren, ook al heeft men het nog zo druk met zijn eigen project. Daarnaast is er altijd tijd voor een ontspannen babbeltje (soms in het Brabants), in het poortgebouw onder het genot van een lekker rondje handgemaakte espresso.

Ook wil ik de collega's bij Medis van AR en R&D bedanken voor het warme welkom toen ik ineens voor deeltijd bij jullie kwam zitten. Ik vond het erg leuk om wat dichter bij de toepassing te zitten en feedback uit het veld te krijgen over nieuwe stukjes onderzoek die in de commerciële software waren geïntegreerd. Joan en Andrei, dank voor alle 'eindeloze' discussies en brainstorm-sessies over contouren, diameters, centerlines en bifurcaties, eerst bij LKEB en later bij Medis. We waren het lang niet altijd eens, maar dat hield ons allemaal scherp en heeft tot mooie ideeën en oplossingen geleid. Gezamenlijk hebben we een analyse-pakket gemaakt waar we trots op mogen zijn.

In het bijzonder wil ik mijn paranimfen Hilde en Patrick bedanken. Hilde, je riep al vanaf het begin dat je paranimf wilde zijn, al had je wellicht niet meer gedacht dat het er ooit nog van zou komen. Patrick, wat een prestatie dat je het al 12 en een half jaar lang bij mij op de kamer uithoudt, van de terminaalzaal tot het poortgebouw. Erg handig om jou altijd in de buurt te hebben voor al mijn vragen.

Naast het werk is volleybal voor mij erg belangrijk. Het sporten geeft me telkens weer de noodzakelijke nieuwe energie. Daarom wil ik al mijn volleybalvriendjes van Donar en Kratos, maar zeker ook de Kannieballen, heel erg bedanken voor de broodnodige ontspanning, de sportieve inspanning, maar vooral ook alle gezelligheid. En Jenneke, wat is de kaft mooi geworden!

"Wanneer ga je nou eens promoveren?" Met deze confronterende vraag was ik niet altijd even blij, maar toch wil ik iedereen die deze vraag de afgelopen jaren aan mij heeft gesteld bedanken. Misschien was dit uiteindelijk toch net een extra motivatie om het af te maken.

Grote dank gaat uit naar mijn lieve ouders en schoonouders voor het vele oppassen op de meiden op mijn papa-dag, zodat ik aan mijn promotie kon werken. Zonder jullie had ik nooit de tijd gehad om het proefschrift daadwerkelijk af te maken.

Pa en ma, jullie in het bijzonder heel veel dank voor alles wat jullie me van kinds af aan hebben meegegeven.

And last but certainly not least: mijn drie kanjers. Lieve Annieke, dankjewel voor je grenzeloze steun, vertrouwen en liefde. Voor het samen genieten van de mooie dingen in het leven, vooral van onze meisjes. Lieve Marloes en Eline, jullie hebben het me soms wel moeilijk gemaakt om voldoende tijd en energie in mijn proefschrift te steken, maar dat geeft niks, want wat maken jullie mij ontzettend blij en trots!

Jasper

List of Publications

- **Janssen JP**, Egmont-Petersen M, Hendriks EA, Reinders MJT, van der Geest RJ, Hogendoorn PCW, et al. Scale-invariant segmentation of dynamic contrast-enhanced perfusion MR images with inherent scale selection. Journal of Visualization and Computer Animation. 2002;13(1):1–19.

- **Janssen JP**, Koning G, de Koning PJH, Bosch JG, Tuinenburg JC, Reiber JHC. A new approach to contour detection in X-ray arteriograms - The Wavecontour. Invest Radiol. 2005;40(8):514–520.

- **Janssen JP**, Koning G, de Koning PJH, Tuinenburg JC, Reiber JHC. Validation of a new method for the detection of pathlines in vascular x-ray images. Invest Radiol. 2004;39(9):524–530.

- **Janssen JP**, Koning G, de Koning PJH, Tuinenburg JC, Reiber JHC. A novel approach for the detection of pathlines in X-ray angiograms: the wavefront propagation algorithm. Int J Cardiovasc Imaging. 2002;18(5):317–324.

- **Janssen JP**, Rareş A, Tuinenburg JC, Koning G, Lansky AJ, Reiber JHC. New approaches for the assessment of vessel sizes in quantitative (cardio-)vascular X-ray analysis. Int J Cardiovasc Imaging. 2010;26(3):259–271.

- Egmont-Petersen M, van der Geest RJ, Vrooman HA, Hogendoorn PCW, van der Woude HJ, **Janssen JP**, et al. Segmentation of Dynamic Contrast-Enhanced MR-Images of Post Chemotherapy Ewing's Sarcoma with a Pharmacokinetic Model and a Neural Network. In: Bildverarbeitung für die Medizin; 1999. p. 87–91.

- Egmont-Petersen M, Hogendoorn PCW, van der Geest RJ, Vrooman HA, van der Woude HJ, **Janssen JP**, et al. Detection of areas with viable remnant tumor in postchemotherapy patients with Ewing's sarcoma by dynamic contrast-enhanced MRI using pharmacokinetic modeling. Magnetic Resonance Imaging. 2000;18(5):525–535.

- de Koning PJH, Schaap JA, **Janssen JP**, Westenberg JJM, van der Geest RJ, Reiber JHC. Automated segmentation and analysis of vascular structures in magnetic resonance angiographic images. Magn Reson Med. 2003;50(6):1189–1198.

- Reiber JHC, Tu S, Tuinenburg JC, Koning G, **Janssen JP**, Dijkstra J. QCA, IVUS and OCT in interventional cardiology in 2011. Cardiovasc Diagn Ther. 2011;1:57–70.

- Reiber JHC, Tuinenburg JC, Koning G, **Janssen JP**, Lansky A, Goedhart B. Quantitative Coronary Arteriography. In: Oudkerk M, Reiser MF, editors. Coronary Radiology Revised 2nd Edition. Medical Radiology, Diagnostic Imaging, Baert, A.L. and Knauth, M. and Sartor, K.. Berlin/Heidelberg/NewYork: Springer-Verlag; 2008. p. 41–65.
- Reiber JHC, Tuinenburg JC, Koning G, **Janssen JP**, Rareş A, Lansky AJ, et al. Quantitative Coronary Arteriography. In: Oudkerk M, Reiser MF, editors. Coronary Radiology. 2nd ed. Medical Radiology. Dordrecht: Springer-Verlag; 2009. p. 41–65. Sub-series: Diagnostic Imaging, Baert, A.L. and Knauth, M. and Sartor, K. (eds).
- Schaap JA, de Koning PJH, **Janssen JP**, van der Geest RJ, Reiber JHC. Quantitative analysis of vascular images, in particular of abdominal aorta aneurysms from 3D CTA data sets. Studies in health technology and informatics. 2004;103:252–8.
- Schaap JA, de Koning PJH, **Janssen JP**, Westenberg JJM, van der Geest RJ, Reiber JHC. 3D quantification visualization of vascular structures in magnetic resonance angiographic images. Computational Science-iccs 2002, Pt Iii, Proceedings. 2002;2331:Univ Amsterdam, Sect Computat Sci; SHARCNET, Canada; Univ Tennessee,EOLEOLDept Comp Sci; Power Comp & Commun BV; Elsevier Sci Publ; SpringerEOLEOLVerlag; HPCN Fdn; Natl Supercomp Facilities; Sun Microsyst Inc; QueensEOLEOL-Univ, Sch Comp Sci.
- Tuinenburg JC, **Janssen JP**, Kooistra R, Koning G, Corral MD, Lansky AJ, et al. Clinical validation of the new T- and Y-shape models for the quantitative analysis of coronary bifurcations: An inter-observer variability study. Cathet Cardiovasc Interv. 2012;Submitted.
- Tuinenburg JC, Koning G, Rareş A, **Janssen JP**, Lansky AJ, Reiber JHC. Dedicated bifurcation analysis: basic principles. Int J Cardiovasc Imaging. 2011;27(2):167–174.
- Tuinenburg JC, Koning G, Rareş A, **Janssen JP**, Louvard Y, Pattenier H, et al. A novel method for the analysis of bifurcation lesions in cardiovascular angiograms. Eur Heart J. 2005;26(1):478. 27th Congress of the European-Society-of-Cardiology, Stockholm, SWEDEN, SEP 03-07, 2005.

Curriculum Vitæ

Johannes Petrus (Jasper) Janssen was born on the 7th of February, 1976 in Heteren. After graduating at the St. Oelbert Gymnasium in Oosterhout in 1994, he started studying Electrical Engineering at the Delft University of Technology. In 1999 he received his Master of Science degree after completing his graduation project on the segmentation of dynamic contrast-enhanced perfusion MR-images using neural networks. This research was carried out at the Division of Image Processing of the Leiden University Medical Center. In September 1999 he accepted a research position in the same lab and started working on the analysis of optical mammography images. In 2001, he started working towards his PhD by researching the automated quantification of lesions in coronary and vascular X-ray angiograms. This was in close collaboration with Medis medical imaging systems bv, Leiden. Before this project was finished, he applied for and received a Casimir grant at NWO to conduct research on the quantification of cerebral aneurysms in MRA and CTA images. In 2006 he started this project, also in cooperation with Medis, where he was posted for half of the time during the project. In the meanwhile he continued the research on the lesion-quantification in X-ray angiograms to finish the software and his PhD. In 2010 he received a new grant from STW (the Carisma program) to continue the research on the cerebral vascular tree analysis, on which he started working as a Postdoc in 2011. His current research includes automatic image analysis and visualization, vascular tree segmentation and registration, vascular abnormality detection and quantification.